Contents of issue 1 vol. L

Polish Academy of Sciences

Institute of Fundamental Technological Research

Archives of Mechanics

Archiwum Mechaniki Stosowanej

volume 50 issue 1

FIFTY YEARS OF THE ARCHIVES OF MECHANICS

Polish Scientific Publishers PWN

Warszawa 1998

ARCHIVES OF MECHANICS IS DEVOTED TO
Theory of elasticity and plasticity • Theory of nonclassical continua • Physics of continuous media • Mechanics of discrete media • Nonlinear mechanics • Rheology • Fluid gas-mechanics • Rarefied gas • Thermodynamics

---

Printed in Poland, Editorial Office: Świętokrzyska 21,
00-049 Warszawa (Poland)

e-mail: publikac@ippt.gov.pl

Arkuszy wydawniczych 10,5. Arkuszy drukarskich 9,25.
Papier offset. kl. III 70 g. B1.
Oddano do składania w lutym 1998 r.
Druk ukończono w kwietniu 1998 r.
Skład i łamanie: "MAT-TEX"
Druk i oprawa: Drukarnia Braci Grodzickich, Żabieniec ul. Przelotowa 7

ARCHIWUM MECHANIKI STOSOWANEJ

ARCHIVES DE MÉCANIQUE APPLIQUÉE

TOM 1

ZESZYT 1

WYDAWNICTWO
ZAKŁADU MECHANIKI BUDOWLI POLITECHNIKI GDAŃSKIEJ
GDAŃSK 1949

Adres Redakcji:

Gdańsk - Wrzeszcz, ul. Narutowicza, Politechnika Gdańska
Zakład Mechaniki Budowli

TREŚĆ ZESZYTU:

ODBITO W DRUKARNI UNIWERSYTETU POZNAŃSKIEGO K-55848

Druk ukończono 13. IV. 1949 r. Nakład 400. Pap. Ilustr. kl. V. form. 70/100 cm 90 g

Arch. Mech., 50, 1, pp. 3–19, Warszawa 1998
FIFTY YEARS OF THE ARCHIVES OF MECHANICS

Internal variables in macrodynamics of two-dimensional periodic cellular media

I. CIELECKA (ŁÓDŹ), C. WOŹNIAK (CZĘSTOCHOWA)
and M. WOŹNIAK (ŁÓDŹ)

A NEW CONTINUUM MODEL for studying the plane strain problems in elastodynamics of a cellular medium having a periodic structure is proposed. The model is based on the concept of macro-internal variables, [17], being capable of describing structures of an arbitrary complex lay-out. The continuum model equations constitute a certain generalization of the plane Cosserat continuum equations coupled with the ordinary differential equations for internal variables. The results are applied to the analysis of free vibration and wave propagation problems. The physical correctness of the model proposed is shown by comparing the obtained solutions to the exact ones.

Notations

Subscripts i, j, k, l run over 1, 2 and are related to a Cartesian orthogonal coordinate system on the plane $0x_1x_2$. Superscripts $a, b, ...$ and $A, B, ...$ run over $1, ..., n$ and $1, ..., N$, respectively, where n is the number of nodes and N is the number of rods in a cell which is assumed to be representative for a periodic structure under consideration. Superscripts α, β run over $1, ..., \nu$ being related to the description of micro-oscillations occurring inside every cell. Summation convention holds for all aforementioned indices unless otherwise stated. Points on the plane $0x_1x_2$ are denoted by $\mathbf{x} = (x_1, x_2)$ and t is the time coordinate.

1. Introduction

THE OBJECTIVE OF THIS CONTRIBUTION is the formulation and application of a continuum model to study linearized elastodynamics for a cellular medium of an arbitrary periodic structure in $0x_1x_2$-plane. Examples of cross-sections for such media are shown in Fig. 1. The considerations are restricted to the plane strain problems.

It is assumed that the length dimensions of a representative cell of the periodic structure are small compared with the minimum characteristic length dimension of the whole medium, and that the mass distribution can be approximated by assigning a concentrated mass and an inertia moment to every nodal point of a periodic lattice. Hence the medium under consideration is represented by a certain plane periodic system of mutually interacting rigid joints. For mass-point systems, problems of this kind were studied in a series of papers which will be not discussed here. An overview of the results, related mainly to the wave propagation and vibration problems, can be found in the known book by BRILLOUIN and PARODI [2].

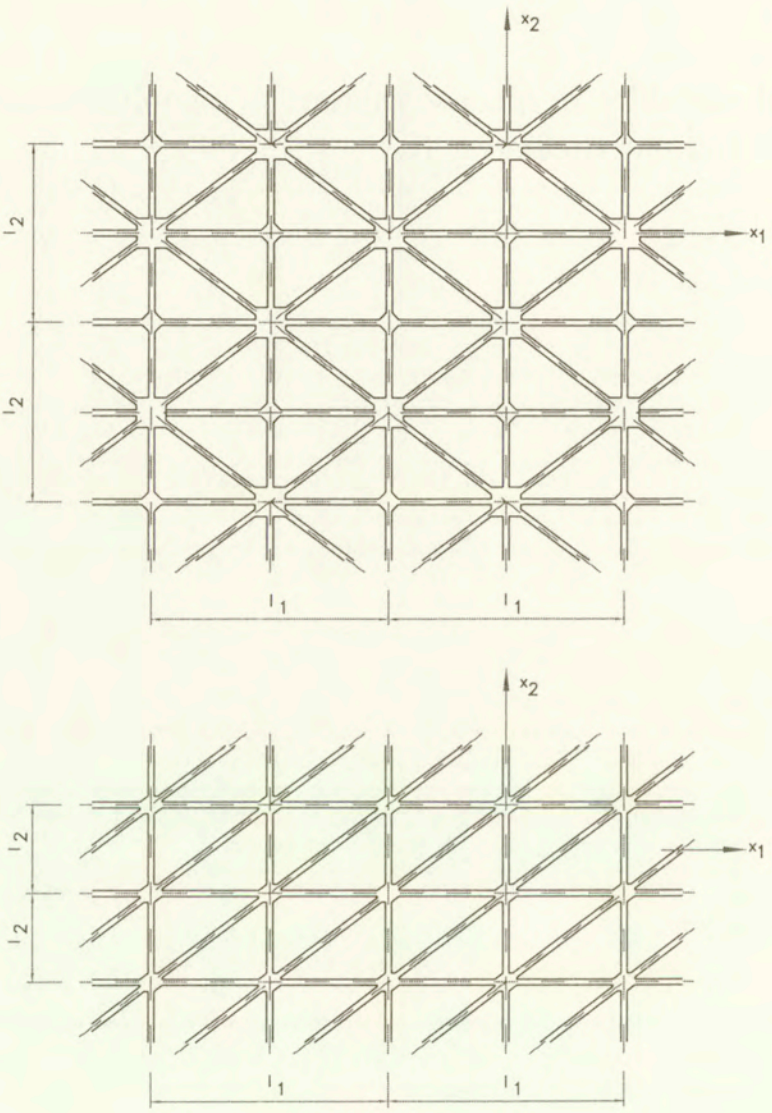

FIG. 1.

It is known that a direct approach to dynamics of periodic systems with a very large number of interacting mass-points or rigid bodies leads to computational difficulties due to a large number of ordinary differential equations describing the problem under consideration. That is why different averaged continuum models of periodic mass-point and rigid-body systems have been proposed in order to reduce the number of basic unknowns and to simplify the analysis of particular problems. From many results obtained in this manner, let us mention those related to periodic structures [5], cellular materials [6], perforated plates [7], and

frame-type lattice structures, summarized in [15], where the list of references can be found. Main attention in [14, 15, 16] was focussed on investigation of engineering problems for framed structures (not only periodic) but the analysis was restricted to static problems. A more sophisticated modelling approach, based on the asymptotic procedures of the homogenization theory (for details see the recent book [8], and the references therein) can be found in a book [1]; a similar approach was also applied in [4].

It has to be emphasized that the asymptotic approaches to the formulation of continuum (homogenized) models for periodic structures neglect the effect of the unit cell size on the global behaviour of discrete medium, because in the course of modelling all length dimensions of every unit cell tend to zero (and number of the cells tends to infinity). On the other hand, the aforementioned effect plays an important role in many dynamic problems being responsible, for example, for dispersion of waves propagating across a periodic system made of interacting mass-points or rigid elements. We can mention here a series of papers [10–13] related to the analysis of hexagonal gridworks, where Rogula–Kunin's approach was applied, cf. [9].

An alternative nonasymptotic continuum model of periodic mass-point systems was formulated in [3]. This model was based on the concepts of refined macrodynamics of composite materials proposed in [17] and then developed in a series of papers (for references cf. [18]). The idea of refined macrodynamics lies in the description of microdynamic effects on the global composite body behaviour in terms of so-called macro-internal variables which are governed by a system of ordinary differential equations and hence do not enter boundary conditions [17, 18].

In this paper, the line of approach is similar to that leading to the refined macrodynamics of composites, but it has been modified in order to derive a continuum model of the plane problem for an arbitrary periodic cellular structure, with nodal joints as rigid elements interconnected by means of linear-elastic thin plates subjected to cylindrical bending. This model also describes a plane framed structure with rigid joints and linear-elastic beams. It is assumed that the length dimensions in $0x_1x_2$ plane of every rigid nodal element are negligibly small as compared with the spans of interconnecting plates or beams.

The present paper constitutes a generalization of the approach to dynamics of periodic trusses proposed in [3] where only axial forces in the interconnecting rods and concentrated masses at the nodal points of the system were taken into account. The aim of this contribution is to formulate a refined continuum model of the medium under consideration (i.e. a nonasymptotic model which describes the effect of size of the representative periodicity cell on the global body behaviour) which can be applied to the analysis of linear elastic plane cellular media with an arbitrary complex lay-out of the representative cell. The main feature of the model is its relatively simple analytical form given by the partial differential equations of the plane Cosserat continuum coupled with the system

of ordinary differential equations involving only second order time derivatives of internal variables. An example is used to show that the proposed model yields physically correct solutions.

2. Preliminaries

Let $\Delta = (-0.5l_1, 0.5l_1) \times (-0.5l_2, 0.5l_2)$ represent a cell which is assumed as representative for of a periodic network on the plane $0x_1, x_2$, cf. Fig. 3. It means that Δ contains the representative structural element for the cellular or framed periodic medium. It has to be emphasized that the choice of this element is not unique and depends not only on the geometry of the network but also on the class of micro-motions we are to investigate using the model proposed in the sequel. It is assumed that the representative element is made of n rigid nodes N^a, $a = 1, ..., n$, interconnected by N linear-elastic homogeneous thin plates R^A, $A = 1, ..., N$ subjected to cylindrical bending in $0x_1x_2$-plane. For framed structures R^A are linear-elastic beams and it is assumed that $0x_1x_2$ is a symmetry plane, both for every beam and every rigid node treated as certain spatial (3-dimensional) elements. By a region occupied by a periodic medium under consideration we shall mean the plane region Ω obtained by a union of all repeated cells. Denoting by L the smallest characteristic length dimension of Ω and setting $l := \sqrt{(l_1)^2 + (l_2)^2}$, it will be assumed that $l/L \ll 1$. This is why l will be referred to as the microstructure length parameter of the medium. It has to be remembered that the periodic structure of the whole medium can be disturbed in the structural elements situated near the boundary $\partial\Omega$ of Ω. An example of a lattice with the representative cell Δ is shown in Fig. 3 but in general, no restrictions are imposed on the form of the lattice and a choice of a representative cell, provided that condition $l/L \ll 1$ holds.

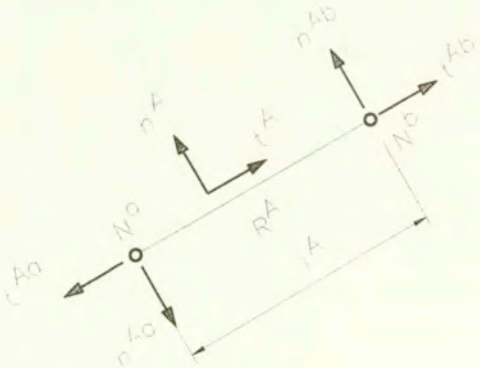

FIG. 2.

Significant properties of a thin plate or a beam R^A will be given by the flexural stiffness B^A in plane $0x_1x_2$, the axial stiffness D^A and the span l^A.

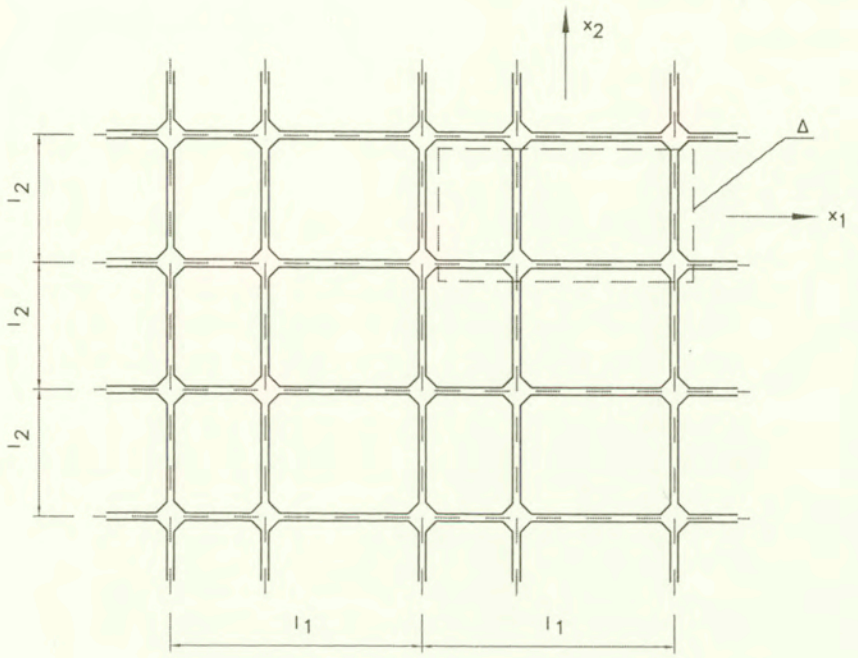

FIG. 3.

The concentrated mass and the rotational moment of inertia (related to the axis normal to the plane $0x_1x_2$) assigned to node N^a will be denoted by M^a, J^a, respectively. Orientation of the plate or the beam R^A interconnecting nodes N^a, N^b will be described by unit vectors $\mathbf{t}^A$, $\mathbf{n}^A$, $\mathbf{t}^{Aa}$, $\mathbf{n}^{Aa}$ shown in Fig. 2. We shall assume that if a plate or a beam R^A is not supported at the nodal point N^a then by definition $\mathbf{t}^{Aa} \equiv \mathbf{0}$, $\mathbf{n}^{Aa} \equiv \mathbf{0}$. Denoting by u_i^a, φ^a displacements and rotation of the node N^a, respectively, let us define

$$(2.1) \qquad \Delta_A u_i := \frac{u_i^b - u_i^a}{l^A}, \qquad \Delta_A \varphi := \varphi^b - \varphi^a, \qquad \varphi_A := \frac{\varphi^a + \varphi^b}{2}.$$

Let us also assume that every plate or beam R^A can be considered in the framework of the Kirchhoff plate theory or the Euler–Bernoulli beam theory, respectively. Then the strain components related to R^A can be taken in the form (no summation over A in formulae (2.2)–(2.4)!)

$$(2.2) \qquad \varepsilon^A := (\Delta_A u_i) t_i^A, \qquad \tilde{\varepsilon}^A := (\Delta_A u_i) n_i^A - \varphi_A, \qquad \kappa^A := \Delta_A \varphi,$$

and at additional notations

$$(2.3) \qquad \Lambda^A := D^A l^A, \qquad \tilde{\Lambda}^A := 12 B^A / l^A, \qquad K^A := B^A / l^A,$$

the strain energy σ^A assigned to plate or beam R^A is equal to

$$\sigma^A = \frac{1}{2}A^A(\varepsilon^A)^2 + \frac{1}{2}\widetilde{A}^A(\widetilde{\varepsilon}^A)^2 + K^A(\kappa^A)^2. \tag{2.4}$$

It has to be remembered that all the aforementioned denotations and formulae are related to an arbitrary but fixed structural element of the periodic lattice under consideration (possibly except some elements situated near boundary $\partial\Omega$ of Ω). Let us denote by $\mathcal{L}$ a set of all points on the plane $0x_1x_2$ which are centers of all disjoined cells constituting the region Ω. Then the displacement vector and rotation of the node N^a belonging to a cell with center $\mathbf{z}$, $\mathbf{z} \in \mathcal{L}$, at an arbitrary instant t, will be denoted by $\mathbf{u}^a(\mathbf{z}, t)$, $\varphi^a(\mathbf{z}, t)$, respectively. All external loads acting on the medium will be applied exclusively to the centers of the nodal joints. The resultant force and moment applied to the node N^a in a cell with a center $\mathbf{z} \in \mathcal{L}$ will be denoted by $\mathbf{f}^a(\mathbf{z}, t)$ and $m^a(\mathbf{z}, t)$, respectively. Introducing the action functional $\mathcal{A} = \mathcal{T} - \mathcal{K} - \mathcal{W}$, where

$$\begin{aligned}
\mathcal{T} &= \frac{1}{2}\sum_{\mathbf{z}\in\mathcal{L}}\sum_{A=1}^{N}\left[A^A(\varepsilon^A(\mathbf{z}, t))^2 + \widetilde{A}^A(\widetilde{\varepsilon}^A(\mathbf{z}, t))^2 + K^A(\kappa^A(\mathbf{z}, t))^2\right], \\
K &= \sum_{\mathbf{z}\in\mathcal{L}}\sum_{a=1}^{n}\left[M^a(\dot{\mathbf{u}}^a(\mathbf{z}, t))^2 + J^a(\dot{\varphi}^a(\mathbf{z}, t))^2\right], \\
\mathcal{W} &= \sum_{\mathbf{z}\in\mathcal{L}}\sum_{a=1}^{n}\left[\mathbf{f}^a(\mathbf{z}, t)\mathbf{u}^a(\mathbf{z}, t) + m^a(\mathbf{z}, t)\varphi^a(\mathbf{z}, t)\right],
\end{aligned} \tag{2.5}$$

and taking into account formulae (2.1), (2.2), from the principle of stationary action we derive equations of motion for $\mathbf{u}^a(\mathbf{z}, t)$, $\varphi^a(\mathbf{z}, t)$, $\mathbf{z} \in \mathcal{L}$, $a = 1, ..., n$. These equations represent a discrete model of a periodic lattice-type structure but are not convenient in investigations of its global dynamic behaviour since the number of points of $\mathcal{L}$ is very large. That is why relations (2.1), (2.2), (2.5) together with assumptions formulated in Sec. 3 will be treated only as a basis for deriving a continuum model of the cellular medium under consideration.

3. Modelling assumptions

In order to formulate the modelling assumptions leading from the discrete model of the periodic medium under consideration to a certain refined (non-asymptotic) continuum model, first of all we have to choose a cell Δ and then to introduce two auxiliary concepts.

The first is the concept of a macro-function related to the choice of a cell Δ. Let $F(\cdot, t)$ be a real-valued function defined on Ω and depending on time t, the values of which, from the computational viewpoint, have to be calculated within the known error ε_F. For a given value of Δ, the microstructure length parameter

l is also known. Function $F(\cdot, t)$ will be called a macro-function (related to ε_F and l) if for every $\mathbf{x}, \mathbf{y} \in \Omega$ such that $\|\mathbf{x} - \mathbf{y}\| < l$ and for every t, condition $|F(\mathbf{x}, t) - F(\mathbf{y}, t)| < \varepsilon_F$ holds. Moreover, if $F(\cdot, t)$ is a differentiable function and similar conditions hold also for all derivatives of F (including time-derivatives), then F will be called a regular macro-function. In the sequel we tacitly assume that every (regular) macro-function F is related to certain parameters ε_F, l.

The second auxiliary concept is that of an oscillation-shape matrix. Define $\nu := n - 1$ and let $h^{a\alpha}$, $g^{a\alpha}$, $\alpha = 1, ..., \nu$ be the real numbers which are elements of $n \times \nu$ matrices of rank ν, satisfying conditions

$$M^a h^{a\alpha} = 0, \qquad J^a g^{a\alpha} = 0, \qquad \alpha = 1, ..., \nu. \tag{3.1}$$

The aforementioned matrices will be referred to as the oscillation-shape matrices. The physical meaning of this concept will be explained below.

The first modelling assumption makes it possible to represent displacement $\mathbf{u}^a(\mathbf{z}, t)$ and rotation $\varphi^a(\mathbf{z}, t)$ of an arbitrary node N^a in a cell with center $\mathbf{z}$, $\mathbf{z} \in \mathcal{L}$, in terms of certain regular macro-functions $U_i(\cdot, t)$, $Q_i^\alpha(\cdot, t)$, $\Phi(\cdot, t)$, $R^\alpha(\cdot, t)$, defined on Ω for every t. This assumption will be referred to as *the macro-kinematic hypothesis* given by

$$\begin{aligned} u_i^a(\mathbf{z}, t) &= U_i(\mathbf{x}, t) + l h^{a\alpha} Q_i^\alpha(\mathbf{x}, t), \\ \varphi^a(\mathbf{z}, t) &= \Phi(\mathbf{x}, t) + l g^{a\alpha} R^\alpha(\mathbf{x}, t), \qquad \mathbf{z} \in \mathcal{L}, \end{aligned} \tag{3.2}$$

where $\mathbf{x}$ is a position vector of the node N^a in a cell with the center $\mathbf{z}$. Because of $|U_i(\mathbf{x}, t) - U_i(\mathbf{z}, t)| < \varepsilon_U$, $|\Phi(\mathbf{x}, t) - \Phi(\mathbf{z}, t)| < \varepsilon_\Phi$, etc., and bearing in mind Eqs. (3.1), we obtain

$$\begin{aligned} U_i(\mathbf{z}, t) &= \frac{M^a u_i^a(\mathbf{z}, t)}{\sum M^a} + \mathcal{O}(\varepsilon_U) + \mathcal{O}(\varepsilon_Q), \\ \Phi(\mathbf{z}, t) &= \frac{J^a \varphi^a(\mathbf{z}, t)}{\sum J^a} + \mathcal{O}(\varepsilon_\Phi) + \mathcal{O}(\varepsilon_R), \qquad \mathbf{z} \in \mathcal{L}. \end{aligned} \tag{3.3}$$

It follows that $U_i(\mathbf{z}, t)$ and $\Phi(\mathbf{z}, t)$ are approximations of weighted averaged displacements and rotations, respectively, within an arbitrary cell. Fields $U_i(\cdot, t)$ and $\Phi(\cdot, t)$ will be called macro-displacements and macro-rotation, respectively, at an instant t. Taking into account Eqs. (3.1) it can be seen that $Q_i^\alpha(\mathbf{z}, t)$, $R^\alpha(\mathbf{z}, t)$ describe oscillations of displacements and rotations at time t within an arbitrary cell. Fields $Q_i^\alpha(\cdot, t)$, $R^\alpha(\cdot, t)$ will be called macro-internal variables; the meaning of this term will be explained in the subsequent section. Roughly speaking, in order to use the macro-kinematic hypothesis we have to choose a certain representative cell Δ, and then to specify oscillation-shape matrices and hence to restrict our considerations to a certain class of motions which can be expected in the problem under consideration. Such situation is met in many dynamic problems of interest in the analysis of special classes of motions.

Let us observe that restrictions imposed on the class of motions under consideration reduce to the requierement that $U_i(\cdot,t)$, $Q_i^\alpha(\cdot,t)$, $\Phi(\cdot,t)$, $R^\alpha(\cdot,t)$ have to be regular macro-functions for every t. Let us also observe that the oscillation-shape matrices are not uniquely determined but their choice is irrelevant.

The second modelling assumption is related to the concept of macro-function and will be called *the macro-approximation hypothesis*. This hypothesis consists of two kinds of postulated approximations:

(i) Finite differences of regular macro-functions within every cell can be approximated by the values of appropriate derivatives.

(ii) Increments of all macro-functions inside an arbitrary cell will be neglected in calculation of averages over this cell.

From (ii) it follows that term $\mathcal{O}(\varepsilon_U)$, $\mathcal{O}(\varepsilon_Q)$, $\mathcal{O}(\varepsilon_\Phi)$, $\mathcal{O}(\varepsilon_R)$ in Eqs. (3.3) in the course of modelling can be neglected. Hence macro-displacements and macro-rotation in the center of an arbitrary cell can be treated as weighted averages of nodal displacements and rotations, respectively, in this cell. From (i) we obtain the formulae for strain components in an arbitrary plate or beam belonging to a cell with the center $\mathbf{z}$. To this end, define $\lambda^A := l/l^A$, $g_A^\alpha := \frac{1}{2}(g^{a\alpha} + g^{b\alpha})$, $g^{A\alpha} := (g^{b\alpha} - g^{a\alpha})$ if nodes N^a, N^b belong to the rod R^A, and

$$
\begin{aligned}
E_{ij}(\mathbf{x},t) &:= U_{i,j}(\mathbf{x},t) + \epsilon_{ij}\Phi(\mathbf{x},t),\\
\Phi_i(\mathbf{x},t) &:= \Phi_{,i}(\mathbf{x},t), \qquad \mathbf{x}\in\Omega,
\end{aligned}
\tag{3.4}
$$

where ϵ_{ij} is the Ricci symbol. After simple calculations we arrive at (no summation over A!)

$$
\begin{aligned}
\varepsilon^A(\mathbf{z},t) &= t_i^A t_j^A E_{ij}(\mathbf{z},t) + \lambda^A t_i^{Aa} h^{a\alpha} Q_i^\alpha(\mathbf{z},t) + \mathcal{O}(\varepsilon),\\
\tilde{\varepsilon}^A(\mathbf{z},t) &= n_i^A t_j^A E_{ij}(\mathbf{z},t) + \lambda^A n_i^{Aa} h^{a\alpha} Q_i^\alpha(\mathbf{z},t) - l g_A^\alpha R^\alpha + \mathcal{O}(\varepsilon),\\
\kappa^A(\mathbf{z},t) &= l^A t_i^A \Phi_i(\mathbf{z},t) + l g^{A\alpha} R^\alpha(\mathbf{z},t) + \mathcal{O}(\varepsilon),
\end{aligned}
\tag{3.5}
$$

where $\mathbf{z}\in\mathcal{L}$ and terms $\mathcal{O}(\varepsilon)$ depend on increments of the pertinent macro-functions inside a cell with center $\mathbf{z}$. Here and in the sequel it has to be remembered that $t_i^{Aa} := 0$, $n_i^{Aa} := 0$ if the node N^a does not belong to the rod R^A.

4. Governing equations

After substituting to (2.5) the right-hand sides of Eqs. (3.2), (3.5) and taking into account the macro-approximation hypothesis (related to calculations of averages), it can be seen that the finite sum over $\mathcal{L}$ can be approximated by an

integral over Ω. Setting $|\Delta| = l_1 l_2$ let us introduce the notations

$$
\begin{aligned}
A_{ijkl} &:= |\Delta|^{-1} \sum_{A=1}^{N} \left(\Lambda^A t_i^A t_k^A + \tilde{\Lambda}^A n_i^A n_k^A \right) t_j^A t_l^A \,, \\
B_{ijk}^{\alpha} &:= |\Delta|^{-1} \sum_{A=1}^{N} \lambda^A \left(\Lambda^A t_i^A t_k^{Aa} + \tilde{\Lambda}^A n_i^A n_k^{Aa} \right) t_j^A h^{a\alpha}, \\
C_{ij}^{\alpha\beta} &:= |\Delta|^{-1} \sum_{A=1}^{N} (\lambda^A)^2 \left(\Lambda^A t_i^{Aa} t_j^{Ab} + \tilde{\Lambda}^A n_i^{Aa} n_j^{Ab} \right) h^{a\alpha} h^{b\beta}, \\
D_{ij} &:= |\Delta|^{-1} \sum_{A=1}^{N} (\lambda^A)^{-2} K^A t_i^A t_j^A \,, \\
G_i^{\alpha} &:= |\Delta|^{-1} \sum_{A=1}^{N} (\lambda^A)^{-1} K^A t_i^A g^{A\alpha}, \\
F^{\alpha\beta} &:= |\Delta|^{-1} \sum_{A=1}^{N} \left(\tilde{\Lambda}^A g_A^{\alpha} g_A^{\beta} + K^A g^{A\alpha} g^{A\beta} \right), \\
B_{ij}^{\alpha} &:= -|\Delta|^{-1} \sum_{A=1}^{N} \tilde{\Lambda}^A n_i^A t_j^A g_A^{\alpha} \,, \\
C_i^{\alpha\beta} &:= -|\Delta|^{-1} \sum_{A=1}^{N} \lambda^A \tilde{\Lambda}^A n_i^{Aa} h^{a\alpha} g_A^{\beta} \,, \\
\chi &:= |\Delta|^{-1} \sum_{a=1}^{n} J^a, \qquad\qquad \varrho := |\Delta|^{-1} \sum_{a=1}^{n} M^a, \\
\chi^{\alpha\beta} &:= |\Delta|^{-1} \sum_{a=1}^{n} J^a g^{a\alpha} g^{a\beta}, \qquad \varrho^{\alpha\beta} := |\Delta|^{-1} \sum_{a=1}^{n} M^a h^{a\alpha} h^{a\beta}.
\end{aligned}
\tag{4.1}
$$

Under the extra assumption that there exist continuous macro-functions $f_i(\cdot, t)$, $f_i^{\alpha}(\cdot, t)$, $m(\cdot, t)$, $m^{\alpha}(\cdot, t)$ defined on Ω for every t, such that the conditions

$$
\begin{aligned}
f_i(\mathbf{z}, t) &= |\Delta|^{-1} \sum_{a=1}^{n} f_i^a(\mathbf{z}, t) + \mathcal{O}(\varepsilon_f), \\
f_i^{\alpha}(\mathbf{z}, t) &= |\Delta|^{-1} \sum_{a=1}^{n} f_i^a(\mathbf{z}, t) h^{a\alpha} + \mathcal{O}(\varepsilon_f), \\
m(\mathbf{z}, t) &= |\Delta|^{-1} \sum_{a=1}^{n} m^a(\mathbf{z}, t) + \mathcal{O}(\varepsilon_m), \\
m^{\alpha}(\mathbf{z}, t) &= |\Delta|^{-1} \sum_{a=1}^{n} m^a(\mathbf{z}, t) g^{a\alpha} + \mathcal{O}(\varepsilon_m),
\end{aligned}
\tag{4.2}
$$

hold for every $\mathbf{z} \in \mathcal{L}$ we arrive, after some manipulations, at the integral form of the action functional $\mathcal{A} = \mathcal{T} - K - \mathcal{W}$, where now

$$\begin{aligned}\mathcal{T} = \int_{\Omega} \Big(& \frac{1}{2} A_{ijkl} E_{ij} E_{kl} + B^{\alpha}_{ijk} E_{ij} Q^{\alpha}_{k} + l B^{\alpha}_{ij} E_{ij} R^{\alpha} \\ & + \frac{1}{2} C^{\alpha\beta}_{ij} Q^{\alpha}_{i} Q^{\beta}_{j} + l C^{\alpha\beta}_{i} Q^{\alpha}_{i} R^{\beta} + l^2 D_{ij} \Phi_i \Phi_j + l^2 G^{\alpha}_{i} \Phi_i R^{\alpha} \\ & + l^2 \frac{1}{2} F^{\alpha\beta} R^{\alpha} R^{\beta} \Big) \, da, \\ K = \int_{\Omega} & \Big(\frac{1}{2} \varrho \dot{U}_i \dot{U}_i + \frac{1}{2} l^2 \varrho^{\alpha\beta} \dot{Q}^{\alpha}_{i} \dot{Q}^{\beta}_{i} + \frac{1}{2} \chi \dot{\Phi} \dot{\Phi} + \frac{1}{2} l^2 \varrho^{\alpha\beta} \dot{R}^{\alpha} \dot{R}^{\beta} \Big) \, da, \\ \mathcal{W} = \int_{\Omega} & \left(f_i U_i + l f^{\alpha}_{i} Q^{\alpha}_{i} + m \Phi + l m^{\alpha} R^{\alpha} \right) da, \qquad da = dx_1 dx_2 \, .\end{aligned} \tag{4.3}$$

From the principle of stationary action we obtain the following equations of motion for macro-displacements U_i and a macro-rotation Φ:

$$\begin{aligned} A_{ijkl} E_{kl,j} + B^{\alpha}_{ijk} Q^{\alpha}_{k,j} + l B^{\alpha}_{ij} R^{\alpha}_{,j} - \varrho \, \ddot{U}_i + f_i = 0, \\ l^2 D_{ij} \Phi_{i,j} + l^2 G^{\alpha}_{i} R^{\alpha}_{,i} - \epsilon_{ij} \left(A_{ijkl} E_{kl} + B^{\alpha}_{ijk} Q^{\alpha}_{k} + l B^{\alpha}_{ij} R^{\alpha} \right) - \chi \, \ddot{\Phi} + m = 0 \end{aligned} \tag{4.4}$$

coupled with equations for macro-internal variables Q^{α}_{i}, R^{α}:

$$\begin{aligned} l^2 \varrho^{\alpha\beta} \, \ddot{Q}^{\beta}_{i} + C^{\alpha\beta}_{ij} Q^{\beta}_{j} + l C^{\alpha\beta}_{i} R^{\beta} + B^{\alpha}_{kji} E_{kj} = l f^{\alpha}_{i} \, , \\ l^2 \chi^{\alpha\beta} \, \ddot{R}^{\beta} + l^2 F^{\alpha\beta} R^{\beta} + l C^{\beta\alpha}_{i} Q^{\beta}_{i} + l^2 G^{\alpha}_{i} \Phi_i + l B^{\alpha}_{ij} E_{ij} = l m^{\alpha}, \end{aligned} \tag{4.5}$$

where E_{ij}, Φ_i are defined by Eqs. (3.4). The obtained equations have to be satisfied for every t in region Ω of the plane $0x_1x_2$, and represent a continuum model of the cellular periodic medium under consideration.

The governing equations (4.4), (4.5) can be also written in the alternative form given by:

(i) Equations of motion

$$\begin{aligned} T_{ij,j} - \varrho \, \ddot{U}_i + f_i = 0, \\ M_{i,i} - \epsilon_{ij} T_{ij} - \chi \, \ddot{\Phi} + m = 0. \end{aligned} \tag{4.6}$$

(ii) Dynamic evolution equations

$$\begin{aligned} l^2 \varrho^{\alpha\beta} \, \ddot{Q}^{\beta}_{i} + S^{\alpha}_{i} = l f^{\alpha}_{i} \, , \\ l^2 \chi^{\alpha\beta} \, \ddot{R}^{\beta} + H^{\alpha} = l m^{\alpha}. \end{aligned} \tag{4.7}$$

(iii) Constitutive equations

$$
\begin{bmatrix} T_{ij} \\ M_i \\ S_i^\alpha \\ H^\alpha \end{bmatrix} = \begin{bmatrix} A_{ijkl} & 0 & B_{ijk}^\beta & lB_{ij}^\beta \\ 0 & l^2 D_{ik} & 0 & l^2 G_i^\beta \\ B_{kli}^\alpha & 0 & C_{ik}^{\alpha\beta} & lC_i^{\alpha\beta} \\ lB_{kl}^\alpha & l^2 G_k^\alpha & lC_k^{\beta\alpha} & l^2 F^{\alpha\beta} \end{bmatrix} \begin{bmatrix} E_{kl} \\ \Phi_k \\ Q_k^\beta \\ R^\beta \end{bmatrix}, \tag{4.8}
$$

which have to be considered together with the notations (3.4). From a formal viewpoint, Eqs. (4.6) are similar to the known plane Cosserat media equations of motion. Hence T_{ij} and M_i can be called components of a macro-stress tensor and a macro-couple-stress vector, respectively. However, contrary to the Cosserat media, we also deal here with the dynamic evolution equations (4.7) which are coupled with the Cosserat equations (4.6) *via* the constitutive equations (4.8).

The first characteristic feature of the obtained model is that it describes, in one formal scheme, a wide class of plane problems for elastic periodic cellular media. Moreover, the effect of the cell size on the dynamic behaviour of the structure is taken into account. This fact is caused by the nonasymptotic modelling procedure which leads to the occurence of the microstructure length parameter l in Eqs. (4.7), related to the coefficients at the second-order time derivatives of macro-internal variables. At the same time, all coefficients in equations (4.4), (4.5) defined by formulae (4.1) are independent of the cell size and hence, the dependence of these equations on l has an explicit form.

The second characteristic feature of the obtained continuum model is that equations (4.5) for Q_i^α, R^α are ordinary differential equations involving exclusively time-derivatives of these fields. Hence functions Q_i^α, R^α are not restricted by boundary conditions, which have to be formulated only for macro-displacements U_i and a macro-rotation Φ. That is why functions Q_i^α, R^α were called macro-internal variables. Thus, in formulation of initial-boundary value problems, Eqs. (4.4), (4.5) have to be considered together with both the boundary and initial conditions for U_i, Φ and only the initial conditions for Q_i^α, R^α. This fact is essential in investigations of special problems since in the framework of the continuum model, only boundary conditions for U_i and Φ have a physical motivation, being independent of possible disturbances of the periodic structure of a medium near the boundary of a region Ω.

It has to be emphasized that solutions to problems described by Eqs. (4.3) – (4.5) together with boundary and initial conditions, have a physical sense only if solutions U_i, Φ, Q_i^α, R^α to these problems are represented by regular macro-functions.

In order to evaluate the cell size effect on the dynamic behaviour of the medium, together with the refined model we can also consider its asymptotic approximation obtained by a formal passage $l \to 0$ in (4.3). In this case we arrive at a special case of results obtained in [3].

At the end of this section let us consider some special cases of the proposed continuum models for discrete periodic structures described in Sec. 3. Firstly, assume that $B^{\alpha}_{ijk} = 0$, $G^{\alpha}_{i} = 0$ and $C^{\alpha\beta}_{i} = 0$. Such situation takes place if x_α are elastic symmetry axes for constitutive equations (4.8). In this case the model will be called macro-ortothropic. Moreover, if $B^{\beta}_{ij} = 0$ then constitutive equations (4.8) reduce to the form

$$T_{ij} = A_{ijkl}E_{kl}\,, \qquad M_i = D_{ij}\Phi_j\,, \tag{4.9}$$

and dynamic evolution equations (4.7) yield

$$\begin{aligned} l^2\varrho^{\alpha\beta}\,\ddot{Q}^{\beta}_{i} + C^{\alpha\beta}_{ij}Q^{\beta}_{j} &= lf^{\alpha}_{i}\,,\\ l^2\chi^{\alpha\beta}\,\ddot{R}^{\beta} + l^2F^{\alpha\beta}R^{\beta} &= lm^{\alpha}. \end{aligned} \tag{4.10}$$

Hence, if $f^{\alpha}_{i} = 0$, $m^{\alpha} = 0$ then under homogeneous initial conditions for macro-internal variables Q^{α}_{i}, R^{α}, we obtain $Q^{\alpha}_{i} = 0$, $R^{\alpha} = 0$. It follows that for this class of problems, there are no oscillations in displacements and rotations within every cell of a structure provided that the external loadings are not oscillating on a cell (i.e. $f^{\alpha}_{i} = 0$, $m^{\alpha} = 0$), and the initial values of macro-internal variables Q^{α}_{i}, R^{α} are equal to zero. Macro-ortothropic models in which $B^{\beta}_{ij} = 0$, will be called uncoupled and their continuum models are represented by equations of motion (4.6) and constitutive equations (4.9) (together with notations (3.4)) for U_i, Φ and indepedently, by the evolution equations (4.10) for Q^{β}_{i}, R^{β}. Now assume that the choice of a cell Δ implies $\nu = n-1 = 0$ and hence there are no macro-internal variables in the considered model. This special discrete medium will be referred to as having a simple lay-out structure [12]; an example of this medium is shown at the bottom of Fig. 1. The detailed analysis of different problems for these media was given in [15] where also the list of references can be found. However, also in the case of media with a simple lay-out structure we can analyse more complicated motions by introducing another cell for which $\nu > 0$. Let us also observe that for quasi-stationary processes, the macro-internal variables can be eliminated from (4.4) by means of (4.5).

5. Example

General results of the previous section will be now illustrated by the analysis of a wave propagation in a periodic medium with a rectangular network shown in Fig. 3. In order to introduce the simplest continuum model of this medium, let the cell Δ be assumed in the form given in Fig. 3. This cell has two nodal points; in this case $n = 2$ and $\nu = n - 1 = 1$, i.e., the oscillation-shape matrices reduce to vectors with components h^{11}, h^{21} and g^{11}, g^{21}. Moreover, let the directions of network be paralell to the coordinate axes x_1, x_2, and let x_1 be a symmetry axis

for the constitutive equations (4.8) which have to be invariant under transformation $x_2 \to -x_2$. We are to show, under what conditions a longitudinal harmonic wave can propagate across such medium and how the dispersion relation depends on the unit cell size.

Taking into account the aforementioned properties of a medium and assuming that all unknown functions depend only on x_1 and time t, from Eqs. (4.4), (4.5), (3.4), bearing in mind definitions (4.1) and neglecting external loadings, we obtain two independent systems of equations. The first system is related to U_1 and Q_1:

$$
\begin{aligned}
&A_{1111}U_{1,11} + B_{111}Q_{1,1} - \varrho\,\ddot{U}_1 = 0,\\
&l^2\varrho^{11}\,\ddot{Q}_1 + C_{11}Q_1 + B_{111}U_{1,1} = 0,
\end{aligned}
\tag{5.1}
$$

and the second one involves U_2, Φ, Q_2 and R:

$$
\begin{aligned}
&A_{2121}U_{2,11} + (A_{2112} - A_{2121})\Phi_{,1} + B_{212}Q_{2,1} - \varrho\,\ddot{U}_2 = 0,\\
&l^2D_{11}\Phi_{,11} + (A_{2112} + A_{1221} - A_{1212} - A_{2121})\Phi\\
&\qquad + (A_{2121} - A_{1221})U_{2,1} + (B_{212} - B_{122})Q_2 + l^2G_1R_{,1} - \chi\,\ddot{\Phi} = 0,\\
&l^2\varrho^{11}\,\ddot{Q}_2 + C_{22}Q_2 + (B_{122} - B_{212})\Phi + B_{212}U_{2,1} = 0,\\
&l^2\chi^{11}\,\ddot{R} + l^2FR + l^2G_1\Phi_{,1} = 0,
\end{aligned}
\tag{5.2}
$$

where the superscripts related to macro-internal variables were neglected, i.e., $Q_1 = Q_1^1$, $Q_2 = Q_2^1$, $R = R^1$ etc.

In this paper investigations will be restricted to longitudinal waves. Substituting $U_1 = U(x_1 - ct)$, $Q_1 = Q(x_1 - ct)$ to Eqs. (5.1), where c is the propagation speed, we obtain

$$
\begin{aligned}
&(A_{1111} - \varrho c^2)U_{,11} + B_{111}Q_{,1} = 0,\\
&l^2\varrho^{11}c^2Q + C_{11}Q + B_{111}U_{,1} = 0.
\end{aligned}
\tag{5.3}
$$

Define

$$
\bar{c}^2 := \frac{A_{1111}}{\varrho}, \qquad \tilde{c}^2 := \frac{1}{\varrho}\left(A_{1111} - \frac{(B_{111})^2}{C_{11}}\right).
\tag{5.4}
$$

It can be shown that $\bar{c}^2 > \tilde{c}^2 > 0$. Analysis of Eqs. (5.1) leads to the three following cases:

CASE 1. If $c < \tilde{c}$ or $\bar{c} > c$ then across a medium under consideration, a harmonic longitudinal wave can propagate. Under the notation

$$
(k(c))^2 := \frac{C_{11}}{l^2\varrho^{11}}\,\frac{\tilde{c}^2 - c^2}{c^2(\bar{c}^2 - c^2)}, \qquad (k(c))^2 > 0,
\tag{5.5}
$$

solution to Eqs. (5.3) will be given by

$$U = A_U \sin[k(c)(x_1 - ct)], \qquad Q = A_Q \cos[k(c)(x_1 - ct)].$$

CASE 2. If $\widetilde{c} < c < \overline{c}$ then we shall deal with the exponential wave. Setting

$$(\kappa(c))^2 := -\frac{C_{11}}{l^2\varrho^{11}} \frac{\widetilde{c}^2 - c^2}{c^2(\overline{c}^2 - c^2)}, \qquad (\kappa(c))^2 > 0, \tag{5.6}$$

we obtain

$$U = A_U \exp[-\kappa(c)(x_1 - ct)] + B_U \exp[\kappa(c)(x_1 - ct)]$$

and

$$Q = -\varrho(B_{111})^{-1}(\overline{c}^2 - c^2)U_{,1}\,.$$

CASE 3. If $c = \widetilde{c}$ then we deal with a degenerate case in which $U_{,11} = 0$, $Q_{,1} = 0$. At the same time, the propagation speed $c = \overline{c}$ cannot be realized in the medium under consideration.

Let $k = 2\pi/L$, where L is the wavelength, be the wave number for a harmonic longitudinal wave. Taking into account (5.5) we obtain the dispersion relation

$$-l^2\varrho^{11}k^2c^4 + \left(C_{11} + l^2\varrho^{11}c^2k^2\right)c^2 - C_{11}\widetilde{c}^2 = 0. \tag{5.7}$$

In the framework of applicability of the proposed continuum model, the wavelength L has to be much longer than the microstructure length parameter; only in this case the obtained solutions to Eqs. (5.3) are represented by macro-functions. Hence $\varepsilon := kl$ is a small parameter, $\varepsilon \ll 1$. For harmonic waves we obtain the following asymptotic formulae related to the lower $c = c_L$ and higher $c = c_H$ propagation speeds

$$\begin{aligned} c_L^2 &= \widetilde{c}^2 - l^2\frac{\widetilde{c}^2}{C_{11}}\left(\overline{c}^2 - \widetilde{c}^2\right)\varrho^{11}k^2 + \mathcal{O}(\varepsilon^4), \\ c_H^2 &= \frac{C_{11}}{l^2\varrho^{11}k^2} + \overline{c}^2 - \widetilde{c}^2 + \mathcal{O}(\varepsilon^2), \end{aligned} \tag{5.8}$$

where $c_L < \widetilde{c}$ and $c_H > \overline{c}$. In the case of an exponential wave, i.e., for $c \in (\widetilde{c}, \overline{c})$, we obtain from (5.3) the dispersion relation

$$c^2 = \widetilde{c}^2 + l^2\frac{\widetilde{c}^2}{C_{11}}\left(\overline{c}^2 - \widetilde{c}^2\right)\varrho^{11}\kappa^2 + \mathcal{O}(\varepsilon^4), \tag{5.9}$$

where $\kappa := \delta^{-1}$ and δ is called the length of the exponential wave; here $\varepsilon := \kappa l$ is a small parameter $\varepsilon \ll 1$.

The above results were obtained by using the proposed continuum model of a periodic discrete medium. In the framework of the asymptotic model, by formal passage with l to zero, we obtain from (5.3) only one propagation velocity $c = \widetilde{c}$.

6. Reliability of the model

In order to investigate the physical correctness of the model we restrict ourselves to equations (5.1). Denoting by M^1, M^2 the masses assigned to nodal points, by l^1, l^2 the distances between them (where $l^1 + l^2 = l_1$, cf. Fig. 3) and by D^1, D^2 the axial stiffnesses of the corresponding plates, under notation $\mu = M^2/M^1$ and assuming $h^{11} = -\mu$, $h^{21} = 1$, from formulae (3.6) we obtain

$$
\begin{aligned}
&A_{1111} = \frac{1}{l_1 l_2}\left(D^1 l^1 + D^2 l^2\right), \qquad C_{11} = \frac{l_1}{l_2}(1+\mu)^2\left(\frac{D^1}{l^1} + \frac{D^2}{l^2}\right),\\
&B_{111} = \frac{1}{l_2}(1+\mu)(D^1 - D^2), \qquad \varrho = (1+\mu)\frac{M^1}{l_1 l_2}, \qquad \varrho^{11} = \mu(1+\mu)\frac{M^1}{l_1 l_2}.
\end{aligned} \tag{6.1}
$$

Setting $A := A_{1111}$, $B := B_{111}$, $C := C_{11}$ and $U := U_1$, $Q := Q_1$, we shall rewrite Eqs. (5.1) to the form

$$
\begin{aligned}
&AU_{,11} + BQ_{,1} - \varrho\,\ddot{U} = 0,\\
&l^2\mu\varrho\,\ddot{Q} + CQ + BU_{,1} = 0
\end{aligned} \tag{6.2}
$$

and look for solutions to (6.2) in the well known form

$$
U = a_U \exp i(\omega t - \kappa x_1), \qquad Q = a_Q \exp i(\omega t - \kappa x_1), \tag{6.3}
$$

where $\kappa = 2\pi/L$ and L is the wavelength. Substituting the right-hand sides of (6.3) into (6.2) and denoting $l := l_1 = l^1 + l^2$, $k := \kappa l = 2\pi l/L$, for the free vibration frequency ω we obtain the dispersion relation

$$
(l)^2\mu\varrho^2\omega^4 - (Ak^2\mu + C)\varrho\omega^2 + \kappa^2(AC - B^2) = 0. \tag{6.4}
$$

The model is applicable only if (6.3) are macro-functions; hence the value k has to be sufficiently small compared to 1 and solutions ω_+, ω_- to (6.4), by taking into account (6.1) and performing some manipulations, will be given by

$$
\begin{aligned}
(\omega_+)^2 = &\left(\frac{1}{M^1} + \frac{1}{M^2}\right)\left(\frac{D^1}{l^1} + \frac{D^2}{l^2}\right)\\
&+ \frac{(D^1 - D^2)^2}{(M^1 + M^2)\left(\frac{D^1}{l^1} + \frac{D^2}{l^2}\right)}\left(\frac{k}{l}\right)^2 + o(k^2),
\end{aligned} \tag{6.5}
$$

$$
(\omega_-)^2 = \left[\frac{D^1 l^1 + D^2 l^2}{M^1 + M^2} + \frac{(D^1 - D^2)^2}{(M^1 + M^2)\left(\frac{D^1}{l^1} + \frac{D^2}{l^2}\right)}\right]\left(\frac{k}{l}\right)^2 + o(k^2).
$$

Exact solution of the discrete problem under consideration is known for $D^1 = D^2$ and can be found in [2]. For the long wave approximation and after neglecting terms k^2 as small compared to 1, it can be easily shown that the model solution (6.5) coincides with the long wave approximation of the exact solution given in [2]. Hence we conclude that the proposed model in the problem under consideration yields the physically correct solutions and can be treated as a reliable one.

7. Conclusions

From the illustrative example given in Sec. 5 and its physical correctness discussed in Sec. 6 it follows that the continuum model of a cellular periodic medium,which was proposed in this contribution, constitutes a useful tool for investigations of certain dynamic problems. We also conclude that the proposed continuum model describes dynamics of a whole class of discrete periodic media in one formal scheme given by equations of motion (4.6), dynamic evolution equations (4.7) and constitutive equations (4.8). It has to be emphasized that the microdynamic phenomena (micro-oscillations of mass-elements inside an arbitrary periodicity cell) are described by the macro-internal variables governed by the ordinary differential equations and not entering the boundary conditions; hence the proposed continuum model have certain features typical for the dynamics of discrete media. Moreover, accuracy of the model proposed can be verified *a posteriori* by evaluations of the computational accuracy parameters ε_U, ε_Q, $\varepsilon_{\nabla U}$, ... related to the obtained macro-functions $U(\cdot)$, $Q_i^\alpha(\cdot)$, ..., which constitute a solution to the problem under consideration.

Application of Eqs. (4.6) – (4.8) to the dynamic analysis of honeycomb cellular structures as well as comparison of the obtained data with those resulting from the known models will be given in the subsequent paper.

For the sake of simplicity, the proposed model was restricted to the plane problems for periodic cellular media or framed linear-elastic structures. However, the proposed general line of modelling can be also applied to spatial periodic systems, to problems with damping and to non-linear dynamic problems. Formulation of these models and their applications will be considered separately.

References

1. N.S. BAKHVALOV and G.P. PANASENKO, *Averaging processes in periodic media* [in Russian], Nauka, Moscow 1984.
2. L. BRILLOUIN and M. PARODI, *Propagation des ondes dans les milieux perodiques*, Dunod, Paris 1956.
3. I. CIELECKA, *On continuum modelling the dynamic behaviour of certain composite lattice-type structures*, J. Theor. Appl. Mech., **33**, 351–359, 1995.

4. D. CIORANESCU and J. SAINT PAULIN, *Asymptotic techniques to study tall structures*, [in:] Trends in Applications of Mathematics to Mechanics, Longman Scientific & Technical, 254–262, Harlow 1991.
5. J.O. DOW, Z.W. SU and C.C. FENG, *Equivalent continuum representation of structures composed of repeated elements*, AIAA J., **23**, 1564–1569, 1985.
6. L.J. GIBSON, M.F. ASHBY and C.I. ROBERTSON, *The mechanics of two-dimensional cellular materials*, Proc. Roy. Soc., Ser. **A 382**, 25–42, London 1982.
7. G. HORVAY, *The plane-stress problem of perforated plates*, J. Appl. Mech., **19**, 355–360, 1952.
8. V.V. JIKOV, S.M. KOZLOV and O.A. OLEINIK, *Homogenization of differential operators and integral functionals*, Springer-Verlag, Berlin 1994.
9. I.A. KUNIN, *Theory of elastic media with microstructure* [in Russian], Nauka, Moscow 1975.
10. T. LEWIŃSKI, *Two versions of Woźniak's continuum model of hexagonal type grid plates*, Mech. Teor. Stos., **22**, 389–405, 1984.
11. T. LEWIŃSKI, *Differential models of hexagonal type grid plates*, Mech. Teor. Stos., **22**, 407–421, 1984.
12. T. LEWIŃSKI, *Physical correctness of Cosserat type models of honeycomb grid plates*, Mech. Teor. Stos., **23**, 53–69, 1985.
13. T. LEWIŃSKI, *Dynamical tests of accuracy of Cosserat models for honeycomb gridworks*, ZAMM, **68**, T 210–T 212, 1988.
14. C. WOŹNIAK, *Load carrying structures of dense lattice type*, Arch. Mech., **18**, 579–796, 1966.
15. C. WOŹNIAK, *Lattice surface structures* [in Polish], PWN, Warszawa 1970.
16. C. WOŹNIAK and P. KLEMM, *The elasticity of dense grids of composite structure* [in Polish], Engng. Trans., **18**, 415–440, 1970.
17. C. WOŹNIAK, *Refined macro-dynamics of periodic structures*, Arch. Mech., **45**, 295–304, 1993.
18. C. WOŹNIAK, *Internal variables in dynamics of composite solids with periodic microstructure*, Arch. Mech., **49**, 421–441, 1997.

DEPARTMENT OF STRUCTURAL MECHANICS,
ŁÓDŹ UNIVERSITY OF TECHNOLOGY
al. Politechniki 6, PL 90-924 Łódź 40, Poland,
INSTITUTE OF MATEMATICS AND COMPUTER SCIENCE,
CZĘSTOCHOWA UNIVERSITY OF TECHNOLOGY
ul. Dąbrowskiego 73, PL 42-200 Częstochowa, Poland
and
DEPARTMENT OF GEOTECHNICAL AND STRUCTURE ENGINEERING
ŁÓDŹ UNIVERSITY OF TECHNOLOGY
al. Politechniki 6, PL 90-924 Łódź 40, Poland.

Received July 8, 1997.

Arch. Mech., **50**, 1, pp. 21–40, Warszawa 1998
FIFTY YEARS OF THE ARCHIVES OF MECHANICS

Continuum damage and failure evolution in inhomogeneous ceramic rods

J. NAJAR and V. SILBERSCHMIDT (MUNICH)

A WELL-POSED CDM model and an adequate representation of deterministic and random inhomogeneity factors, combined with an efficient numerical algorithm of modified lattices, yield a realistic simulation of the rupture properties of alumina ceramic specimens at tensile tests. Effects of energy dissipation and acoustic emission, the load-carrying capacity and the post-critical response are analysed in dependence of the heterogeneity realisations, which are related to the initial damage distribution within the specimen. This distribution is shown to be a crucial factor determining the response of brittle damaging ceramics at rupture.

1. Introduction

THE MECHANICAL RESPONSE and failure of brittle materials, monolithic alumina ceramics in particular, are commonly described by means of linear elasticity capped by some rupture condition [1]. Basically, models of this kind are not in the position to explain various experimental observations; these are e.g. acoustic emission and energy dissipation at subcritical loads [2, 3], excessive energy spent at rupture, as compared with single crack-based fracture energy estimates [4], post-critical response [5], size effects in the rupture strength [6], and many others. On the other hand, continuum damage mechanics (CDM) models [7], although reflecting some of the above effects, seem to be not flexible enough to encompass the whole variety of experimental observations, as long as the most fundamental feature of these materials, namely, their inhomogeneity, is not properly accounted for.

The aim of the present paper is to show that a well-posed continuum damage model, [8, 9], and an adequate representation of the deterministic and stochastic factors influencing the inhomogeneity of a sintered ceramic rod, combined with an efficient numerical procedure, result in a realistic simulation of the rupture properties of an alumina specimen in uniaxial tension. The results show also the influence of various realisations of the inhomogeneity on the rod rupture evolution.

The calculations presented in the paper are based on the simulations of the experimental results, [4], obtained with sintered cylindrical specimens of alumina ceramics (diameters 4 to 12 mm, grain size $10 - 20\,\mu$m, tensile strength ca. 300 MPa, compressive strength ca. 3000 MPa, Young modulus 350 GPa); for computational details see [10]. Micromechanical aspects of the damage model

[8, 9], to be presented in Sec. 2, are not discussed in the paper. The applied discretisation, Sec. 3.1, represents rather a mesoscale model (discrete element size ca. 300 μm as compared to the grain size), mainly of the inhomogeneity and randomness of mechanical parameters, Sec. 3.2, as well as mechanisms of local failure development and energy balance of interactions between the elements, Sec. 3.4.

2. Damage evolution law and local failure condition

Basic results on the continuum damage model for brittle ceramics presented in [8, 9] are recalled and extended in this section. The stress-strain relation for uniaxial tensile loading

$$\sigma = E(1 - D)\varepsilon, \tag{2.1}$$

contains the damage variable D, which is governed by the damage evolution law

$$D = D_0 \exp\left(\frac{E\varepsilon^2}{2W^*}\right). \tag{2.2}$$

Here, D_0 denotes the initial damage at the onset of the tensile deformation ε in the current tensile loading branch of the process; the parameter W^*, characterising material's intake of the energy at damage, is denoted further as damage absorbing capacity. The stress-strain relation at damage (2.1) – (2.2) reaches a maximum, see Fig. 1, at the damage value D_m, which can be calculated from the relation

$$D_m \exp\left(\frac{D_m - 1}{2D_m}\right) = D_0\,, \tag{2.3}$$

depending thus solely on the initial damage D_0. The corresponding values of stress σ_m and strain ε_m characterise the load-carrying capacity and material's compliance. The latter can be expressed as a function of initial damage D_0 by the relation

$$\varepsilon_m = \sqrt{\frac{2W^*}{E}}\sqrt{\ln\frac{D_m}{D_0}}\,. \tag{2.4}$$

Expressions (2.3), (2.4) serve as the basis for the determination of the failure criterion in damage. It can be shown, namely, that shortly beyond the stress maximum (m) the uniaxial extension becomes unstable at a point (s) of a strain-controlled process, Fig. 1. Therefore, it can be further assumed that at arriving at the (m)-point, the material undergoes a rapid decay and the damage grows from the value D_m to the nominal value $D = 1$ corresponding to complete

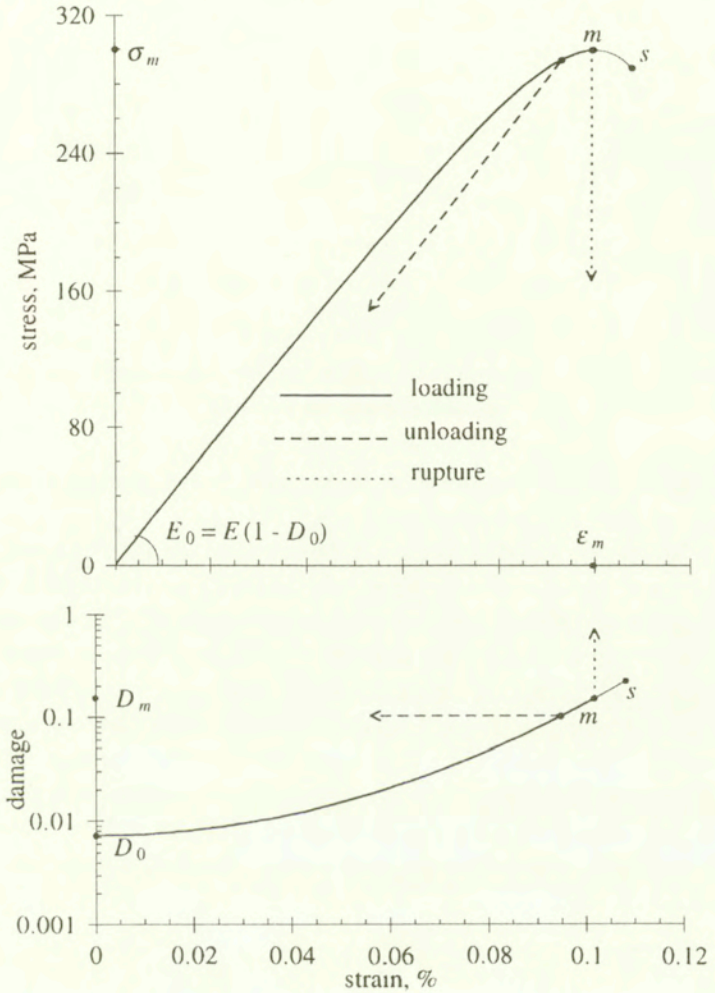

FIG. 1. Stress- and damage-strain curves at tensile loading, unloading and rupture; data for alumina ceramics: $E = 350\,\mathrm{GPa}$, $W^* = 59\,\mathrm{kJ/m^3}$; initial damage $D_0 = 0.73\%$ corresponds to $\sigma_m = 350\,\mathrm{MPa}$ and $\varepsilon_m = 0.1\%$.

failure. Although at increasing initial damage D_0 the failure damage D_m also increases, cf. Eq. (2.3), the load-carrying capacity σ_m and the strain at failure ε_m drop substantially, Fig. 2.

At a strain increment from ε_1 to ε_2, deformation work is performed

$$\Delta W_\sigma = \int_{\varepsilon_1}^{\varepsilon_2} \sigma \, d\varepsilon = \frac{E}{2}\left(\varepsilon_2^2 - \varepsilon_1^2\right) - D_0 W^* \left(\exp\frac{E\varepsilon_2^2}{2W^*} - \exp\frac{E\varepsilon_1^2}{2W^*}\right). \tag{2.5}$$

It can be split into increments of recoverable strain energy ΔW_r and the dissipation related to material damage and associated acoustic and heat losses [8].

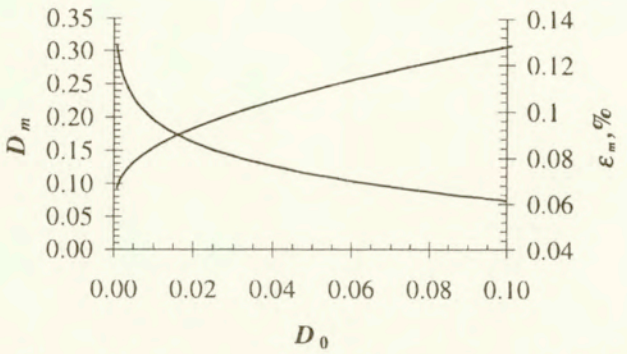

FIG. 2. Damage D_m and strain ε_m at failure, in dependence of the initial damage D_0 (data for alumina, see Fig. 1).

At modest compressive loads, or in unloading from tensile branches of the process, the ceramics follow the incremental Hooke's law $\Delta\sigma = E\Delta\varepsilon$, where E denotes the Young's modulus of the undamaged material [8]; here, no change of damage and no dissipation increment take place. The recoverable strain energy released at complete unloading from a stress σ equals $\sigma^2/2E$. Failure at σ_m leads to the release of the whole stored energy $\sigma_m^2/2E$ in a violent event.

Consider partial unloading from the state characterised by stress σ and damage D to the stress $\sigma_* > 0$, see Fig. 3. Under the branch-invariance conditions discussed in [9], it follows that the state of damage remains unchanged, i.e. $D_* = D$; the strain ε_* undergoes a shift $\delta\varepsilon_s$ to a secondary state of reference 0_s, from which the secondary strain ε_s is counted. The secondary state corresponds also to a secondary initial damage value D_{0s}. The following relations are valid for these quantities:

$$\varepsilon_* = \frac{\sigma_*}{E} + \varepsilon D, \tag{2.6}$$

$$\varepsilon_s = \frac{\varepsilon_* - \varepsilon D}{1 - D}, \tag{2.7}$$

$$\Delta\varepsilon_s = \frac{D}{1 - D}(\varepsilon - \varepsilon_*), \tag{2.8}$$

$$D_{0s} = D \exp\left(-\frac{E\varepsilon_s^2}{2W^*}\right). \tag{2.9}$$

During the partial unloading, the following amount of strain energy is released, see Fig. 3:

$$\Delta W_r = \frac{1}{2E}\left(\sigma^2 - \sigma_*^2\right) = \frac{E}{2}\left[\varepsilon_* + \varepsilon(1 - 2D)\right](\varepsilon - \varepsilon_*). \tag{2.10}$$

The tensile reloading branch, which begins at the state (σ_*, D) is governed by the branch-invariant relations Eq. (2.1) – (2.4), as applied to the secondary initial

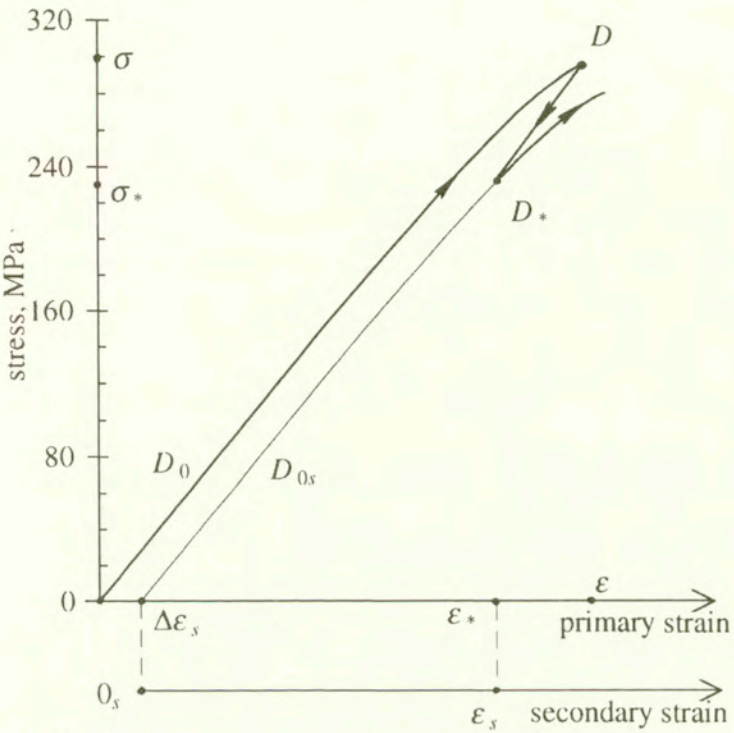

FIG. 3. Partial unloading and reloading in tension (data for alumina, see Fig. 1); the secondary reference state 0_s corresponds to the strain shift $\Delta\varepsilon_s$, Eq. (2.8).

damage D_{0s} and the secondary strain ε_s, while preserving the material parameters E and W^*.

3. Formulation of the problem

A ceramic cylindrical rod will be considered under the conditions of a uniform extension. The modelling of the rod inhomogeneity within its cross-section is based on the combination of a discretization procedure, given in Sec. 3.1, and the material modelling presented in Sec. 2, as applied to single discrete elements. This is complemented by an analysis of the initial damage distribution within a ceramic rod based on experimental data, Sec. 3.2, and by modelling of element's interactions at extension and local failures, Sec. 3.4.

3.1. Discretization

A nonuniform distribution of microdefects in a ceramic rod must result in its inhomogeneous response even at uniform uniaxial extension. A $2d$-formulation, with parameters of the ceramics depending on the position within the cross-section, becomes thus necessary for the analysis of its damage evolution. Such

formulation is implemented in this paper for a cylindrical rod by means of a cross-section discretization into elements of equal area, Fig. 4. The size of the elements must secure the applicability of the continuum damage model presented in Sec. 2. In the following computations, corresponding to the evaluations of the ceramics test presented in [4], the typical size of the elements is ca. 300 μm, as compared to the grain size of the alumina not exceeding 20 μm, which seems to fit well the above mentioned condition. A $3d$-discretization, although basically possible, is not presently considered due to the lack of particular data on the axial distribution of the inhomogeneities along ceramic specimens under investigation.

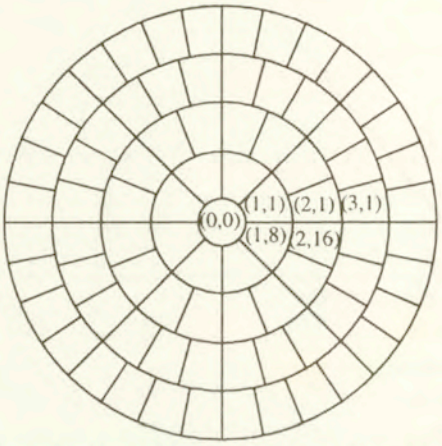

FIG. 4. Cross-section discretisation for $N = 4$, $M = 81$; double indexation of elements facilitates the local failure interaction analysis, see Sec. 3.4.

The cross-section of radius R is divided into N rings of elements, with a circular central element of radius $r_0 = R/(2N + 1)$; all other elements have the radial height $h = 2r_0$ and the angular width $\theta_k = \pi/4k$. Here, k denotes the ring number, with $k = 1$ for the ring next to the central element and $k = N$ for the external ring. The cross-section is divided thus into $M = 1 + 8 \sum_{k=1}^{N} k$ elements, each having the same area of $\pi R^2/M$. Element dimensions are chosen to meet the requirements for a representative unit cell, being small enough with respect to the characteristic length R of the macroscopic field of the rod, and sufficiently large as compared to the size of the microscopic structure of the ceramic material.

3.2. Inhomogeneity

Two main factors determine the features of the distribution of mechanical properties in the rod cross-section:

a) general heterogeneity, linked to the randomness of imperfections in ceramics [11];

b) specific radial distribution, due to the rod-manufacturing technology.

For the case under study, we may assume that all the nonuniformity of the process is based on the features of the initial damage distribution. For the given ceramic material it is, namely, this parameter that influences both the damage accumulation and the response at failure, see Sec. 2. Introducing a $2d$-distribution of initial damage, and putting it at the basis of the two above factors, we express the rod response problem in terms of a $2d$ stochastics.

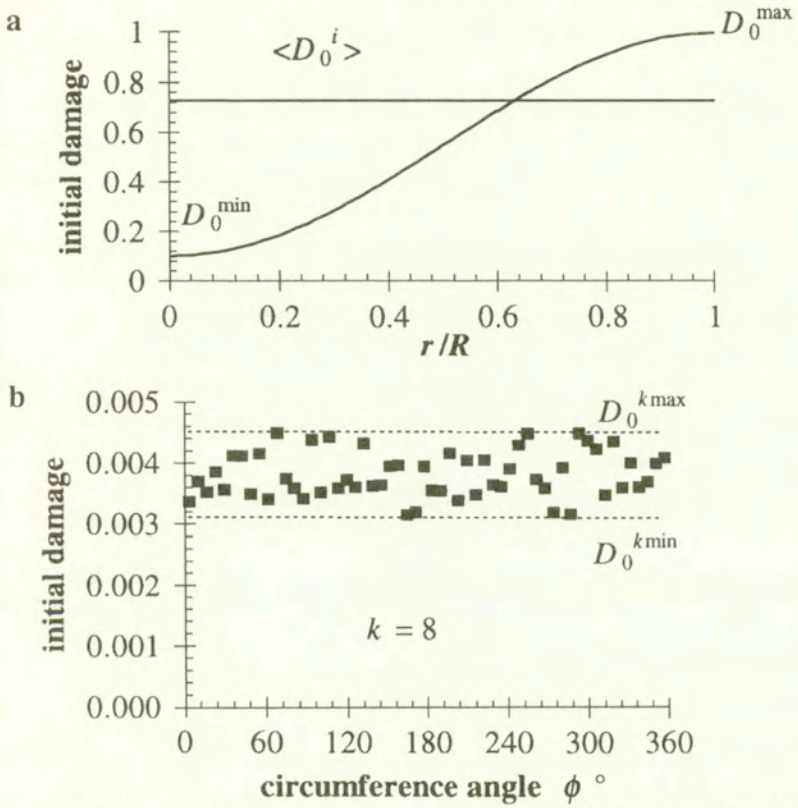

FIG. 5. Initial damage distributions: a) deterministic, over rod radius; b) random, over circumference; exemplary realisation at ring $k = 8$, with scatter band width constant $k_s = 0.1$.

In order to model the D_0-distribution, we recall the elementary notion of damage as a volumetric ratio of voids in a material [12]; the ratio is inversely related to the material's density. We take the radial distribution of density in sintered rods [13] with its drop from the centre to the periphery of the specimen as indicative for the following initial damage function of the radius r:

$$D_0(r) = D_0^{\min} + (D_0^{\max} - D_0^{\min}) \sin^2 \frac{\pi r}{2R}. \tag{3.1}$$

Here, $D_0^{\min}$ relates to the maximum material density, i.e. to the lowest level of initial defects, in the rod centre, while $D_0^{\max}$ corresponds to lower density at

$r = R$, Fig. 5 a. A reference value

$$\overline{D}_0 = \frac{1}{A}\int_A D_0\, dA = \langle D_0^i \rangle\Big|_{M\to\infty} \tag{3.2}$$

for the distribution (3.1) is given by

$$\overline{D}_0 = D_0^{\min} + \left(D_0^{\max} - D_0^{\min}\right)\left(\frac{2}{\pi^2} + \frac{1}{2}\right),$$

corresponding in the discretization to the $M \to \infty$ limit of the initial damage D_0^i $(i = 1, ..., M)$ averaged over all M elements; (3.2) means averaging over the cross-section area A. The reference quantity $\overline{D}_0$ can be used for comparing various discretization and statistical realisations.

To account for the randomness in the $2d$-distribution of defects, we introduce a stochastic sample of the initial damage within each ring separately. It is based on the experimental observations, [13, 14], showing a substantial density scatter within sintered specimens. Here, uniform probability distribution of D_0 within a range $[D_0^{k\,\min}; D_0^{k\,\max}]$ is assumed for each k-th ring separately. The bounds are related to the $D_0(r)$-dependence given by Eq. (3.1), and take the form

$$\left.\begin{matrix} D_0^{k\,\min} \\ D_0^{k\,\max} \end{matrix}\right\} = D_0(r_0(2k \mp 1))(1 \mp k_s), \tag{3.3}$$

where k_s is a scatter band width constant. In numerical simulations, a random number generator is used for the distribution of initial damage. A typical distribution is shown in Fig. 5 b.

3.3. Damage evolution in elements

The cross-section discretization and the distribution of D_0^i over the elements imply the application of the constitutive equations (2.1) – (2.3) to each i-th element separately in the form

$$\begin{aligned} \sigma^i &= E(1 - D^i)\varepsilon, \\ D^i &= D_0^i \exp\left(\frac{E\varepsilon^2}{2W^*}\right), \\ D_m^i \exp\left(\frac{D_m^i - 1}{2D_m^i}\right) &= D_0^i, \qquad i = 1, ..., M_0\,. \end{aligned} \tag{3.4}$$

It is assumed here that all the elements in the cross-section are exposed to the same external strain ε. They exhibit the same material properties regarding the elasticity modulus E and the damage absorbing capacity W^*. The differences in the response of the elements are in the first stage of the loading solely due to the initial damage distributions (3.2) – (3.3).

The situation changes somewhat as soon as the rod extension ε arrives at the strain-at-failure ε_m^w of the weakest w-th element with the highest initial damage within the cross-section, cf. Eq. (2.4). In order to further the numerical simulation of the rod response under tension, Eqs. (3.4) need to be now completed by interaction-at-failure conditions for the elements.

3.4. Local failure and interaction of elements

Until the failure of the w-th element, see Sec. 3.3, there is no interaction between the uniformly extended finite elements assumed to be in the uniaxial state of strain. With the failure of the first element, considered within the framework of the damage model described in Sec. 2, the standard situation is the following one: an i-th element, with a higher initial damage D_0^i than all p elements in its vicinity, reaches its respective failure strain ε_m^i sooner than any j-th element of the neighbourhood, compare Eq. (2.4) and Fig. 2. Upon reaching the state of failure, the element loses its carrying capacity, and its damage catastrophically grows from D_m^i to the nominal level $D^i = 1$ corresponding to $\sigma^i = 0$, see Eq. (2.1).

Such events occur randomly in various regions of the cross-section and at various instants of the strain history. Each spatially separate event increases the connectivity of the region under study. These features make the use of established numerical codes based on the finite elements method (FEM) rather cumbersome; the modelling would demand a reformulation of the boundary-value problem nearly at each strain step after the first element's failure. An alternative is provided by utilisation of the modified lattice algorithms, developed originally in statistical physics, and lately applied in stochastic fracture problems, [15, 16]. An advantage of this approach lies in the possibility to analyse highly heterogeneous media and complicated failure morphology. Recently, this modelling approach has been considered in the analysis of the macroscopic response to the development of defect ensembles in disordered brittle materials under stress-controlled tension [17, 18], as a unification of the CDM and lattice algorithms.

In order to describe the strain-controlled process, the following simplified algorithm is suggested, Fig. 6. The failure of the i-th element results in a violent release of its stored elastic energy, ${\sigma_m^i}^2/(2E)$, see Sec. 2. The energy is transferred to p nearest neighbours possessing a common boundary with the failed one. It is equally partitioned between them, independently of the size of their contact. The j-th element, which has been in the state *1*, $(\varepsilon, \sigma_1^j, D_1^j)$, receives thus at best a $(1/p)$-th share of the released energy. Under unconstrained circumstances, the energy share is transformed into the deformation work performed on the j-th element, see the area under the stress-strain curve segment *1* – *2*, Fig. 6. The state *2*, $(\varepsilon_2^j, \sigma_2^j, D_2^j)$, corresponds to the increments in strain $\delta\varepsilon^j$, stress $\delta\sigma^j$ and damage δD^j, cf. Eqs. (2.5) and (3.4).

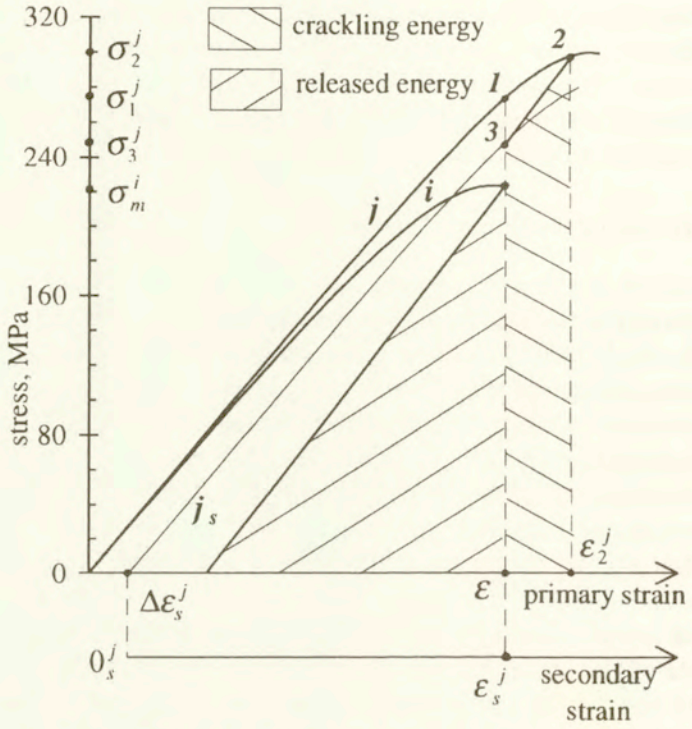

FIG. 6. Energy release at failure of the i-th element and interaction with the j-th element: loading *1* – *2*, unloading *2* – *3*, acoustic crackling emission.

Due to the kinematical constraint of the common external strain ε, however, the j-th element must undergo simultaneously an unloading by the strain decrement $-\delta\varepsilon^j$, resulting in the relaxation path *2* – *3*, Fig. 6. The element returns to the strain ε, although at lower stress σ_3^j, and remains at the damage value of $D_3^j = D_2^j$. The energy released at this relaxation process, cf. Eq. (2.10), causes acoustic effects, further referred to as crackling.

The energy flux due to the failure of one element induces thus in all neighbouring elements transitions analogous to the path *1* – *2* – *3*: from their respective states *1*, the elements undergo intermediate loading *1* – *2*, followed by relaxation *2* – *3*. Has one of the neighbouring elements been already broken in a previous event, its share of the violently released energy is irradiated directly into the environment as an acoustic snap.

The energy balance for the j-th element in the vicinity of the failed i-th element is

$$\frac{E}{2}\left(\varepsilon_2^{j\,2} - \varepsilon^2\right) - D_0^j W^* \left(\exp\frac{E\varepsilon_2^{j\,2}}{2W^*} - \exp\frac{E\varepsilon^2}{2W^*}\right) = \frac{\sigma_m^{i\,2}}{2Ep} \tag{3.5}$$

cf. (2.5), and yields the strain ε_2^j at the state *2*. The resulting damage in state *3*

$$D_3^j = D_2^j = D_0^j \exp\left[\frac{E{\varepsilon_2^j}^2}{2W^*}\right] \tag{3.6}$$

and the relaxation *2* - *3* lead to a secondary state of reference [9], with a strain shift

$$\Delta\varepsilon_s^j = \frac{D_2^j}{1 - D_2^j}\left(\varepsilon_2^j - \varepsilon\right), \tag{3.7}$$

cf. Eq. (2.8) and Fig. 3, and to a secondary initial damage, cf. Eq. (2.9)

$$D_{0s}^j = D_3^j \exp\left[-\frac{E{\varepsilon_s^j}^2}{2W^*}\right], \tag{3.8}$$

where $\varepsilon_s^j = \varepsilon - \Delta\varepsilon_s^j$ is the secondary strain in the j-th element, cf. Sec. 2.

The damage increment in the j-th element may lead to the damage D_3^j, Eq. (3.6), exceeding the respective damage at failure $D_m^j(D_{0s}^j)$, see Eqs. (3.4) and (3.8). This would mean that the local failure of the i-th element induces the failure of the j-th element. The latter, in its turn, may further induce failures in its own neighbourhood. Thus, a cascade of events of local failures can be generated.

4. Numerical realisation and results

In the numerical realisation, extension of a cylindrical rod made of alumina ceramics Al23 (Frialit - Degussit), tested in [4], has been modelled. The material data E and W^* have been taken according to the average response of the tested specimens. At 12 mm diameter, the cross-section has been divided into 20 rings with 1521 elements, cf. the procedure of Sec. 3.1. The characteristic size of the element is thus about 300 μm, i.e. by an order of magnitude larger than the mean grain size (10 – 20 μm) in the ceramics, allowing for the application of the CDM model to single elements. A program assigns to each element not only its "global" number from 1 to M but also a pair of indices, cf. Fig. 4, denoting its ring and position within the ring. An effective algorithm for finding the nearest neighbours has been based on it, generalising the experience with orthogonal grids in [17, 18].

In the first step, initial values of damage D_0^j are distributed with the use of a random number generator on the basis of relations (3.1), (3.3). In the following examples, we take $k_s = 1$, which results in the presence of some initially undamaged elements in each ring and thus in an overestimation of the post-critical

deformation. In order to exclude the effect of the variation of the mean value

$$\langle D_0^i \rangle = \frac{1}{M} \sum_{i=1}^{M} D_0^i \tag{4.1}$$

for different realisations, the random values D_0^i are corrected by multiplication with a renormalisation parameter $k_{\text{ren}} = \overline{D}_0 / \langle D_0^i \rangle$, cf. Eq. (3.2).

The next step is the determination of the local failure conditions for all elements from the relation $(3.4)_3$. Applying in steps equal strain increments $\Delta\varepsilon$ to all elements, we obtain that damage evolves with different rates, see Eq. $(3.4)_2$, due to different initial conditions. The evolution in the elements is independent of each other up to the moment of the first local failure.

Here, a transition according to Sec. 3.4 takes place in the neighbourhood of the weakest element $w = i$. The solution of Eq. (3.5) with respect to ε_2^j is carried out by an iterative Newton procedure, until the criterion $\|\varepsilon_2^{j(q+1)} - \varepsilon_2^{j(q)}\| \leq \alpha\varepsilon$ is fulfilled. Here, q is the step of iteration, parameter α equals 10^{-6} in our simulations.

After each event of local failure and interaction, see Sec. 3.4, the neighbourhood is examined with the purpose to check the induced failure conditions, and to account for the possibility of a failure cascade. After the completion of all cascades within the current step, the value of the load is computed as

$$F = A_{\text{el}} \sum_{i=1}^{M} \sigma^i,$$

where A_{el} is the element area. Also, the current damage level D is obtained by averaging of D^j over all elements by a formula analogous to Eq. (4.1), and the number of failed elements n is calculated in the cross-section. To the elements, which have undergone the *1 - 2 - 3* - transition, the algorithm assigns their secondary strain ε_s and secondary initial damage D_{0s} values to be reckoned with at further steps.

At this instance, the algorithm goes into the next step, resulting in dependences $F(\varepsilon)$, $D(\varepsilon)$ and $n(\varepsilon)$, see Fig. 7. The load-strain relation, Fig. 7 a, demonstrates a response that is characteristic for brittle ceramics [1]: a practically linearly ascending loading curve arrives at the limit which may be identified with rupture load, followed by a rapid descent. The latter can be roughly subdivided into two stages: a sharp drop after the rupture load, and a tail of dropping residual load-carrying capacity. This result follows alone from the collective response of the set of elements exhibiting the CDM properties under consideration: no specific rod rupture cap was needed in these simulations.

A comparison of $F(\varepsilon)$ with $D(\varepsilon)$ and $n(\varepsilon)$ explains the strongly non-linear behaviour. After the monotonous damage accumulation, stage 1, Fig. 7 b-c, a substantial share of elements approaches the pre-failure state. A relatively small

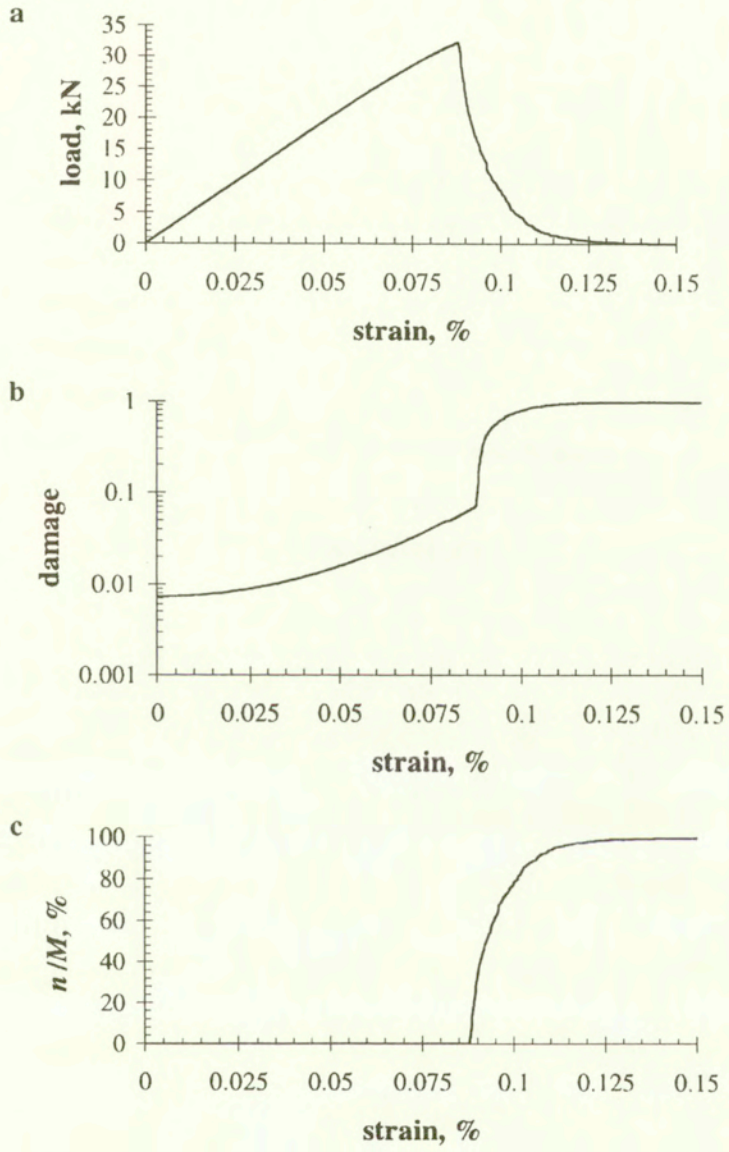

FIG. 7. Computational results for $\overline{D}_0 = 0.73\%$, in a 12 mm diameter ceramic rod (data for alumina, see Fig. 1): a) load F, b) mean damage D, c) number of failed elements n, as function of rod extension ε.

increase in the strain ε causes now an extensive process of element failures, stage 2, enhanced by the energy release effects, Sec. 3.4. Elements with low initial damage (close to $\inf_k D_0^{k\,\min}$) are responsible for the third characteristic stage of the curve: an extended post-critical response of the few remaining elements. These three stages are reflected also in the $D(\varepsilon)$ diagram, see Fig. 7 b.

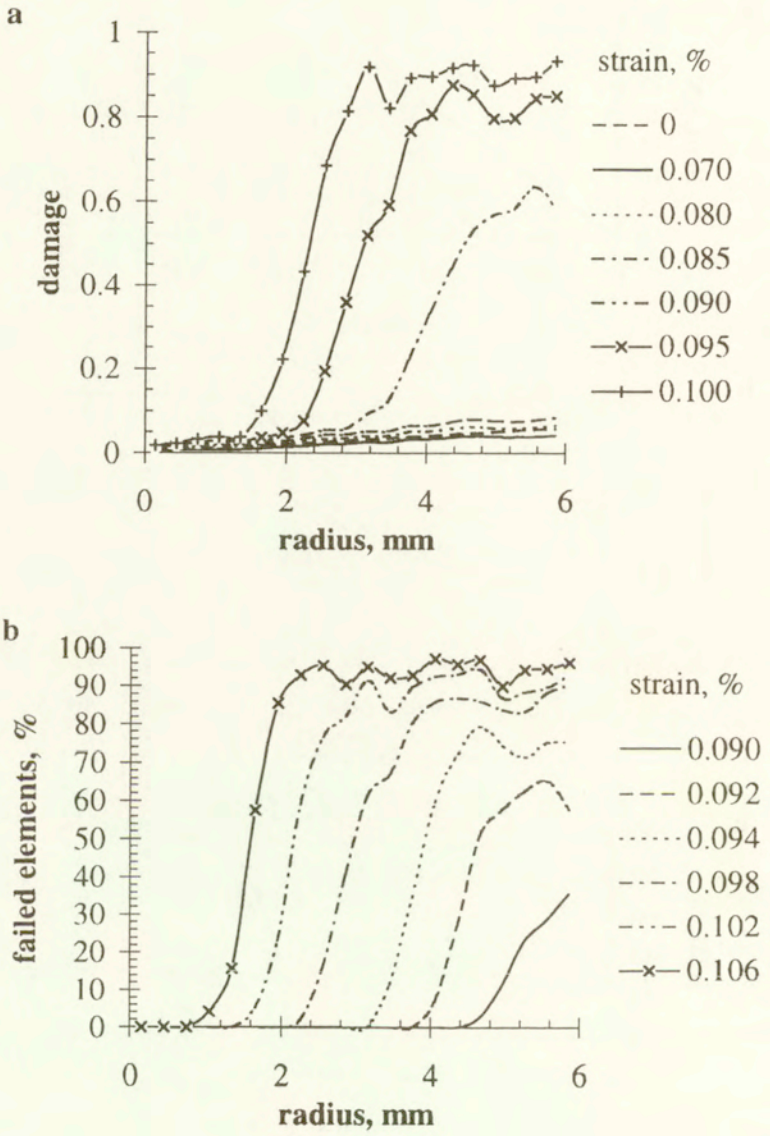

FIG. 8. Radial distributions of (a) the damage (mean values in rings) and (b) the number of failed elements (percentage of elements in rings), in dependence of rod extension.

Figure 8 demonstrates the evolution of radial distributions of damage and of the number of failed elements in rings. It is obvious, that damage at the stage 2 of extensive failure shows a high extent of localisation in peripheral rings (here: above $\varepsilon = 0.085$, Fig. 8 a). This is also reflected in the localisation of the number of failed elements (Fig. 8 b): failures occur initially in external rings only; with the strain development they increasingly take place in the central rings.

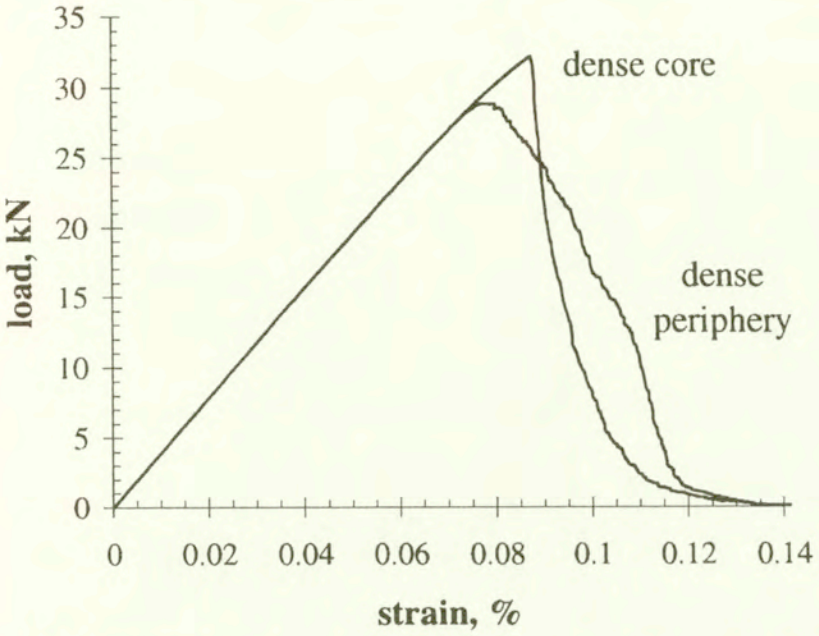

FIG. 9. Comparison of load-extension curves (specimen data, see Fig. 7) for two opposite radial distributions of the initial damage D_0 at the same value $\overline{D}_0 = 0.73\%$; for the dense core specimen, see Eq. (3.1); for the dense periphery specimen, $D_0^{\max}$ is at $r = 0$.

In order to analyse the effect of the type of randomness on the mechanical response of ceramics, let us study an opposite radial distribution of initial damage. We assume now the maximum of D_0 in the rod centre, and its minimum in external rings, i.e. consider a rod with a denser periphery than its core, compare Sec. 3.2. The resulting rupture load and the post-critical response, Fig. 9, differ substantially from the previously studied case. At the same level of mean initial damage $\overline{D}_0$, Eq. (3.2), the load-carrying capacity of the rod with a more porous core is by 10.3 percent lower than that for a more dense core, and the respective strain value is also lower by 9.5 percent. On the other hand, the descending branch of the $F(\varepsilon)$-curve is more protracted for the rod with more porous core.

The analysis of the released acoustic energy at failure evolution, Fig. 10, obtained by our numerical simulation, reflects the non-uniformity of the process. The distribution of the irradiated energy density over the strain closely reminds the data on acoustic emission in ceramics [2, 3]. With the progress of rod extension, the snapping component of the energy increases faster than the crackling one, cf. Sec. 3.4. It is the result of the advancing failure of elements and the increase of the connectivity of the cross-section, at which the relative portion of unbroken elements in immediate neighbourhoods at local failure events continuously diminishes.

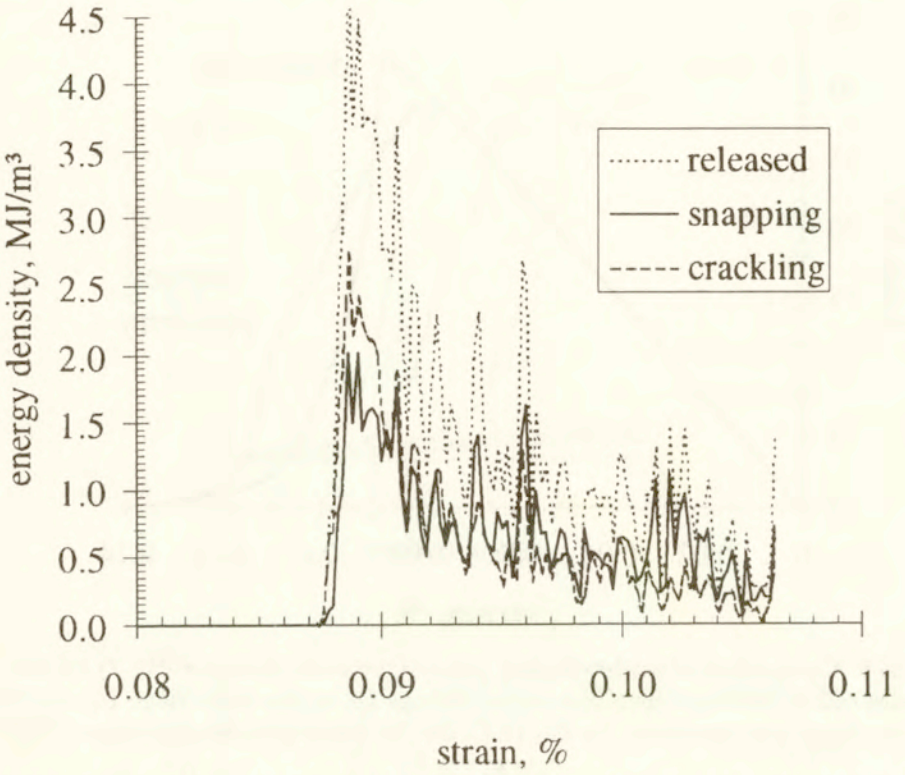

FIG. 10. Energy release at elements' failure, interpreted as acoustic effects of crackling and snapping, as functions of rod extension.

One of the much discussed problems of the mechanical response of damaging materials is the analysis of their unloading properties in the post-critical state. According to most CDM models, e.g. [7], the unloading modulus of a damaged material is $E_u = \underset{\sim}{E}(1 - D_u)$, where D_u denotes the damage at unloading. The non-unique relation between E_u and D_u would yield thus the basis for experimental determination of damage, mostly for ductile materials, [7]. Experimental data on unloading in brittle materials are limited mainly to the bending of notched specimens with initial cracks [5], while data on uniaxial tensile tests with smooth specimens are practically nonexistent due to the difficulties, [19], connected with the extremely low strain-to-failure values in ceramics and to their rapid rupture.

In our numerical simulations, unloading was performed at a certain share of failed elements (between 5 and 70 percent) in the cross-section, Fig. 11. Thus, the unloading begins at some load F_u and strain ε_u of the descending branch of the load characteristic, and can be characterised by the corresponding mean damage D_u exceeding the damage at the onset of rupture. The slopes of the unloading branches steadily decrease with the increase of D_u and with the advance of the rupture. They yield some non-vanishing residual strain ε_r, which seems to

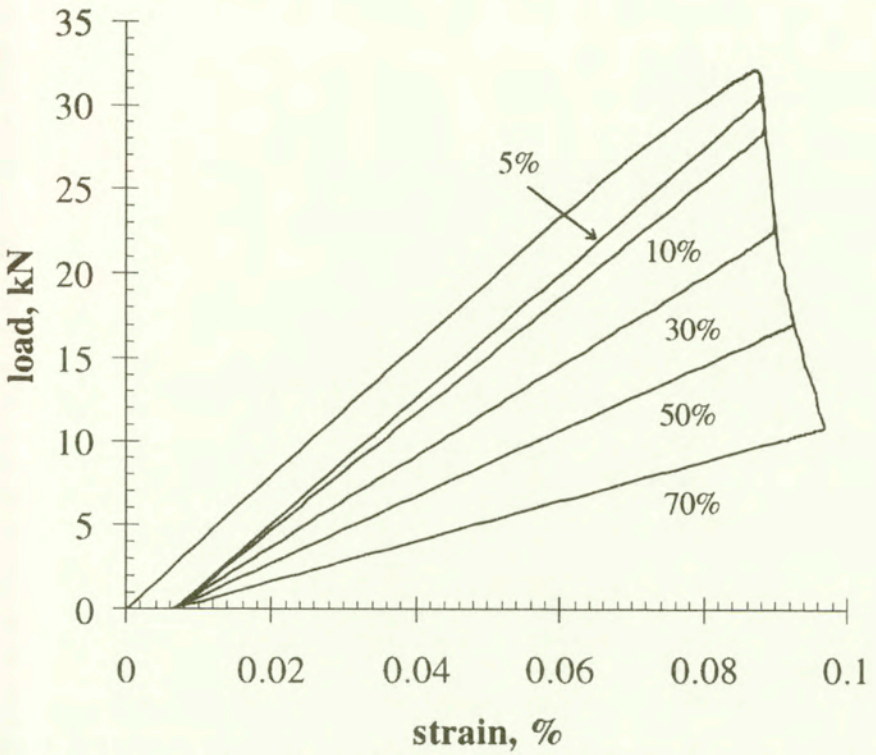

FIG. 11. Unloading characteristics at a given percentage number of failed elements (specimen data, see Fig. 7).

be nearly independent of D_u, although it clearly depends on the choice of the inhomogeneity realisation, cf. Fig. 9.

However, the dependence of the unloading slope on the mean damage at unloading D_u differs substantially from the predictions in [7]. Moreover, there is an obvious difference in the dependence of the slope on D_u for the two different inhomogeneity realisations discussed above. Let us compare the mean unloading modulus

$$E_u = \frac{F_u}{A(\varepsilon_u - \varepsilon_r)}$$

with the value $E(1 - D_u)$, as predicted in [7]; Fig. 12 presents their ratio against the mean damage at unloading D_u. We observe that in both inhomogeneity realisations, the unloading modulus steadily exceeds the predictions by values up to more than 10 per cent. This indicates that a phenomenological extraction of the damage values from measurements in unloading must be done with care; it may yield doubtful results when no data on the inhomogeneity distribution in specimens are available.

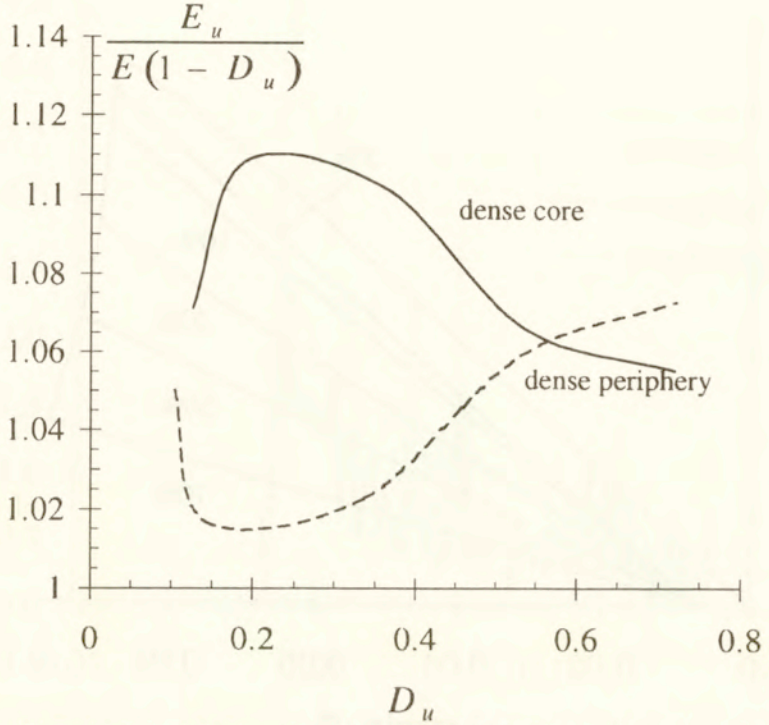

FIG. 12. Comparison of the mean unloading modulus E_u and the quantity $E(1 - D_u)$ based on the mean damage D_u at unloading, for two radial distributions of D_0, compare Fig. 9.

5. Conclusions

The proposed $2d$ approach, based on the damage evolution law [8] as applied to a set of discrete elements with deterministically and randomly distributed initial damage, allows for efficient numerical simulations of a whole range of characteristic response features of brittle specimens. The qualitative differences in response between homogeneous and heterogeneous specimens become quite obvious in the proposed numerical procedure, [17], since the process can be followed in all details concerning each single element of the system.

For the particular problem under consideration, it has been shown that certain characteristics of the damage evolution and rupture strongly depend on the kind of the cross-section heterogeneity of the specimen. This should be treated as a call for caution at certain CDM interpretations of experimental results, which may lead to doubtful conclusions when the type of inhomogeneity within the tested specimens is not known *a priori*.

The tensile rod simulations presented here can easily be extended to the study of heterogeneity scale effects, i.e. the dependence of the rupture strength on the

specimen size, [10], damage evolution and failure in ceramic beams and similar problems. The procedure contains further capabilities with regard to unloading and reloading under strain-controlled conditions, being thus potentially applicable to problems of cyclic fatigue. Finally, the applications of the procedure in composite mechanics represent an obviously important field of further research.

References

1. M.V. SWAIN [Ed.], *Structure and properties of ceramics*, Material Science and Technology, Vol. 11, VCH, Weinheim 1994.
2. L.J. GRAHAM and G.A. ALERS, *Microstructural aspects of acoustic emission generation in ceramics*, [in:] Fracture Mechanics of Ceramics. Volume 1. Concepts, Flaws and Fractography, R.C. BRANDT, D.P.H. HASSELMAN and F.F. LANGE [Eds.], pp. 175–188, Plenum Press, New York - London 1973.
3. M.J. NOON and R.R. MEHAN, *Observation of crack propagation in polycrystalline ceramics and its relationships to acoustic emissions*, [in:] Fracture Mechanics of Ceramics. Volume 1. Concepts, Flaws and Fractography, R.C. BRANDT, D.P.H. HASSELMAN and F.F. LANGE [Eds.], pp. 201–229, Plenum Press, New York - London 1973.
4. S. BIERWIRTH, *Verfahren zur Bestimmung dynamischer Zugbruchparameter von Hochleistungskeramik*, VDI Verlag, Düsseldorf, **18**, 148, 1994.
5. R.W. STEINBRECH, A. REICHL und W. SCHAARWÄCHTER, *Einfluß von Rißflankeneffekten auf das Rißwiderstandsverhalten von* Al_2O_3- *Keramik*, [in:] Mikrobruchvorgänge in Al_2O_3-Keramik. DFG-Kolloquium, H. NICKEL and R.W. STEINBRECH [Eds.], pp. 57–89, Forschungszentrum Jülich 1991.
6. D. MUNZ and T. FETT, *Mechanisches Verhalten keramischer Werkstoffe*, Springer-Verlag, Berlin 1989.
7. J. LEMAITRE, *A course in damage mechanics*, Springer-Verlag, Berlin 1992.
8. J. NAJAR, *Continuous damage of brittle solids*, [in:] Continuum Damage Mechanics. Theory and Applications, D. KRAJCINOVIC and J. LEMAITRE [Eds.], pp. 233–294, Springer, Wien - New York 1987.
9. J. NAJAR, *Brittle residual strain and continuum damage at variable uniaxial loading*, Int. J. Damage Mech., **3**, 2, 260–276, 1994.
10. V.V. SILBERSCHMIDT and J. NAJAR, *Computational modelling of the size effect of damage inhomogeneity in ceramics*, Comput. Materials Sci. [in print].
11. J.B. WATCHMAN, *Mechanical properties of ceramics*, John Wiley & Sons, New York 1996.
12. A.L. GURSON, *Continuum theory of ductile rupture by void nucleation and growth. Part I. Yield criteria and flow rules for porous ductile media*, J. Engng. Mater. Technol., **99**, 1, 2–15, 1977.
13. O. BEER, *Verdichtung von Metallpulvern*, VDI Verlag, Düsseldorf, **5**, 458, 1996.
14. S. SHIMA and K. MIMURA, *Densification behaviour of ceramic powder*, Int. J. Mech. Sci., **28**, 1, 53–59, 1986.
15. H.J. HERRMANN and S. ROUX [Eds.], *Statistical models for the fracture of disordered media*, North Holland, Amsterdam 1990.
16. A. DELAPLACE, G. PIJAUDIER-CABOT and S. ROUX, *Progressive damage in discrete models and consequences on continuum modelling*, J. Mech. Phys. Solids, **44**, 1, 99–136, 1996.

17. V.V. SILBERSCHMIDT, *Mathematical modelling and fractal analysis of stochastic fracture process*, [in:] Mathematical Modelling and Applied Mathematics. Proc. IMACS Conf., A.A. SAMARSKY and M.P. SAPAGOVAS [Eds.], pp. 399–406, Elsevier Science Publishers B.V., North Holland, 1992.

18. V.V. SILBERSCHMIDT and J.-L. CHABOCHE, *The effect of material stochasticity on crack-damage interaction and crack propagation*, Engng. Fracture Mech., **48**, 3, 379–387, 1994.

19. C.W. MARSCHALL and A. RUDNICK, *Conventional strength testing of ceramics*, [in:] Fracture Mechanics of Ceramics. Volume 1. Concepts, Flaws and Fractography, R.C. BRANDT, D.P.H. HASSELMAN and F.F. LANGE [Eds.], pp. 69–92, Plenum Press, New York - London 1973.

LEHRSTUHL A FÜR MECHANIK
TECHNISCHE UNIVERSITÄT MÜNCHEN
Boltzmannstr. 15, D-85748 Garching b. München, Germany
e-mail: najar@lam.mw.tu-muenchen.de

Received July 18, 1997.

Arch. Mech., 50, 1, pp. 41–52, Warszawa 1998
FIFTY YEARS OF THE ARCHIVES OF MECHANICS

Dynamic solutions of non-uniform extensional motions as applied to instability of fibre-forming processes

S. ZAHORSKI (WARSZAWA)

THE CONCEPT of non-uniform extensional motion of materially non-uniform simple, locally isotropic materials is applied to the case of dynamic solutions of fibre-forming processes. The approach presented enables discussion of instability problems taking into account inertia as well as shearing effects. It is shown that small stationary disturbances may lead to unstable situations while small oscillatory disturbances grow limitlessly only for certain discrete frequencies. Some comparisons with previous results are made.

1. Introduction

THIS PAPER PRESENTS further application of the theory of non-uniform extensional motions (NUEM) of materially non-uniform (inhomogenous) media developed in [1, 2] and applied to kinematic description of steady fibre-forming processes in [3]. Under the assumption that the filament shape slightly differs from the cylindrical one, we used a consequent linearization procedure leading to the relatively simple equations describing also shearing effects.

In the present paper, in a way similar to that developed in [3], we consider the corresponding approximations of the unsteady governing equations taking into account shearing as well as inertial effects. Such an approach leads to the dynamic solutions enabling effective discussion of instability problems of the stationary and oscillatory types. Certain comparisons of our results with those obtained so far for the instability problems and draw-resonance phenomena in non-isothermal fibre-spinning processes (cf. [4, 5, 6]) are discussed in grater detail at the end.

It is worth noting that certain particular instability problems were also considered in the case of flows with dominating extension (FDE) in our previous papers [7, 8]. Apart from formal similarities to the present results, the solutions obtained for FDE refer rather to the sensitivity problems caused by disturbances superposed on the corresponding stresses, velocity gradients, etc.

In Sec. 2 we remind the concept of steady NUEM of materially non-uniform media and introduce the additional motions superposed on the quasi-elongational ones and formulate the relevant constitutive equations. This section is based in whole on our previous considerations [3]. Section 3 briefly presents the equations of dynamic equilibrium and the boundary conditions appropriate for fibre-forming processes. The subsequent approximations of the governing equations are

considered in Sec. 4. The dynamic solutions and the instability problems of the stationary and oscillatory types are discussed in greater detail in Sec. 5. The last Sec. 6 summarizes certain conclusions and compares our results on instability with those obtained previously under different assumptions.

2. Non-uniform extensional motions (NUEM) of materially non-uniform media

Consider an isochoric, quasi-elongational motion in cylindrical coordinates for which the deformation gradient at the current time t, relative to a configuration at time 0, is of the following diagonal form:

$$[\mathbf{F}(\mathbf{X},t) = \begin{bmatrix} \lambda^{-1/2} & 0 & 0 \\ 0 & \lambda^{-1/2} & 0 \\ 0 & 0 & \lambda \end{bmatrix}, \qquad \det \mathbf{F} = 1, \tag{2.1}$$

where the non-uniform stretch ratio $\lambda(\mathbf{X},t)$, depending on the position $\mathbf{X}$ of a particle in the reference configuration at time 0, is defined as

$$\lambda = V/V_0\,, \qquad \dot{\lambda} = V'\lambda, \tag{2.2}$$

where V and V_0 denote the variable axial velocity and the velocity at the exit, respectively, and the prime denotes derivative with respect to the axial coordinate z.

It has been shown in [3] that the quasi-elongational motion described by Eq. (2.1) is consistent with the definition of NUEM and enables determination of such quantities as the velocity gradient $\mathbf{L}(\mathbf{X},t)$, the left Cauchy–Green deformation tensor $\mathbf{B}(\mathbf{X},t)$ and the first Rivlin–Ericksen kinematic tensor $\mathbf{A}_1(\mathbf{X},t)$ (cf. [9]). For steady NUEM these quantities are independent of time and the constitutive equations of materially non-uniform, simple, locally isotropic media can be written in the following spatial form:

$$\mathbf{T}(z) = \mathbf{k}(V'(z),\ V(z),\ \varrho(z);\ z), \tag{2.3}$$

where $\mathbf{k}$ is a tensor function of scalar arguments: the velocity V, the velocity gradient V', the density ϱ, and the axial coordinate z. An explicit dependence of the stress tensor $\mathbf{T}$ on the coordinate z takes into account the material properties variable along the axis and caused by the corresponding temperature, crystallization, orientation, solidification, etc. effects (cf. [6, 3]).

For axisymmetric, quasi-elongational motions Eq. (2.3) leads to

$$\begin{aligned} T^{11} &= T^{22} = \sigma_1(V', V, \varrho; z), \\ T^{33} &= \sigma_3(V', V, \varrho; z), \\ T^{13} &= 0. \end{aligned} \tag{2.4}$$

Since for steady flows the pair of variables V, V' is equivalent to the pair ε, $\dot{\varepsilon}$ (ε denotes the Hencky strain), we may quote PETRIE'S [10] statement that "... the use of rate of strain and strain as independent variables, was the most plausible choice. The fact that this choice is appropriate for both extremes of material behaviour, the purely viscous and the purely elastic, lend weight to the argument."

If the inclination of filament surface is a small quantity, i.e. $R' = 0(\varepsilon)$, $\varepsilon = R_0/L \ll 1$, where R, R_0 and L denote the outer current radius $R(z)$, the radius at the exit and the total length, respectively, we consider the following small additional velocity field superposed on the fundamental motion characterized by the axial velocity V:

$$[w(r,z,t)] = \begin{bmatrix} u \\ 0 \\ w \end{bmatrix} = [0(\varepsilon)]. \tag{2.5}$$

The above additional velocity field depens on both coordinates r and z, on time t, and enables determination of all the linear increments necessary for further considerations (cf. [3]). We have, in particular,

$$\Delta\lambda = \frac{w}{V_0}, \qquad \Delta\lambda' = \frac{1}{V_0}\frac{\partial w}{\partial z}. \tag{2.6}$$

Under the assumption that, in the perturbed expressions for stresses, viz.

$$T^*(z) = T(z) + \Delta T(r,z,t), \tag{2.7}$$

only the increments ΔT may depend on time, we finally arrive at the following equations:

$$\begin{aligned}
T^{*11} &= \sigma_1 + \frac{\partial\sigma_1}{\partial V}w + \frac{\partial\sigma_1}{\partial V'}\frac{\partial w}{\partial z} + \frac{\partial\sigma}{\partial\varrho}\Delta\varrho + \alpha\frac{\partial u}{\partial r}, \\
T^{*22} &= \sigma_1 + \frac{\partial\sigma_1}{\partial V}w + \frac{\partial\sigma_1}{\partial V'}\frac{\partial w}{\partial z} + \frac{\partial\sigma}{\partial\varrho}\Delta\varrho + \beta\frac{u}{r}, \\
T^{*33} &= \sigma_3 + \frac{\partial\sigma_3}{\partial V}w + \frac{\partial\sigma_3}{\partial V'}\frac{\partial w}{\partial z} + \frac{\partial\sigma}{\partial\varrho}\Delta\varrho, \\
T^{*13} &= \eta\left(\frac{\partial u}{\partial z} + \frac{\partial w}{\partial r}\right) + \gamma u,
\end{aligned} \tag{2.8}$$

where α, β, γ and η are new material functions depending on the same arguments as σ_1 and σ_3.

It has been proved in [3] that for steady fundamental motions for which, moreover, div.$V = 0$, the density ϱ is constant and $\Delta\varrho$ denotes the corresponding

increment depending on r and z. Similarly, from the global continuity condition, viz.

$$W = \varrho \pi R^2 V = \text{const}, \tag{2.9}$$

where W denotes the mass output, it results that for density increments

$$\int_0^R \Delta\varrho\, r\, dr = 0, \tag{2.10}$$

if the additional velocity distribution over the fibre cross-section is such that (see Sec. 4)

$$\int_0^R w\, r\, dr = 0. \tag{2.11}$$

In what follows, we assume validity of the so-called thin-thread approximation (cf. [3]) introducing the following dimensionless quantities marked with broken dashes

$$u = \varepsilon U \hat{u}, \qquad w = U \hat{w}, \qquad r = R_0 \hat{r}, \qquad z = L \hat{z}, \tag{2.12}$$

where U is some characteristic velocity. Therefore, it is a consequence of the assumption (2.5) that $u = 0(\varepsilon^2)$, if $w = 0(\varepsilon)$.

3. Equations of dynamic equilibrium and boundary conditions

The axisymmetric equations of dynamic equilibrium can be written in the form:

$$\begin{aligned} &\frac{\partial T^{*11}}{\partial r} + \frac{1}{r}\left(T^{*11} - T^{*22}\right) + \frac{\partial T^{*13}}{\partial z} = \varrho\left(\frac{\partial u}{\partial t} + V\frac{\partial u}{\partial z}\right), \\ &\frac{\partial T^{*13}}{\partial r} + \frac{1}{r}T^{*13} + \frac{\partial T^{*33}}{\partial z} = \varrho\left(\frac{\partial w}{\partial t} + VV' + V\frac{\partial w}{\partial z} + V'w\right). \end{aligned} \tag{3.1}$$

Introducing the stresses defined by Eq. (2.8), differentiating with respect to z and r, and subtracting the first Eq. (3.1) from the second one, we arrive, after integration with respect to r, at

$$\begin{aligned} \eta\frac{1}{r}\frac{\partial}{\partial r}\left(r\frac{\partial w}{\partial r}\right) + r\frac{d}{dz}\left(\sigma + \frac{\partial\sigma}{\partial V}w + \frac{\partial\sigma}{\partial V'}\frac{\partial w}{\partial z} + \frac{\partial\sigma}{\partial\varrho}\Delta\varrho\right) \\ = C + \varrho\left(\frac{\partial w}{\partial t} + VV' + V\frac{\partial w}{\partial z} + V'w\right) - \frac{\gamma}{r}\frac{\partial}{\partial r}(ru), \end{aligned} \tag{3.2}$$

where C is an integration constant,

$$\sigma = T^{33} - T^{11} = \sigma_3 - \sigma_1 , \tag{3.3}$$

and only terms up to ε^2 have been retained. Here, the symbol d/dz denotes the total derivative with respect to z.

For the fibre-forming processes considered in the present paper it is usually assumed that at the exit (the feeding velocity V_0) and at the end (the take-up velocity V_L), the following boundary conditions are satisfied:

$$V(0) = V_0 \qquad \text{and} \qquad V(L) = V_L , \tag{3.4}$$

respectively. Since by assumption $R'(z) = 0(\varepsilon)$, it is reasonable to consider that the additional velocity field only modifies the uniform velocity profile of the fundamental motion. Thus, if the mass output W is constant along the fibre, we should apply the additional condition in the integral form (2.11).

On the free surface of the filament all the forces acting have to be mutually balanced. For small R' this leads to (cf. [3])

$$R' \left(T^{*33} - T^{*11}\right)_{r=R} = T^{*13}\Big|_{r=R} , \tag{3.5}$$

or alternatively to

$$R' \left[\sigma + \frac{\partial \sigma}{\partial V} w + \frac{\partial \sigma}{\partial V'} \frac{\partial w}{\partial z} + \frac{\partial \sigma}{\partial \varrho} \Delta \varrho\right]_{r=R} = \eta \left(\frac{\partial w}{\partial r} + \frac{\partial u}{\partial z}\right)_{r=R} + \gamma u\Big|_{r=R} , \tag{3.6}$$

where only terms of order ε^2 have been retained.

4. Approximations of governing equations

Assuming on the basis of Eq. (2.5) that the additional velocity field can be written as

$$w = \varepsilon w_1 + \varepsilon^2 w_2 \ldots , \qquad u = \varepsilon^2 u_1 + \varepsilon^3 u_2 \ldots , \tag{4.1}$$

Eq. (3.2) amounts to

$$\eta \frac{1}{r} \frac{\partial}{\partial r} \left(r \frac{\partial w_1}{\partial r}\right) + \frac{d}{dz} \sigma = C_1 + \varrho \frac{\partial w_1}{\partial t} + \varrho V V' , \tag{4.2}$$

for terms of order ε, and to

$$\eta \frac{1}{r} \frac{\partial}{\partial r} \left(r \frac{\partial w_2}{\partial r}\right) + \frac{d}{dz} \left(\frac{\partial \sigma}{\partial V} w_1 + \frac{\partial \sigma}{\partial V'} \frac{\partial w_1}{\partial z} + \frac{\partial \sigma}{\partial \varrho} \Delta \varrho\right) = C_2 + \varrho \left(\frac{\partial w_2}{\partial t} + V' w_1 + V \frac{\partial w_1}{\partial z}\right) - \gamma \frac{\partial}{\partial r} (r u_1), \tag{4.3}$$

for terms of order ε^2. C_1 and C_2 are the corresponding integration constants for the first and second approximation, respectively, and u_1 results from the continuity equation.

Being interested in dynamic (harmonic) solutions of the problems considered, we postulate that the total additional velocity field consists of steady part $\overline{w}$ and dynamic part $\widetilde{w}$, viz.

$$w_1 = \overline{w}_1 + \widetilde{w}_1 \exp \omega(t - t_0), \tag{4.4}$$

where the quantity ω may be complex, real or purely imaginary. Equation (4.4) implies that also

$$\begin{aligned} C_1 &= \overline{C}_1 + \widetilde{C}_1 \exp \omega(t - t_0), \\ R' &= \overline{R}' + \widetilde{R}' \exp \omega(t - t_0), \\ \Delta\varrho &= \Delta\overline{\varrho} + \Delta\widetilde{\varrho} \exp \omega(t - t_0), \end{aligned} \tag{4.5}$$

where $\overline{R}'$ denotes the surface inclination in a steady-state motion, and $\widetilde{R}$ is the amplitude of dynamic increment. Similar notations are used for the density increments $\Delta\overline{\varrho}$ and $\Delta\widetilde{\varrho}$.

Under the above assumptions the first approximation of the governing equations (4.2) leads to

$$\eta \frac{1}{r} \frac{\partial}{\partial r} \left(r \frac{\partial \overline{w}_1}{\partial r} \right) + \frac{d\sigma}{dz} + \varrho V V' = \overline{\overline{C}}_1 , \tag{4.6}$$

for steady-state motions, and to

$$\eta \frac{1}{r} \frac{\partial}{\partial r} \left(r \frac{\partial \widetilde{w}_1}{\partial r} \right) - \varrho \omega \widetilde{w}_1 = \widetilde{C}_1 \tag{4.7}$$

for dynamic (harmonic) motions.

Of course, the condition (2.11) takes the forms:

$$\int_0^{\overline{R}} \overline{w}\, r\, dr = 0, \qquad \int_0^{\overline{R}} \widetilde{w}\, r\, dr = 0. \tag{4.8}$$

Similarly, the boundary condition (4.2), after taking into account Eqs. (4.4), (4.5), gives

$$\overline{R}' \sigma = \eta \frac{\partial \overline{w}_1}{\partial r}\bigg|_{r=\overline{R}}, \tag{4.9}$$

for steady-state motions, and

$$\widetilde{R}' \sigma = \eta \frac{\partial \widetilde{w}_1}{\partial r}\bigg|_{r=\overline{R}}, \tag{4.10}$$

for dynamic (harmonic) motions. It is worthwhile to remember that Eqs. (4.7) and (4.10) are valid only if the first harmonics are analysed.

5. Dynamic solutions and instability problems

The governing differential equation (4.6) together with the conditions $(4.8)_1$ and (4.9) can be integrated in a straightforward manner leading to the solution

$$\overline{w}_1 = \frac{\sigma}{2\eta}\frac{\overline{R}'}{R}\left(r^2 - \frac{\overline{R}^2}{2}\right), \tag{5.1}$$

describing steady-state motions. This is exactly the same result as that obtained previously in [3].

The governing differential equation (4.7) can easily be solved, leading to the expression

$$\widetilde{w}_1 = \widetilde{D}_1 I_0\left(\sqrt{\frac{\varrho\omega}{\eta}}r\right) - \frac{\widetilde{C}_1}{\varrho\omega}, \tag{5.2}$$

where I_0 denotes the modified Bessel function of the first kind and order 0, and $\widetilde{D}_1$ is a new integration constant. Taking into account the conditions $(4.8)_2$ and (4.10), we arrive at

$$\widetilde{C}_1 = 2\sigma\frac{\widetilde{R}'}{\overline{R}}, \qquad \widetilde{D}_1 = \frac{\sigma\widetilde{R}'}{\eta\sqrt{\frac{\varrho\omega}{\lambda}}I_1\left(\sqrt{\frac{\varrho\omega}{\eta}}\right)}, \tag{5.3}$$

and finally at

$$w_1 = 2\widetilde{R}'\overline{R}\frac{\sigma}{\eta}\left[\frac{1}{2x}\frac{I_0\left(x\frac{r}{\overline{R}}\right)}{I_1(x)} - \frac{1}{x^2}\right], \qquad x = \sqrt{\frac{\varrho\omega}{\eta}}\overline{R}, \tag{5.4}$$

where I_1 denotes the modified Bessel function of the first kind and order 1.

Since, in general, the quantity ω is complex, viz.

$$\omega = \omega_1 - i\omega_2, \tag{5.5}$$

where both ω_1 and ω_1 are real (the minus sign is a matter of convention), the result (5.2) can also be presented as

$$\widetilde{w}_1 = \widetilde{D}_2 J_0(M)e^{i\varphi} - \frac{\widetilde{C}_1}{\varrho(\omega_1 - i\omega_2)}, \tag{5.6}$$

where J_0 denotes the ordinary Bessel function of the first kind and order 0. The corresponding modulus M and the argument φ are defined as follows:

$$M^2 = \sqrt{\omega_1^2 + \omega_2^2}\frac{\varrho r^2}{\eta}, \tag{5.7}$$

$$\operatorname{tg}^2\varphi = \left(\pm\sqrt{\omega_1^2 + \omega_2^2} + \omega_1\right) / \left(\pm\sqrt{\omega_1^2 + \omega_2^2} - \omega_1\right). \tag{5.8}$$

In the particular case of $\omega_1 \equiv 0$, the solution (5.4) can easily be presented by the real and imaginary parts, viz.

$$\tilde{w}_1 = \operatorname{Re}\tilde{w}_1 + i\operatorname{Im}\tilde{w}_1, \tag{5.9}$$

where

$$\operatorname{Re}\tilde{w}_1 = \frac{\sigma}{\varrho\omega_2}\frac{\tilde{R}'}{\overline{R}}\frac{J_0(M)}{J_1(M(\overline{R}))}, \tag{5.10}$$

$$\operatorname{Im}\tilde{w}_1 = -2\frac{\sigma}{\varrho\omega_2}\frac{\tilde{R}'}{\overline{R}}\left[\frac{1}{2}\frac{J_0(M)}{J_1(M(\overline{R}))}\sqrt{\frac{\varrho\omega_2}{2\eta}}\overline{R} - 1\right], \tag{5.11}$$

and according to Eqs. (5.7), (5.8),

$$M^2(\overline{R}) = \frac{\varrho\omega_2}{\eta}\overline{R}^2, \qquad \operatorname{tg}^2\varphi = 1. \tag{5.12}$$

Although the above solutions resemble those widely discussed in [3], it should be emphasized, however, that they have different meanings and are based on different model assumptions.

In the case of harmonic disturbances in the form (4.4) and (4.5), the motion is said to be unstable, if there exists at least one solution for which the amplitudes limitlessly increase in time. If we assume that ω is written in the form (5.5), the sufficient condition of instability can be expressed as

$$\operatorname{Re}\omega = \omega_1 > 0. \tag{5.13}$$

We have the case of "neutral" stability, if $\operatorname{Re}\omega = 0$, passing from negative to positive values. Depending on what value is taken by $\operatorname{Im}\omega$, two types of the stability loss may be observed: the stationary type when $\omega_2 = 0$, and the oscillatory type when $\omega_2 \neq 0$.

In the motions discussed all the types of instability may occur independently, and "the principle of exchange of stabilities" (cf. [11]), valid for purely viscous fluids, cannot be proved in general. Thus, we discuss separately the following cases.

1. *The case of stationary instability*

If $\omega_2 = 0$ and $\omega_1 \geq 0$, the particular dynamic solution takes the form:

$$\tilde{w} = \tilde{w}_1 \exp\omega(t - t_0), \tag{5.14}$$

where the additional velocity amplitude $\tilde{w}_1$ is determined by Eq. (5.4) with ω replaced by ω_1. Since for finite x the quantity ω_1 is also finite, the result (5.14) implies that any small disturbances imposed on the additional velocity field either will be preserved ($\omega_1 = 0$) or will increase limitlessly in time (for $\omega_1 > 0$). In

other words, this means that various types of spots, neckings and corrugations occuring along the filament either will be preserved or will grow limitlessly in time.

2. *The case of oscillatory instability*

If $\omega_1 = 0$ and $\omega_2 \neq 0$, the solution (5.14) is valid with ω replaced by $-i\omega_2$, where the real and imaginary parts of the additional velocity amplitude $\tilde{w}_1$ are given by Eqs. (5.10), (5.11).

Assuming that only the real part of Eq. (5.14) has physical meaning, we obtain the implication:

$$\text{Im}\,\tilde{w} = 0 \quad \Rightarrow \quad \sin\omega_2(t-t_0) = \frac{\text{Im}\,\tilde{w}_1}{\text{Re}\,\tilde{w}_1}\cos\omega_2(t-t_0) \tag{5.15}$$

and finally

$$\begin{aligned}\text{Re}\,\tilde{w} &= \left(\text{Re}\,\tilde{w}_1 + \frac{(\text{Im}\,\tilde{w}_1)^2}{\text{Re}\,\tilde{w}_1}\right)\cos\omega_2(t-t_0) \\ &= 2\frac{\sigma}{\varrho\omega_2}\frac{\tilde{R}'}{\overline{R}}\left(p + \frac{(p-1)^2}{p}\right)\cos\omega_2(t-t_0),\end{aligned} \tag{5.16}$$

where

$$p = \frac{1}{2}\frac{J_0(M)}{J_1(M(\overline{R}))}\sqrt{\frac{\varrho\omega_2}{2\eta}}\,\overline{R}^2, \tag{5.17}$$

and M, $M(\overline{R})$ have been defined through Eqs. (5.7), $(5.12)_1$, respectively.

It is seen by inspection from Eq. (5.16) that the real part of the additional velocity $\text{Re}\,\tilde{w}$ tends to infinity, if the quantity p, defined in Eq. (5.17), tends to infinity. This is the case, if

$$J_1(M(\overline{R})) = 0, \tag{5.18}$$

i.e. for $M(\overline{R}) = 3.83$, 7.02, 10.17, etc. The above result means that any small oscillatory disturbances imposed on the additional velocity field will increase limitlessly only for the frequencies determined from

$$\omega_2 = \frac{M^2(\overline{R})\eta\lambda}{\varrho R_0^2} = \frac{\pi M^2(\overline{R})V_0}{W}\eta(z)\lambda(z), \tag{5.19}$$

where W denotes the constant mass ouput and $\lambda(z) = V(z)/V_0$ is the stretch ratio at the position z along the filament. In other words, this means that various oscillatory disturbances may grow limitlessly only for particular frequencies. For given values of the stretch ratio λ, the viscosity η etc., the least value of the frequency ω_2 results from Eq. (5.19) for $M(\overline{R}) = 3.83$.

Similar results can be obtained from the analysis of the radial components of additional velocities $\tilde{u}$. To this end, we introduce Eq. (5.2) into the local continuity condition expressed by the corresponding increments (cf. [3]):

$$\operatorname{div} \tilde{w}_1 = \frac{1}{r}\frac{\partial}{\partial r}(r\tilde{u}_1) + \frac{\partial \tilde{w}_1}{\partial z} = -\frac{V}{\varrho}\frac{\partial \Delta\tilde{\varrho}}{\partial z}. \tag{5.20}$$

Such a procedure leads to the equation for $\tilde{u}_1$, the solution of which, after integration with respect to r, and taking into account the conditions $(4.8)_2$ and (4.10), amounts to

$$\tilde{u}_1 = -\frac{d}{dz}\left\{\frac{\sigma\tilde{R}'}{\varrho\omega}\left[\frac{I_1\left(\sqrt{\frac{\varrho\omega}{\eta}}\,r\right)}{I_1\left(\sqrt{\frac{\varrho\omega}{\eta}}\,\overline{R}\right)} - \frac{r}{\overline{R}}\right]\right\} - \frac{1}{r}\frac{V}{\varrho}\frac{\partial}{\partial z}\int_0^r \Delta\tilde{\varrho} r\, dr. \tag{5.21}$$

We obtain, moreover, the following results:

$$\tilde{u}_1\Big|_{r=0} = 0, \qquad \tilde{u}_1\Big|_{r=\overline{R}} = 0, \tag{5.22}$$

if Eq. (2.10) is satified for $R = \overline{R}$ and $\Delta\varrho = \Delta\tilde{\varrho}$. Presentation of the above solution in forms similar to (5.9), (5.10) and (5.11) immediately leads to the conditions (5.18) or (5.19).

6. Conclusions and comparisons

The results obtained in the paper enable formulation of the following conclusions.

1. The dynamic solutions discussed in the paper essentially depend on the material properties of the non-uniform medium: the normal stress difference σ and the viscosity function η. For purely viscous fluids this dependence can be expressed by the kinematic quantities: the axial velocity V and its axial gradient V'. A change of material behaviour from a fluid-like to a solid-like (freezing process) can also be taken into account.

2. As a consequence of the first conclusion, the amplitudes of disturbances depend on the material properties, while their limitless growth does not. In particular, the stationary type of stability loss (neckings, corrugations etc.) is always possible for arbitrarily small disturbances distributed in any way along the filament axis.

3. Contrary to the previous well-known studies (cf.[4, 5, 6]), it results from our considerations that the hydrodynamic instability or the draw-resonance are not the only reasons for the appearance of irregular fibres, or for the breakage of the spinning line. This point of view is consistent with that expressed by ZIABICKI [6].

4. The oscillatory type of instability is possible only for certain frequencies of disturbances, depending on the viscosity $\eta(z)$ and velocity $V(z)$ distributions along the filament. The least value of frequency amounts to

$$\omega_{\min} = \frac{\pi \cdot 14.67}{W} \eta(z) V(z), \tag{6.1}$$

where W is a constant mass output.

5. The above result is similar to that discussed in the previous references [4, 5], in the sense that the oscillatory type of instability arise when the draw ratio $\mathrm{Dr} = V_L/V_0$ is greater than some critical value (e.g. $\mathrm{Dr} = 20.2$ for isothermal Newtonian flow) determined on the basis of the neutral stability curves depending on certain dimensionless groups. In our case the role of various dimensionless groups (e.g. Stanton number, Reynolds number, etc.) is replaced by the axial variability of $\eta(z)$ and $V(z)$ for any material described by the assumed pretty general constitutive equation (2.3).

When making various comparisons of the present results with those from other references, one has to bear in mind the fundamental differences between the compared approaches to instability problems. In our considerations we assumed, in particular, that:

- the additional disturbances as well as steady-state solutions depend on the radius r (or R), not only on the axial coordinate z;
- the boundary conditions at both ends of the fibre are quasi-homogeneous, in the sense that for additional velocity they are satified in an integral form;
- the additional disturbances of the stationary and oscillatory types are finite as compared with the additional steady-state velocity fields, responsible for realistic variability of the fibre geometry.

References

1. S. ZAHORSKI, *Non-uniform stagnant motions of materially non-uniform simple fluids*, Arch. Mech., **48**, 577–582, 1996.
2. S. ZAHORSKI, *Non-uniform extensional motions of materially non-uniform simple solids*, Arch. Mech., **48**, 747–751, 1996.
3. S. ZAHORSKI, *Steady non-uniform extensional motions as applied to kinematic description of polymer fibre formation*, Arch. Mech., **49**, 963–975, 1997.
4. J.R.A. PEARSON, *Mechanics of polymer processing*, Elsevier Appl. Sci. Publ., London - New York 1985.
5. M.M. DENN and J.R.A. PEARSON, *An overview of the status of melt spinning instabilities*, Proc. 2nd Word Congr. Chem. Engng., Montreal 1981, p. 354.
6. A. ZIABICKI, *Fundamentals of fibre formation. The science of fibre spinning and drawing*, Wiley, London 1976, p. 229.
7. S. ZAHORSKI, *Instability of disturbed elongational flows of viscoelastic fluids*, Arch. Mech., **47**, 647–659, 1995.

8. S. ZAHORSKI, *Comments on instability of disturbed elongational flows of viscoelastic fluids*, Arch. Mech., **47**, 1189–1192, 1995.
9. S. ZAHORSKI, *Mechanics of viscoelastic fluids*, Martinus Nijhoff, The Hague 1982.
10. C.J.S. PETRIE, *Three-dimensional presentation of extensional flow data*, J. Non-Newtonian Fluid Mech., **70**, 205–218, 1997.
11. S. CHANDRASEKHAR, *Hydrodynamic and hydromagnetic stability*, Oxford University Press, Oxford 1961.

POLISH ACADEMY OF SCIENCES
INSTITUTE OF FUNDAMENTAL TECHNOLOGICAL RESEARCH
e-mail: szahor@ippt.gov.pl

Received August 7, 1997.

Arch. Mech., 50, 1, pp. 53–81, Warszawa 1998
FIFTY YEARS OF THE ARCHIVES OF MECHANICS

A thermodynamical description of the martensitic transformation
A model with small volume of averaging

J. KACZMAREK (GDAŃSK)

IN THE PAPER a thermomechanical model of the martensitic transformation in a single crystal is introduced. The model is related to a small volume of averaging. It means that detailed phenomena such as motion of single interfaces, internal rotations towards habit planes, separate mechanisms of dissipation or nucleation of different martensite variants can be discussed in the framework of the model. Such a description is attained mainly by means of the introduced free energy. Therefore, the construction of this function is a central part of this paper. The free energy depends on the Lagrangean strain tensor which describes the dominant part of deformation, relative displacement vectors for modelling shuffles and variables which are introduced with the aid of material directors. With the help of the last variables, an internal rotation is discussed. Furthermore, higher gradients of deformation are also taken into account. A general thermodynamical formulation for this small scale model is considered.

1. Introduction

THE MARTENSITIC TRANSFORMATION appears in many alloys, organic materials and even in living organisms. This transformation is diffusionless and is characterized by dominant shear strain. In case of moving interfaces between martensite variants or between martensite and austenite, such a transformation leads to shape memory phenomenon [1].

In general, the martensitic transformation creates complicated microstructure. In the case of moving interfaces, the microstructure has its own complex dynamics. This dynamics becomes still much more complicated when thermal processes are taken into account. They cause the stabilization martensite phenomenon. The stabilization can considerably influence temperatures of the transformation.

The martensitic transformation is a subject of intensive investigations in metallurgy. Such a transformation is the main mechanism of the shape memory phenomenon [1]. Increasing interest in this phenomenon appears in mechanics for the last twenty years. This is possible owing to results which were attained in metallurgy. Very helpful in mechanical description are, for instance, crystallographic structures of CuAl [2] or CuAlNi [3] alloys, positions of their habit planes or forms in which their martensitic structures appear in the material.

Miscellaneous points of view are presented in mechanical description of the martensitic transformation. One-dimensional models are discussed in order to give a qualitative mechanical description for some special behaviour of a material (see for instance [4, 5]). There are some models related to a single crystal [6, 7, 8]. A statistical approach is presented in [9, 10]. On the other hand, very averaged descriptions over the composition of martensite variants and austenite are discussed in the literature, see for instance [11 – 16]. They are simpler and are more applicable.

Complicated behaviour of materials which undergo the discussed transformation suggests a multiscale approach. Such point of view is presented by the author of this paper. Consequently, two models should be introduced. The first one is a model with small scale of averaging. It means that many detailed phenomena are taken into account in this description. There are single martensite variants, moving interfaces, shuffles which are usually neglected in description of the martensitic transformation, internal rotations towards habit planes or separated mechanisms of dissipation. However, such a model is rather complicated and difficult in applications. Some elements of such a description are discussed in [17, 18].

The model with small scale of averaging is viewed to be a theoretical and numerical basis for a more averaged model. The last one would have a reduced number of variables and more simple constitutive equations which would be derived from the small scale model. A concept of multiscale approach of this kind has been discussed in [20]. The program discussed here is too large for one paper. On the other hand, the model of small volume of averaging is complicated itself. Therefore, the purposes should be more limited at the moment.

Consequently, the aim of this paper is to introduce a thermomechanical model of the martensitic transformation related to a small volume of averaging which takes into account the detailed phenomena accompanied by this transformation.

2. Crystallographic considerations related to the martensitic transformation

The model of small volume of averaging will be constructed mainly by introduction of appropriate form of the free energy. Properties of the free energy are responsible for the detailed behaviour of the material in the frame of the model. However, in order to determine this function, variables which are appropriate for description of kinematics of the martensitic transformation and some internal state variables should be introduced. Selection of these variables depends on understanding the crystallographic properties of the material undergoing the considered phase transformation.

The crystallographic structure of the martensitic transformation will be discussed with the help of the CuAl alloy. Properties of this alloy are representative for a large class of shape memory alloys based on copper.

Let us discuss a process of nucleation of martensite variant from austenitic structure in a single crystal.

The austenite single crystal has a cubic body-centered structure bcc which is shown in Fig. 1. This structure is also called the β phase [2]. A face-centered structure which is not cubic can be distinguished in the frame of the bcc one. This is marked by a bold line. Furthermore, four planes are displayed by means of thin lines. They are called basal planes and are connected with the $0Y$ axis. We can distinguish in a similar manner next four basal planes assigned to $0X$ and next to $0Z$ axes, respectively. Thus, we have twelve basal planes. Some of them coincide in the undeformed state of austenite. Thus, in this undeformed state we have six different basal planes.

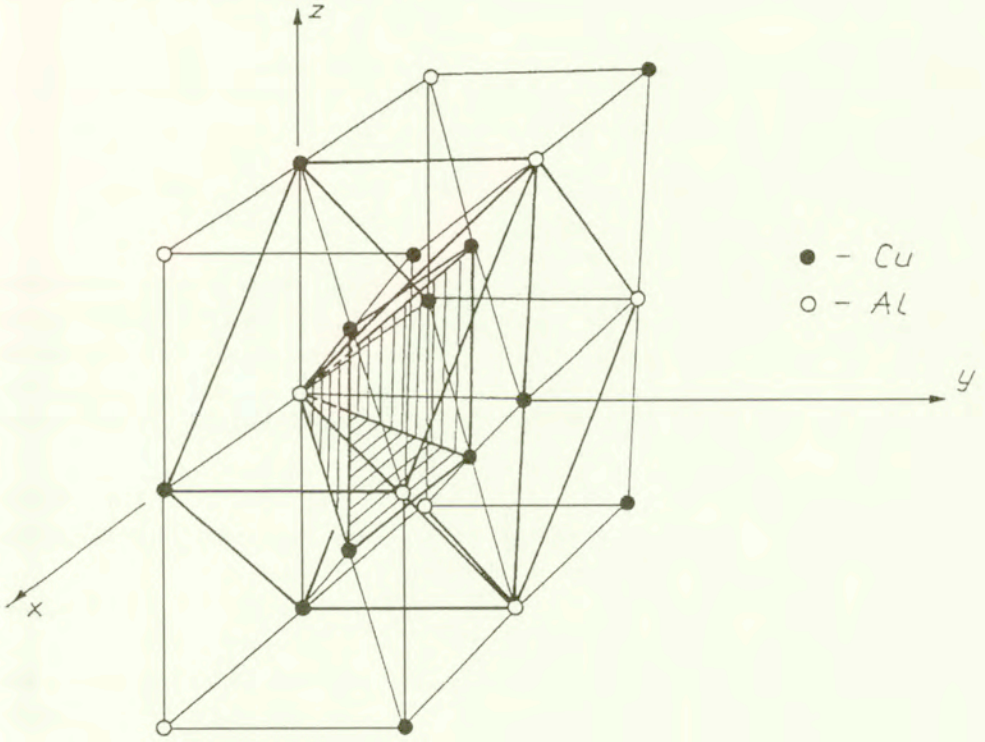

FIG. 1. Structure of austenite for CuAl alloy.

We can distinguish three stages of the martensitic transformation. The first stage consist in realization of the Bain strain. Let us select, for instance, $0Y$ axis. If we apply an extension along $0Y$ then, the previously discussed face-centered structure can be transformed into a cubic fcc one. The strain of this kind is called just the Bain strain.

The second stage of the martensitic transformation is a micrononhomogeneous shear. This deformation appears on one of four possible basal planes related to the $0Y$ axis. Micrononhomogeneous deformation of this kind is shown at Fig. 2 and

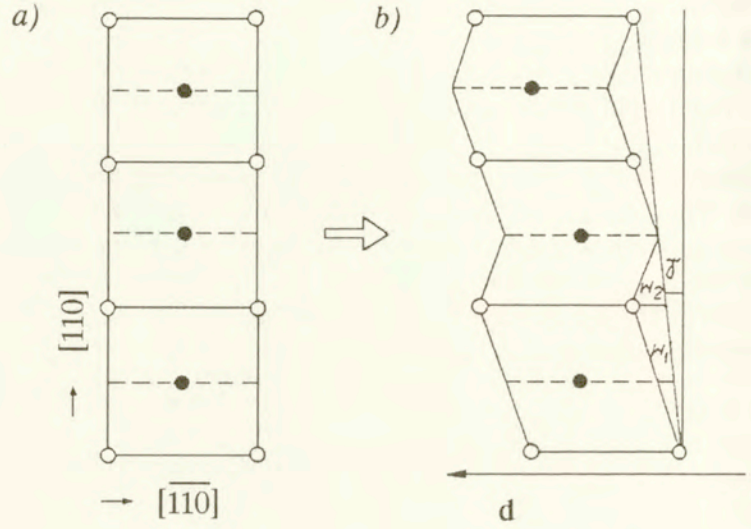

FIG. 2. Micrononhomogeneous shear on the basal plane of CuAl alloy.

is connected with shuffles. The micrononhomogeneous shear occurs in direction **d** which lies on the basal plane. We have four such directions accompanied by the $0Y$ axis. They are fixed to point 0 and lie on each of the basal planes and on the ZY and XY plane, respectively. The shuffles marked by w_1 and w_2 in Fig. 2 are a measure of deviation of atoms from the position indicated by a homogeneous deformation.

The third stage of transformation considered is a rotation of the hitherto obtained structure towards a habit plane. We have two possible habit planes related to each structure obtained in the discussed manner.

In real evolution of the crystal structure these three stages are not separated so clearly.

Thus, we can obtain twenty four martensite variants. Indeed, we have four micrononhomogeneous shears accompanied by the $0Y$ axis and next two possible rotations. This gives eight martensite variants related to the $0Y$ axis. Similarly, martensite variants can be obtained for the remaining axes.

Orientations of basal planes and habit planes are shown at Fig. 3 where notations from [21] are used. Capital letters denote Bain axes. Small letters are connected with directions of nonhomogeneous shear. Variants which are different by rotation are marked by primes at the capital letter.

Possible twenty four martensite variants appear in the material in six self-accommodating groups. Consequently, each group has four marensite variants separated by habit-type or twin-type planes. Four martensite variants organized in one self-accommodating group are shown at Fig. 4.

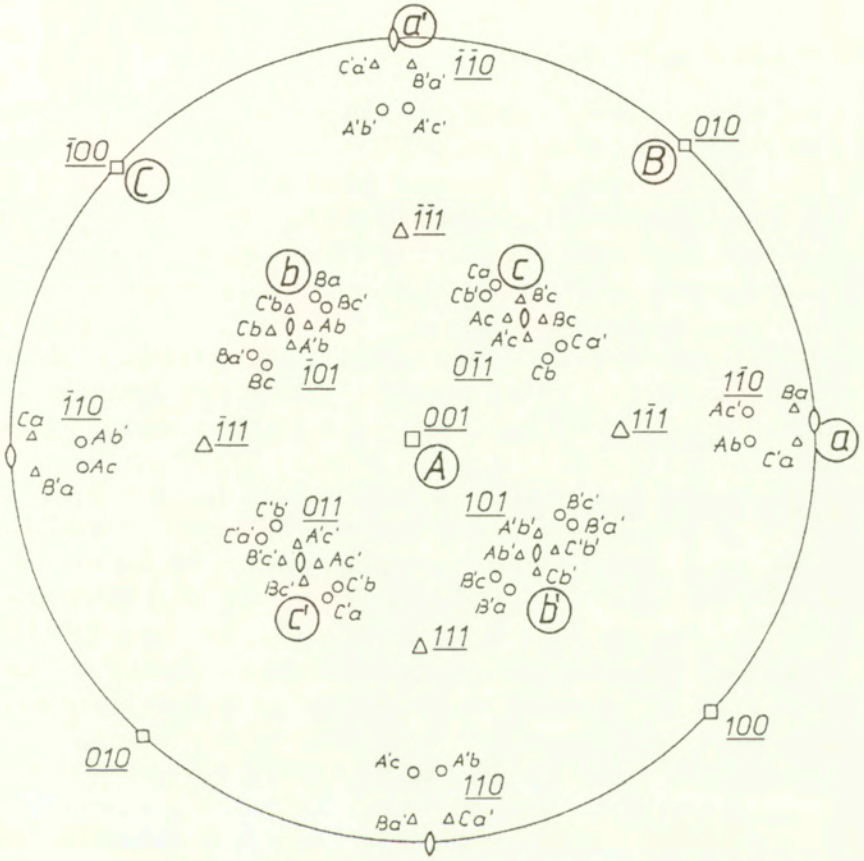

FIG. 3. Distribution of basal planes and habit planes for CuAl alloy.

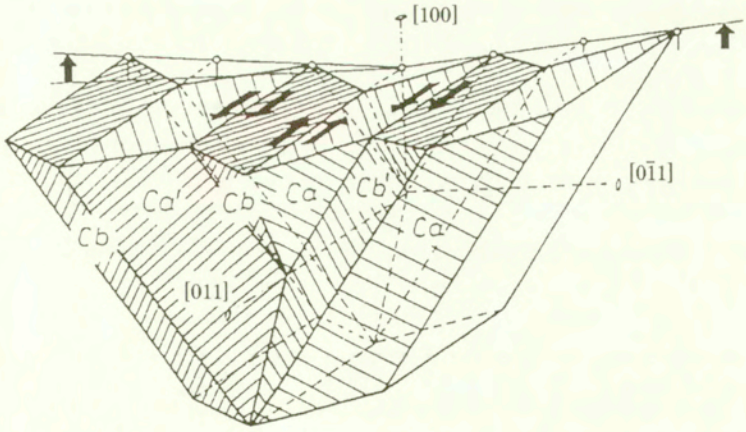

FIG. 4. A selfaccommodating group of four martensite variants in CuAl alloy.

3. Kinematical considerations

Crystallography of the martensitic transformation discussed in the last section suggests the measures of deformation which should be assumed. They should give a possibility of classification of martensite variants.

Let us introduce a system of orthonormal base vectors $\mathbf{b} = \{\mathbf{b}_1, \mathbf{b}_2, \mathbf{b}_3\}$. Directions of these vectors coincide with axes $0X$, $0Y$, $0Z$ as in Fig. 1, respectively.

We introduce also the sets of vectors which define the shear systems connected with the micrononhomogeneous shears.

Let us consider a vector $\mathbf{b}_i$. We assign to this vector two planes which contain the vector $\mathbf{b}_i$ and vectors $\mathbf{b}_j$, $j \neq i$, respectively. Thus, a double index is assigned to each plane of this kind as $I = \{i, j\}$, $j \neq i$. The first index is related to the Bain axis and the second one determines the plane introduced.

With the help of these planes we define vectors $\mathbf{d}_{I\alpha}$, $\alpha = 1, 2$. They are unit vectors with their initial points in 0 and lie on the lines which appear as intersections of plane I with a pair of basal planes related to axis i. Their positions are illustrated in Fig. 6. Pair of vectors $\{\mathbf{d}_{I1}, \mathbf{d}_{I2}\}$ determine a shear system. Furthermore, we create new basis $\mathbf{d}_I = \{\mathbf{d}_{I1}, \mathbf{d}_{I2}, \mathbf{d}_{I1} \times \mathbf{d}_{I2}\}$.

Let $\mathbf{e}$ be the Lagrangean strain tensor. Then $e_{I12} = \mathbf{d}_{I1}\mathbf{e}\mathbf{d}_{I2}$ is a measure of shear strain in this shear system. Vectors $\mathbf{d}_{I1}$ and $\mathbf{d}_{I2}$ indicate possible directions of shuffles.

Let us notice that structures given on Fig. 5 c and Fig. 5 d have the same strain given by e_{I12}. They differ only by shuffles. Thus, the shuffles which are small and usually neglected in description of the martensitic transformation are important for distinguishing different martensite variants. Moreover, we can say that during deformation given by $\mathbf{e}$, a bifurcation between two direction of shuffles appears.

However, qualitative meaning of shuffles is still greater. Namely, the possible habit planes towards which the structures rotate, depend just on the kind of shuffles which have previously appeared. Accordingly, the shuffles influence the kind of internal rotation.

Let us notice that micrononhomogeneous deformation appears as a consequence of complex crystal lattice accompanied by a multicomponent alloy. Therefore, a natural way of introducing the shuffles follows from multicomponent considerations.

Consequently, let us introduce a set of displacement functions

$$\mathbf{z}_\mu(\mathbf{X}, t) = \{\mathbf{x}(\mathbf{X}, t), \mathbf{y}_\lambda(\mathbf{X}, t)\}, \tag{3.1}$$

where $\lambda \in \Lambda = \{1, ..., N_\lambda\}$. It is assumed that the function $\mathbf{x}$ is accompanied by the microhomogeneous deformation assigned to the body, and functions $\mathbf{y}_\lambda$ indicate the positions which differ from the homogeneous one. Thus, the relation between $\mathbf{x}$ and $\mathbf{y}_\lambda$ has the form

$$\mathbf{y}_\lambda = \mathbf{x} + \boldsymbol{\xi}_\lambda. \tag{3.2}$$

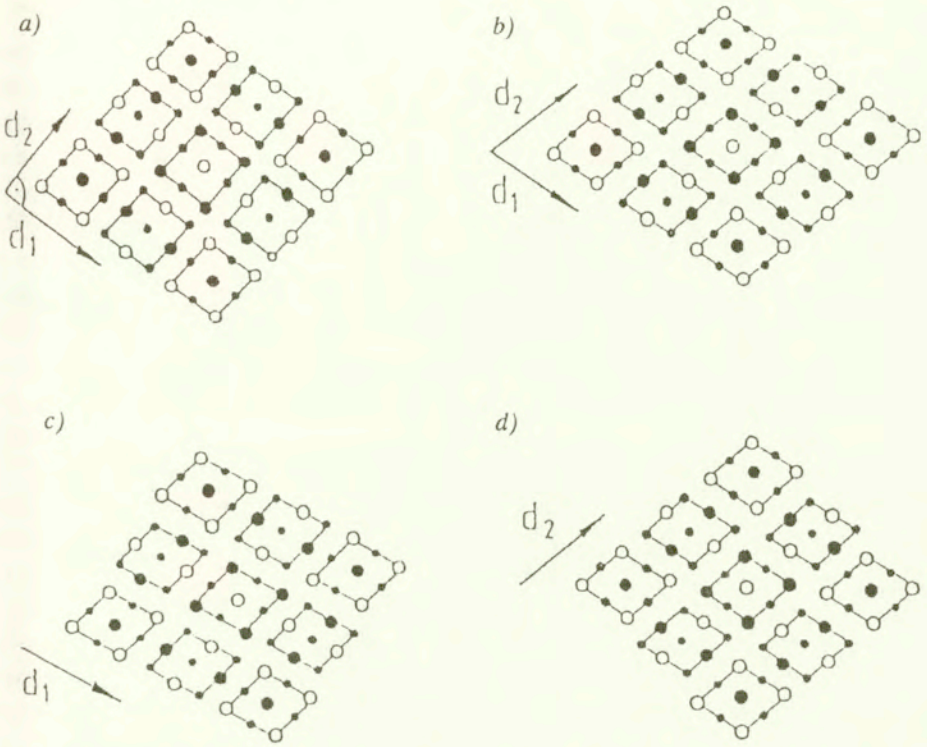

FIG. 5. Evolution of crystal structure during shear strain in the shear system $(\mathbf{d}_1, \mathbf{d}_2)$.

ξ_λ is an independent variable. However, we have observed that shuffles appear in $\mathbf{d}_{I1}$ or $\mathbf{d}_{I2}$ direction in the I-th shear system. Let us note that the base vectors $\mathbf{d}_{I1}$, $\mathbf{d}_{I2}$ can be also viewed as material directors which are deformed as $\mathbf{d}'_{I\alpha} = \mathbf{F}\mathbf{d}_{I\alpha}$ for $\alpha = 1, 2$, where $\mathbf{F}$ is the deformation gradient related to $\mathbf{x}$.

Taking into account the above remark we can assume that $\xi_\lambda = w_\lambda \mathbf{d}'_{I1}$ or $\xi_\lambda = w_\lambda \mathbf{d}'_{I2}$. Then, for instance for $\alpha = 1$, we obtain $\xi_\lambda = w_\lambda \mathbf{F}\mathbf{d}_{I1}$. Putting $\mathbf{w}_\lambda = w_\lambda \mathbf{d}_{I1}$ we have $\xi_\lambda = \mathbf{F}\mathbf{w}_\lambda$.

The gradient of deformation transforms orthonormal vectors $\mathbf{d}_{I\alpha}$ into $\mathbf{d}'_{I\alpha}$ which are usually not orthonormal. In some cases, it is convenient to assume approximately that $\mathbf{d}'_\alpha = \mathbf{R}\mathbf{d}_{I\alpha}$, where $\mathbf{R}$ is a rotation tensor which appears in polar decomposition $\mathbf{F} = \mathbf{V}\mathbf{R}$ [28]. Taking into considerations (3.2) we can also write that $\mathbf{y}_\lambda = \mathbf{x} + \mathbf{F}\mathbf{w}_\lambda \approx \mathbf{x} + \mathbf{R}\mathbf{w}_\lambda$. Such an approximation will be useful in further derivations.

Let us notice that the approximation $\mathbf{F}\mathbf{w}_\lambda \approx \mathbf{R}\mathbf{w}_\lambda$ suggests some constraints related to the gradient of deformation. However, this approximation appears in displacement function $\mathbf{y}_\lambda$ only. Then, the gradient of deformation $\mathbf{F}$ related to $\mathbf{x}$ defines $\mathbf{y}_\lambda$. As a result of this, constraints are related to $\mathbf{y}_\lambda$ and finally to $\mathbf{w}_\lambda$ but not to $\mathbf{F}$.

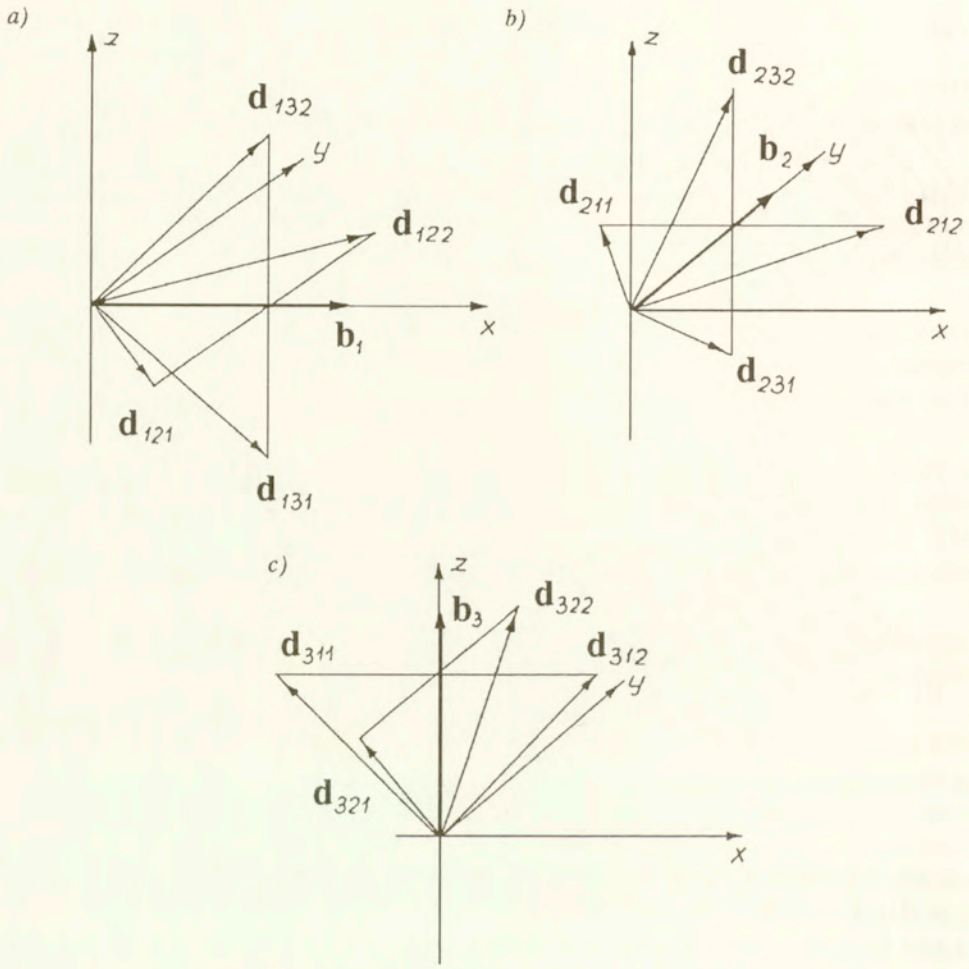

FIG. 6. Distributions of vectors $\mathbf{d}_{I\alpha}$ in the austenite structure.

The vector $\mathbf{w}_\lambda$ is a variable which characterizes relative translation of sublattices. Thus, in the above approximation, it is assumed that the rotation is the most valid part of the gradient of deformation for kinematics. It characterizes the change of directions in rotating lattice. In general, relative displacement vectors should depend on the remaining components of the gradient of deformation. However, such a dependence should not follow from kinematics but from dependence of the free energy on $\mathbf{F}$ and $\mathbf{w}_\lambda$. This kind of dependence in the equilibrium case is discussed in what follows.

In general, the relative displacement vector $\mathbf{w}_\lambda$ has not to be considered as $\mathbf{w}_\lambda = w_\lambda \mathbf{d}_{I1}$ because the last relation is a constraint in fact. Consequently, the vector $\mathbf{w}_\lambda$ will be viewed as an independent variable which is convenient for modelling the shuffles in the free energy.

The approximations discussed above related to $\mathbf{w}_\lambda$ have an interpretational meaning and are applied further during the derivation of equations. It is assumed that they do not influence integrability of the finally obtained fields. The main interpretational aspect related to $\mathbf{w}_\lambda$ rests on elucidating the fact that $\mathbf{w}_\lambda$ appears as a result of multicomponent considerations and is not directly related to defects.

Next problem is connected with a rotation towards the habit plane. This rotation is caused by forces in the material which act in order to fit together the austenite and creating martensite variants. The habit plane is a plane on which the mentioned structures are fitted together and which is undeformed. We may say that the austenite attracts a creating martensite variant until this variant takes appropriate, energetically most advantageous position in the crystal. This attraction is accompanied by two habit planes. Thus, a bifurcation process related to the internal rotation can take place.

The internal rotation will be introduced here with the help of variables which are defined by means of material directors. Let $\mathbf{p}_1$ and $\mathbf{p}_2$ be a pair of material directors which lie on a habit plane. In other words, the habit plane is spanned by these directors. They transform as $\mathbf{p}'_\beta = \mathbf{F}\mathbf{p}_\beta$, $\beta = 1, 2$.

The directors are transformed during the martensitic transformation. We try to describe the forces in the material. Therefore, the discussed variable should exclude an external rotation. Taking it into account, the following measure of deviation of directors is introduced:

$$\mathbf{a}_\beta = \mathbf{R}^{-1}(\mathbf{F} - \mathbf{R})\mathbf{p}_\beta = (\mathbf{R}^{-1}\mathbf{F} - 1)\mathbf{p}_\beta \,, \tag{3.3}$$

where $\mathbf{R}$ is an external rotation. At this moment, a problem of separation of internal and external rotations appears. An idea of this separation is introduced by assuming some additional auxiliary configurations.

It is assumed that the internal rotation develops only when the shear strain e_{I12} in the I-th shear system is between the given values e^*_{I12} and e^{**}_{I12}. This follows from the fact that the internal rotation appears only if an elastic region is exceeded. Indeed, in the usual elasticity problems related to such a rotation are not observed.

Let us distinguish some special configurations. The first one is the reference configuration which coincides with the natural state of austenite. The second configuration $x_\alpha = x_\alpha(X_N)$ is connected with the deformation for which the strain e^*_{I12} is attained in a given point of the body. The third configuration $x_\mu = x_\mu(x_\alpha)$ is connected with deformation for which the strain e^{**}_{I12} is attained and the fourth configuration is an actual configuration x_i.

Configurations x_α and x_μ are fixed and are different for different points $\mathbf{X}$. Thus, they are accompanied by retaining in memory the state of deformation in a given point attained in the past.

The deformation gradients are assigned to the mentioned configurations $\mathbf{F}^{ea} = [x_{\alpha,N}]$, $\mathbf{F}^s = [x_{\nu,\alpha}]$, $\mathbf{F}^{em} = [x_{i,\nu}]$ and the total gradient takes the form $\mathbf{F} = \mathbf{F}^{em}\mathbf{F}^s\mathbf{F}^{ea}$.

At the moment we are able to separate internal and external rotations. Let us assume that deformation occurs in region S, i.e. between the second and third fixed configurations. Then, an external rotation follows from polar decomposition $\mathbf{F}^{ea} = \mathbf{VR}$. Then, the definition of variable $\mathbf{a}_\beta$ is more precise. Let us assume $\mathbf{F}^s = \mathbf{R}^s\mathbf{U}^s$. In such a case, Eq. (3.3) can be rewritten as

$$\mathbf{a}_\beta = \mathbf{R}^{-1}(\mathbf{R}^s\mathbf{U}^s\mathbf{VR} - \mathbf{R})\mathbf{p}_\beta \,. \tag{3.4}$$

It is assumed that the internal rotation is identified with $\mathbf{R}^s$. It means that in the S domain only this rotation appears. Thereby, the evolution of the internal rotation is viewed as relatively faster than the external rotation in the considered domain.

Let us note that the definition of variables $\mathbf{a}_\beta$ depends on the selection of vectors $\mathbf{p}_\beta$. In the simplified case it is possible to take into account one director lying on the rotation axis of the martensitic structure. This axis can be approximately considered as unchanged with respect to austenite. In this case the number of variables is reduced.

Let $\mathbf{U}^c = \mathbf{U}^s\mathbf{V}$ and $\mathbf{Rp}_\beta = \overline{\mathbf{p}}_\beta$. With the help of this, a variable $\overline{\mathbf{a}}_\beta = \mathbf{Ra}_\beta$ is introduced. This variable can also be expressed as $\overline{\mathbf{a}}_\beta = (\mathbf{R}^s\mathbf{U}^c - \mathbf{1})\overline{\mathbf{p}}_\beta$. With the help of the last formula we can discuss a problem of existence of the internal rotation.

The plane spanned on $\overline{\mathbf{p}}_1$, $\overline{\mathbf{p}}_2$ is undeformed if

$$\begin{aligned} \mathbf{U}^c\overline{\mathbf{p}}_1\mathbf{U}^c\overline{\mathbf{p}}_1 &= \overline{\mathbf{p}}_1\overline{\mathbf{p}}_1 \,, \\ \mathbf{U}^c\overline{\mathbf{p}}_1\mathbf{U}^c\overline{\mathbf{p}}_2 &= \overline{\mathbf{p}}_1\overline{\mathbf{p}}_2 \,, \\ \mathbf{U}^c\overline{\mathbf{p}}_2\mathbf{U}^c\overline{\mathbf{p}}_2 &= \overline{\mathbf{p}}_2\overline{\mathbf{p}}_2 \,. \end{aligned} \tag{3.5}$$

Furthermore, we assume that austenite and martensite are fitted together if $\overline{\mathbf{a}}_\beta = 0$. It means that

$$(\mathbf{R}^s\mathbf{U}^c - \mathbf{1})\overline{\mathbf{p}}_1 = 0, \qquad (\mathbf{R}^s\mathbf{U}^c - \mathbf{1})\overline{\mathbf{p}}_2 = 0. \tag{3.6}$$

It is known from crystallographic considerations that $\mathbf{U}_c$ can be interpreted to be responsible for the Bain strain and micrononhomogeneous shear. On the other hand, we have obtained in (3.5) and (3.6) nine equations and nine variables $\mathbf{U}^c$ and $\mathbf{R}^s$. It is known from crystallographic considerations that for equilibrium martensite $\mathbf{U}^c \neq 1$. Thus, if $\mathbf{R}^s = 1$ then Eqs. (3.6) are not satisfied. Consequently, there exist $\mathbf{R}^s \neq 1$.

4. Free energy

A model of the free energy plays a key role in the discussed small-scale approach. Detailed phenomena modelled by the free energy give evidence of what

kind of averaging is used. We have discussed the evolution of crystal structure during the martensitic transformation. As a result, components of the deformation measure are introduced in order to describe this process.

Consequently, we take into account the shear strain in separate shear systems, shuffles represented by relative displacement vectors, internal rotations towards habit planes which can be modelled with the help of directors. Furthermore, we observe in Fig. 4 that the interfaces are flat. Such a phenomenon should appear as a result of mechanical properties of interfaces. Therefore, this fact should also influence the free energy form.

Accordingly, the most important independent variables of the free energy were discussed in the previous section. Furthermore, we assume that the free energy depends on temperature and some internal state variables which will be discussed later.

The free energy will be introduced with the help of the following program:

1. The skeleton of the free energy is based on geometrical objects distinguished in crystal structure of austenite. They are:
   - Bain axes,
   - six different basal planes in undeformed state of austenite,
   - twenty four habit planes,
   - directions of micrononhomogeneous shear.
2. It is assumed that elastic properties of austenite and martensite are known. The free energy is defined in the neighbourhood of equilibrium of austenite and martensite as a positive definite quadratic form with appropriate symmetry properties.
3. The boundary of elastic range for austenite and martensite are given as five-dimensional hypersurfaces in the space of strain E. In this region the phase transformation is initiated.
4. The first stage of construction of the free energy consists in defining its part which depends mainly on the strain tensor.
5. The second stage consists in introducing relative displacement vectors in order to describe the evolution of shuffles.
6. The third stage consists in taking into account internal rotations towards possible habit planes.
7. The last stage consists in introducing higher gradients of deformation.

First, the part of the free energy which depends mainly on the Lagrangean strain tensor $\mathbf{e}$ is introduced. As follows from crystallographic considerations, this part of the free energy should have six minima for martensite and one for austenite. Furthermore, the elastic properties of austenite and martensite near their equilibrium position are assumed to be modelled by a quadratic form with respect to the strain tensor $\mathbf{e}$.

Let E be a set of all strain tensors $\mathbf{e}$ expressed in the basis $\mathbf{b}$. Let us assume that E can be decomposed into the sum $E = A \cup S \cup \bigcup_I M_I$ of sets which represents elastic range for austenite, a spinodal region and elastic range for the

I-th variant of martensite, respectively. These sets are defined as

$$A = \{\mathbf{e} : F_{ijkl}(\mathbf{e}) > 0,\ l(\mathbf{0},\ \mathbf{e}) \subset A\}, \tag{4.1}$$

$$M_I = \{\mathbf{e} : F_{ijkl}(\mathbf{e}) > 0,\ l(\mathbf{e}_{MI},\ \mathbf{e}) \subset M_I\}, \tag{4.2}$$

where

$$F_{ijkl}(\mathbf{e}) = \frac{\partial F}{\partial e_{ij}\partial e_{kl}}(\mathbf{e}),$$

$l(\mathbf{e}',\ \mathbf{e}'')$ means a segment with ends $\mathbf{e}'$, $\mathbf{e}''$, $\mathbf{e}_{MI}$ is a strain assigned to I-th martensite variant in equilibrium. The set S is a domain where $F_{ijkl}(\mathbf{e})$ is not positive definite. Let us remark that $\partial S_A = \partial A$ and $\partial S_{MI} = \partial M_I$.

Let $\overline{F}_A = c_{ijkl}e_{ij}e_{kl}$ be a positive definite form which describes elastic properties of austenite near the equilibrium point $\mathbf{e} = \mathbf{0}$. Such elastic properties are real only in some neighbourhood U_A of this point. On the ∂S_A the free energy is not positive definite. Thus, the function $\overline{F}_A$ should be appropriately modified in domain $A - U_A$. Similarly, a positive definite quadratic form $\overline{F}_{MI} = c_{MIijkl}(e_{ij} - e_{MIij})(e_{kl} - e_{MIkl}) + d$ which represents elastic properties of I-th martensite is introduced. Furthermore, we assume that a critical stress as well as the corresponding strain for which martensitic transformation is initiated is known. It means that forms of hipersurfaces ∂S_A and ∂S_{MI} are postulated in E where the free energy should be semipositive only.

It is convenient to discuss the form of the free energy or, more exactly, the graph of the free energy as a fiber bundle. The fiber bundle is understood here as a generalization of Cartesian product of basis manifold and a fiber manifold [30].

Let $A_I : E \to E_I$ be a mapping which transforms the strain tensors expressed in basis $\mathbf{b}$ into the strain tensors expressed in basis $\mathbf{d}_I$. Let $e_{I12} = \mathbf{d}_{I1}\mathbf{e}\mathbf{d}_{I2}$ be a component of strain tensor $\mathbf{e}_I \in E_I$. It is known from previous considerations that the most characteristic feature of the martensitic transformation is the shear strain. In the discussed case it is the shear strain in shear system $\{\mathbf{d}_{I1},\ \mathbf{d}_{I2}\}$. Accordingly, e_{I12} is just the main feature of martensite variants created in this shear system.

Let us introduce sets $N_{IA} = \{e_{I12} : 0 \leq e_{I12} \leq e^*_{I12}\}$, $N_{IS} = \{e_{I12} : e^*_{I12} \leq e_{I12} \leq e^{**}_{I12}\}$, $N_{IM} = \{e_{I12} : e^{**}_{I12} \leq e_{I12} \leq e_{MI12}\}$ and $N_I = N_{IA} \cup N_{IS} \cup N_{IM}$, where e^*_{I12} and e^{**}_{I12} are components of strains such that $e^*_I \in \partial S_A$ and $e^{**}_I \in \partial S_{MI}$. Functions $\overline{F}_A$ and $\overline{F}_{MI}$ are expressed in the basis $\mathbf{d}_I$ as $\overline{F}_{AI}(\mathbf{e}_I) = \overline{F}_A \circ A_I^{-1}(\mathbf{e}_I)$ and $\overline{F}_{MII}(\mathbf{e}_I) = \overline{F}_{MI} \circ A_I^{-1}(\mathbf{e}_I)$.

Let $h_{AI}(e_{I12}) : \partial S_A \to f(e_{I12})$, $e_{I12} \in N_{IA} - \{0\} = N_0$ be a family of homeomorphisms. Then, N_0 can be seen as a basis of a fiber bundle and $f(e_{I12})$ as a family of fibers. As a result, we consider the elastic domain $A = \bigcup_{e_{I12} \in N_0}\{e_{I12},\ f(e_{I12})\} = N_0 \times \partial S_A$ as a fiber bundle or, in other words, as a generalized Cartesian product of N_0 and ∂S_A. The projection in this bundle acts as $\pi(f(e_{I12})) = e_{I12}$. We discuss one coordinate representation. Then, the structural group consists of one element only.

Let us introduce the following sets in $E_I \times R$ space:

$$\overline{B}_{IA} = \{b_{IA12} = \{e_{I12},\ \overline{F}_{AI}(e_{I12})\} :\ e_{I12} \in N_{IA}\}$$

and

$$\overline{B}_{IM} = \{b_{IM12} = \{e_{I12},\ \overline{F}_{MI}(e_{I12})\} :\ e_{I12} \in N_{IM}\}.$$

Let us consider also the sets $\overline{F}_{\partial S} = \{\{e_I,\ \overline{F}_{AI}|_{\partial S_A}\} :\ e_I \in \partial S_A = f(e^*_{I12})\}$ and $F_{f(e_{I12})} = \{\{e_I,\ \overline{F}_{AI}|_{f(e_{I12})}\} :\ e_I \in f(e_{I12})\}$. With the help of these sets we can determine the graph of $\overline{F}_{AI}$ as a fiber manifold

$$\overline{F}_{AI} = \bigcup_{e_{I12} \in N_0} \left\{b_{IA12},\ F_{f(e_{I12})}\right\} = \overline{B}_{IA} \times \overline{F}_{\partial S} \tag{4.3}$$

with projection π in the bundle as $\pi(F_{f(e_{I12})}) = b_{IA12}$.

As it was mentioned previously, $\overline{F}_A$ has not an appropriate form because it is not positive definite on ∂S_A. Therefore, $\overline{F}_A$ should be modified on $A - U_A$.

It is assumed that $\mathbf{0} \in U_A$, $U_A \subset \operatorname{int} A$ and there exists e_{I12} which gives $\partial U_A = f(e_{I12})$. The idea of modification (4.3) consists in introduction of a modifying function C such that we obtain from $\overline{F}_{AI}$ a new function F_{AI} in the form

$$F_{AI} = \begin{cases} \overline{F}_{AI}|_{U_A}, & \mathbf{e}_I \in U_A\,, \\ \overline{F}_{AI} + C, & \mathbf{e}_I \in A - U_A\,. \end{cases} \tag{4.4}$$

The graph of the map C is assumed as

$$C = \begin{cases} \{\mathbf{e}_I,\ 0\}, & \mathbf{e}_I \in U_A,\ \ e_{I12} \leq \bar{e}_{I12} = N_{IA} \cap \partial U_A\,, \\ \{\mathbf{e}_I,\ C_{e_{I12}}(\mathbf{e}_I)\}, & \mathbf{e}_I \in f(e_{I12}),\ \ \bar{e}_{I12} < e_{I12} < e^*_{I12}\,, \end{cases} \tag{4.5}$$

where the condition

$$\frac{\partial^2(\overline{F}_{AI} + C)}{\partial e^2_{I12}}(e^*_{I12}) = 0$$

is fulfilled and F_{AI} is semipositive definite on the whole ∂S_A.

Let furthermore $B_{IA} = \{\{e_{I12}, F_{AI}(e_{I12})\} :\ e_{I12} \in N_{IA}\}$ and $F_{\partial S_A} = \{\{e_I, (\overline{F}_{AI} + C)\}|_{\partial S}\} :\ e_I \in \partial S_A\}$. Then, we have defined the free energy F_{AI} in the domain A and the graph of this function can be identified with the generalized product $B_{IA} \times F_{\partial S_A}$.

The function F_{AI} can be expressed in basis $\mathbf{b}$ as $F_A = F_{AI} \circ A_I(\mathbf{e})$. There are six shear systems I. Such a construction can be carried out in six ways. We assume that they lead to the same results since we have only one variant of austenite.

Similar construction will be carried out for martensite variants. Let $h_{MI}(e_{I12})$: $\partial S_{MI} \to f(e_{MI})$, $e_{I12} \in N_{IM} - \{e_{MI12}\} = N_{IMo}$ be a family of homeomorphisms. Then, the elastic domain for the I-th martensite variant can be expressed as $M_I = \bigcup_{e_{I12} \in N_{IMo}} \{e_{I12},\ f_{MI}(e_{I12})\} = N_{IMo} \times \partial S_{MI}$.

Let us consider the sets $\overline{F}_{\partial S_{MI}} = \{\{e_I,\ \overline{F}_{MII}|_{\partial S_{MI}}\} :\ e_I \in \partial S_{MI} = f(e^{**}_{I12})\}$ and $F_{MIf}(e_{I12}) = \{\{e_I,\ \overline{F}_{MII}|_{f_{MI}(e_{I12})}\} :\ e_I \in f_{MI}(e_{I12})\}$. Then, the function $\overline{F}_{MII}$ takes the form

$$\overline{F}_{MII} = \bigcup_{e_{I12} \in N_{IMo}} \{b_{IM_{12}},\ F_{MIf}(e_{I12})\} = \overline{B}_{IM} \times \overline{F}_{\partial S_{MI}}\,. \tag{4.6}$$

Let us assume that the elastic properties of the I-th martensite are given in elliptic form only in a set $U_{MI} \subset intM_I$, and that there exists $\check{e}_{I12} \in N_{IMo}$ which gives $\partial U_{MI} = f_{MI}(\check{e}_{I12})$. Then, a correction function C_{MI} induces a new form $\overline{F}_{MII}$ as

$$F_{MII} = \begin{cases} \overline{F}_{MII}\,, & \mathbf{e}_I \in U_{MI}\,, \\ \overline{F}_{MII} + C_{MI}\,, & \mathbf{e}_I \in M_I - U_{MI}\,. \end{cases} \tag{4.7}$$

The map C_{MI} is assumed in the following form:

$$C_{MI} = \begin{cases} \{\mathbf{e}_I,\ 0\}, & \mathbf{e}_I \in U_{MI}\,, \\ \{\mathbf{e}_I,\ C_{MI}(e_{I12})\}, & \mathbf{e}_I \in f(e_{I12}),\quad e^{**}_{12} \le e_{I12} \le \check{e}_{I12} \end{cases} \tag{4.8}$$

with the following condition

$$\frac{\partial^2(\overline{F}_{MII} + C_{MI})}{\partial e^2_{I12}}(e^{**}_{I12}) = 0,$$

and F_{MII} is semipositive definite on the whole ∂S_{IM}.

Let furthermore $B_{IM} = \{\{e_{I12}, F_{MII}(e_{I12})\} :\ e_{I12} \in N_{IM}\}$ and $F_{\partial S_{MI}} = \{\{e_I, (\overline{F}_{IMI} + C_{MI})\}|_{\partial S_{MI}}\} :\ e_I \in \partial S_{MI}\}$. Then, we have defined the free energy F_{MII} in the domain M_I and the graph of this function can be identified with generalized product $B_{IM} \times F_{\partial S_{MI}}$.

The function F_{MII} can be expressed as $F_{MI} = F_{MII} \circ A_I(\mathbf{e})$ in basis $\mathbf{b}$. Let us note that an internal rotation can appear. Then, the martensite becomes rotated with respect to the austenite. As a result of this, elastic constants undergo a transformation being dependent on the possible rotation. In order to stress this fact we write $F_{MI} = F_{MII}(\mathbf{R}) \circ A_I(\mathbf{e})$. It is assumed that $\mathbf{R}$ is not variable at this place but is fully determined.

The form of the free energy function in the S domain is less precisely determined. It follows from the fact that we have not too many detailed information on this subject. Therefore, we assume only general properties for this part of the free energy. Thus, we assume that the following conditions are fulfilled by this function:

$$\begin{aligned} &F_S|_{N_{IS}} = B_{IS}\,, \qquad F_S|_{\partial S_A} = F_A|_{\partial S_A}\,, \qquad F_S|_{\partial S_{MI}} = F_{MI}|_{\partial S_{MI}}\,, \\ &\frac{\partial F_S}{\partial \mathbf{e}}\Big|_{\partial S_A} = \frac{\partial F_A}{\partial \mathbf{e}}\Big|_{\partial S_A}\,, \qquad \frac{\partial F_S}{\partial \mathbf{e}}\Big|_{\partial S_{MI}} = \frac{\partial F_{MI}}{\partial \mathbf{e}}\Big|_{\partial S_{MI}}\,, \\ &\frac{\partial^2 F_S}{\partial \mathbf{e}\partial \mathbf{e}}\Big|_{\partial S_A} = \frac{\partial^2 F_A}{\partial \mathbf{e}\partial \mathbf{e}}\Big|_{\partial S_A}\,, \qquad \frac{\partial^2 F_S}{\partial \mathbf{e}\partial \mathbf{e}}\Big|_{\partial S_{MI}} = \frac{\partial^2 F_{MI}}{\partial \mathbf{e}\partial \mathbf{e}}\Big|_{\partial S_{MI}}\,, \end{aligned} \tag{4.9}$$

where B_{IS} should be postulated.

General features of temperature dependence are presented by means of plotting components of the free energy $c_{ijkl}(T)$, $\partial S_A(T)$, $C(T)$, $c_{MIijkl}(T)$, $\partial S_{MI}(T)$, $C_{MI}(T)$ with temperature. Increasing temperature we can pass from stable martensite to a pseudoelastic case. It is displayed by conditions $\frac{\partial F}{\partial \mathbf{e}}(\mathbf{e}_{MI}) = 0$ in the first case, and by $\frac{\partial F}{\partial \mathbf{e}}(\mathbf{e}_{MI}) \neq 0$ in the second case.

Finally, the free energy part F_E which depends mainly on the strain tensor $\mathbf{e}$ has the form

$$F_E = \begin{cases} F_A\,, & \mathbf{e} \in A\,, \\ F_{MII}(\mathbf{R}) \circ A_I\,, & \mathbf{e} \in M_I\,, \\ F_S\,, & \mathbf{e} \in S\,. \end{cases} \tag{4.10}$$

Another part of the free energy is related to micrononhomogeneous deformation. We have discussed previously that the shuffles appear in two possible directions $\mathbf{d}_{I1}$ or $\mathbf{d}_{I2}$ in a given I-th shear system. Thus, a bifurcation process related to shuffles should be modelled.

Let $\mathbf{w}_\lambda$, $\lambda \in \Lambda$ be the λ-th relative displacement vector which can appear in the I-th shear system. Let us introduce also a function $C_\alpha(z)$, $\alpha = 1,\ 2$ which is symmetric, positive, and $C_\alpha(0) = 0$, $\frac{\partial C_\alpha}{\partial z}(0) = 0$ and $\frac{\partial^2 C_\alpha}{\partial z^2}(0) > 0$. This function has one minimum in $z = 0$ and for increasing z it increases up to a certain determined value.

With the help of C_α, a bifurcation for evolution of $\mathbf{w}_\lambda$ can be modelled. To this end let us introduce a function of variable $\mathbf{w}_\lambda$ given by

$$M_{I\lambda} = C_1(\mathbf{w}_\lambda \mathbf{d}'_{I2})(\mathbf{w}_\lambda \mathbf{d}'_{I1})^2 + C_2(\mathbf{w}_\lambda \mathbf{d}'_{I1})(\mathbf{w}_\lambda \mathbf{d}'_{I2})^2\,. \tag{4.11}$$

Properties of functions C_α produce evolution of the relative displacement vector $\mathbf{w}_\lambda$ in two possible dominant directions $\mathbf{d}'_{I1}$ or $\mathbf{d}'_{I2}$. Evolution along $\mathbf{d}'_{I1}$ eliminates evolution in $\mathbf{d}'_{I2}$ and inversely. However, we have a group of vectors $\mathbf{w}_\lambda$ since $\lambda \in \Lambda$. Kinematical considerations indicate that all vectors of this group should develop in the same directions after a bifurcation (Fig. 2). Thus, we have a collective bifurcation. Therefore, an energetic barrier should make impossible a bifurcation of $\mathbf{w}_\lambda$ and $\mathbf{w}_{\lambda'}$, $\lambda \neq \lambda'$ in two different directions.

Let us introduce some additional notations. By $d_{\alpha\lambda\lambda'} = d(\mathbf{w}_\lambda \mathbf{d}'_{I\alpha},\ \mathbf{w}_{\lambda'} \mathbf{d}'_{I\alpha})$ we denote a distance between $w_{\lambda\alpha} = \mathbf{w}_\lambda \mathbf{d}'_{I\alpha}$ and $w_{\lambda'\alpha}$. We use functions C_α again. Let us consider next the function of variables $\mathbf{w}_\lambda$ and $\mathbf{w}_\lambda$ in the form

$$M_{I\lambda\lambda'} = C_1(d_{2\lambda\lambda'})d^2_{1\lambda\lambda'} + C_2(d_{1\lambda\lambda'})d^2_{2\lambda\lambda'}\,. \tag{4.12}$$

This function has a similar structure as function (4.11). Therefore, if $\mathbf{w}_\lambda$ develops in one direction then an energetic barrier appears and blocks evolution of $\mathbf{w}_{\lambda'}$ in the other direction.

The functions introduced above describe the process of collective evolution of relative displacement vectors in two possible directions. During evolution of $\mathbf{w}_\lambda$, $\lambda \in \Lambda$, different arrangements of these vectors appear. Previous discussion does not provide appropriate justification for considering separate evolutions $\mathbf{w}_\lambda$ for different λ. However, special arrangements of these vectors lead to two-path martensitic transformation. This phenomenon happens, for instance, in CuAlNi alloy. In this case, during loading and unloading, vectors $\mathbf{w}_\lambda$ change in two different ways. Then, new stress-induced phases appear. They can be distinguished only by positions of the relative displacement vectors. In order to obtain a possibility of modelling such a phenomenon, the following function is postulated:

$$M_{WI\lambda} = \Psi(a_\lambda(e_{I12}) + w_\lambda) - f_\lambda(e_{I12})(a_\lambda(e_{I12}) + w_\lambda), \tag{4.13}$$

where $w_\lambda = |\mathbf{w}_\lambda|$. Form of this function allows to model the evolution of $\mathbf{w}_\lambda$ by dependence on e_{I12} and by control positions of minima of the introduced functions with the help of a_λ and f_λ. By means of similar functions, the two-path martensitic transformation has been discussed in [19].

Finally, the part of the free energy which describes shuffles is suggested in the form

$$F_{W(J)} = \sum_\lambda M_{I\lambda} + \sum_{\lambda \neq \lambda',\ \lambda > \lambda'} M_{I\lambda\lambda'} + \sum_\lambda M_{WI\lambda}\,, \tag{4.14}$$

where $J = (I,\ \alpha)$.

Next component of the free energy describes the evolution of internal rotation towards a habit plane. We have twenty four possible habit planes. They can be marked by multi-index $K = (I,\ \alpha,\ \beta) = (J,\ \beta)$, $\alpha, \beta = 1,\ 2$. The habit plane can be represented by a pair of linearly independent vectors $\mathbf{p}_{K\mu}$, $\mu = 1,\ 2$ which are determined in the crystal structure of austenite. In Sec. 3 we have discussed variables which are appropriate for description of the internal rotation. Let us introduce these variables in a convenient form

$$a_{K\mu} = \mathbf{R}^{-1}(\mathbf{F}^{ea})(\mathbf{F}^s\mathbf{F}^{ea} - \mathbf{R}^{-1}(\mathbf{F}^{ea}))\mathbf{p}_{K\mu}\,. \tag{4.15}$$

The deformation gradient $\mathbf{F}^{ea}$ is assigned to the configuration known and fixed at the moment. Thus, all variables $\mathbf{a}_{K\mu}$ depend in fact only on $\mathbf{F}^s$ as independent variable.

Let V_s be a space of all admissible $\mathbf{F}_s \in V_s(x_\alpha(\mathbf{X}_P))$. V_s depends on a fixed configuration $x_\alpha(\mathbf{X}_P)$ for the considered point $\mathbf{X}_P$.

In the space V_s we define curves $K_{J\beta}(e_{I12})$ which are parameterized by $e_{I12} \in N_{IS}$. They have the following properties: $K_{J1}(e_{I12}) = K_{J2}(e_{I12})$ for $e^*_{I12} < e_{I12} < \bar{e}_{I12}$, where $\bar{e}_{I12}$ only slightly exceeds e^*_{I12}. $K_{J1}(\bar{e}_{I12}) \cap K_{J2}(\bar{e}_{I12}) = B \in V_s$, where B is a bifurcation point for these curves which do not coincide for points $e_{I12} > \bar{e}_{I12}$. Thus, the two curves coincide up to the bifurcation point B accompanied by $\bar{e}_{I12}$. By this we introduce the assumption that internal rotation appears

directly after exceeding e^*_{I12}, and then also the bifurcation process starts. We assume that for $K_{J1}(e^{**}_{I12})$ and $K_{J2}(e^{**}_{I12})$, the following conditions are satisfied: $\mathbf{a}_{J1} = 0$, $\mathbf{a}_{J2} \neq 0$ and $\mathbf{a}_{J2} = 0$, $\mathbf{a}_{J1} \neq 0$, respectively. It means that austenite and martensite are fitted together at the end of these curves. Thus, the $K_{J\beta}$ are viewed as certain paths of deformation and create a skeleton for this part of the free energy.

Let us introduce also a function $g : K_{J\beta} \to R$ which has the following properties:

1. $g(K_{J1}(e_{I12})) = g(K_{J2}(e_{I12}))$ for $e_{I12} \in N_{IS}$,
2. $g(K_{J1}(e^*_{I12})) = 0$, $\dfrac{\partial g}{\partial e_{I12}}(e^*_{I12}) = 0$, $\dfrac{\partial^2 g}{\partial e^2_{I12}}(e^*_{I12}) = 0$,
3. g monotonically decreases on N_{IS},
4. $\dfrac{\partial g}{\partial e_{I12}}(e^{**}_{I12}) = 0$, $\dfrac{\partial^2 g}{\partial e^2_{I12}}(e^{**}_{I12}) > 0$.

These properties prove the symmetry of evolution for two possible internal rotations.

Construction of the part of the free energy which depends on rotation is introduced also with the help of the basis and fibers which together create a graph manifold as a fiber bundle. Let us consider a basis

$$b_{J\beta}(e_{I12}) = \{K_{J\beta}(e_{I12}),\ g(K_{J\beta}(e_{I12}))\}.$$

It is assumed also that parts of the domain can be represented as a generalized product in the form $D_{RJ\beta} = K_{J\beta}(e_{I12}) \times D_{J\beta}(e_{I12}) \subset V_s$ and $D_{RJ1} \cap D_{RJ2} \neq \emptyset$, $D_{RJ1} \cup D_{RJ2} = V_s$. Then, we are able to define

$$f_{J\beta}(e_{I12}) = \{\{D_{J\beta}(e_{I12}),\ g_f(\mathbf{F})(e_{I12})\} :\ \mathbf{F} \in D_{J\beta}(e_{I12})\}$$

with the property that $\inf_{\mathbf{F}} g_f(\mathbf{F}) = g(K_{J\beta}(e_{I12}))$. The infimum is attained for $\mathbf{F} \in K_{J\beta}(e_{I12}) \cap D_{J\beta}(e_{I12})$. $f_{J\beta}$ is viewed as a fiber for defining the graph of the considered part of the free energy. Function g_f attains minimum at intersection of $D_{J\beta}$ and $K_{J\beta}$ or, in other words, at the intersection with the basis $b_{J\beta}$.

Now the mentioned part of graph of the free energy can be defined as

$$F_{R(K)}(\mathbf{F}^s) = \begin{cases} b_{J1}(e_{I12}) \times f_{J1}(e_{I12}), & \mathbf{F}^s \in D_{RJ1}, \\ b_{J2}(e_{I12}) \times f_{J2}(e_{I12}), & \mathbf{F}^s \in D_{RJ2}. \end{cases} \tag{4.16}$$

It is assumed that for $\mathbf{F}^s \in D_{RJ1} \cap D_{RJ2}$ these functions coincide.

The model considered is related to a small volume of averaging. Then, nonlocal effects become more important. These effects can be approximated by higher gradients of deformation.

During the martensitic transformation we observe, in a small scale, the thickness of the interface. On the other hand, the interfaces are flat during the transformation. Furthermore, we can consider breaking of interfaces during the appropriate loading process [27]. Thus, interfaces have many fine features which

should be modelled in a small scale. These phenomena suggest the necessity of taking into consideration higher gradients of deformation as an approximation of nonlocal effects.

Some models which take into account this kind of description of the martensitic transformation are considered in literature. See for instance [22, 23, 4].

In the paper, a concept of application of higher gradients in description of fine features of the interfaces is discussed. First, let us introduce this concept with the aid of a two-dimensional example on a plane. Let ϕ be a field on the plane and $\mathbf{m}$ and $\mathbf{n}$ be two linearly independent vectors. Let us consider a free energy as an example, in the following form:

$$F_\phi = C_m(D_{\mathbf{m}}\phi)^2 + C_n(D^s_{\mathbf{m}}\phi)(D_{\mathbf{n}}\phi)^2. \tag{4.17}$$

It is assumed that the function C_n has properties shown at Fig. 7. It means that it is a symmetric positive function of its argument, it has maximum at point 0 and strongly decreases to zero if the argument increases. If the derivative of rank s in direction $\mathbf{m}$ is large enough, then the dependence of F_ϕ on $D_{\mathbf{n}}\phi$ vanishes. Consequently, propagation of ϕ will be continued first in the $\mathbf{m}$ direction. It happens since the gradient dependence on $D_{\mathbf{m}}\phi$ accelerates the equalization of field ϕ in the $\mathbf{m}$ direction. As a consequence, $D^s_{\mathbf{m}}\phi$ gradually vanishes and propagation in direction $\mathbf{n}$ becomes more active. This concept will be next generalized to a three-dimensional model.

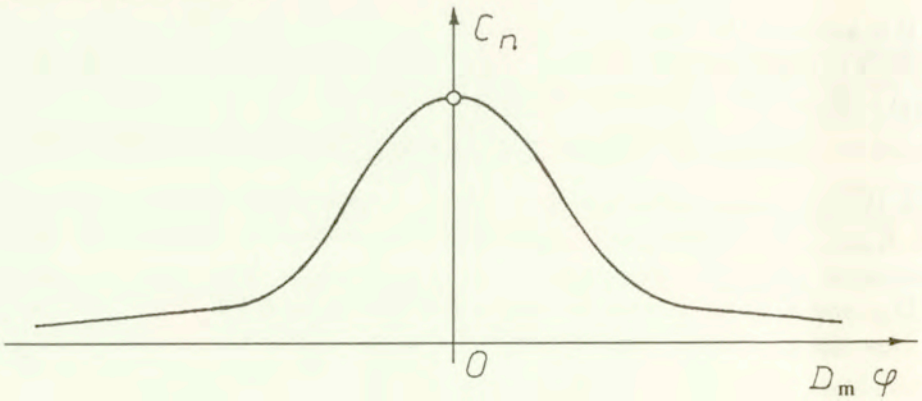

FIG. 7. A qualitative form of function C_n.

A crystal structure, in general, has some distinguished directions. They are connected with arrangement of the atoms. If the interface appears, then some directions can be distinguished on this interface for the same reason.

Let $B_K = \{\mathbf{b}_1, .., \mathbf{b}_N\}$ be a set of distinguished directions on the habit plane HP_K and $\mathbf{v}_K$ be a vector which is perpendicular to this plane. Vectors $\mathbf{b}_1, .., \mathbf{b}_N$ are in general linearly dependent.

Let us consider a point $\mathbf{X}$ which lies on the interface. This fact can be recognized by the state of deformation. Furthermore, we can investigate a deformation

in the neighbourhood of this point and determine what is a preferred direction lying on this habit plane HP_K for this point. More exactly, if the point lies on a flat interface, no direction is preferred. However, if the interface is curved at this point then, it is assumed, a kind of edge on this plane appears. This "edge" reflects the arrangement of atoms and, as a consequence, a preferred direction of the crystal structure. It is assumed that the set B_K is just a set of these preferred directions and they can be recognized by the analysis of deformation near the point $\mathbf{X}$.

Let us introduce a function $p(\mathbf{X}) = \{\mathbf{k},\ \mathbf{l},\ \mathbf{v}_K\}$ which assigns a triplet of vectors to point $\mathbf{X}$. The vector $\mathbf{k} \in B_K$ indicates the preferred direction, $\mathbf{l} \in HP_K$ and $\mathbf{lk} = 0$. Let, furthermore, $\mathbf{M} = \{M_q\} = \{F_{iM},\ w_{\lambda N}\}$ be a set of variables.

After these preparations, the following form of the free energy dependent on higher gradients of deformation is assumed:

$$F_{\mathcal{B}(K)} = \sum_q \Big[C_{kq}(p(\mathbf{X}),\ \mathbf{k})(D_{\mathbf{k}}M_q)^2 + C_{lq}(p(\mathbf{X}),\ \mathbf{l},\ D_{\mathbf{k}}M_q)(D_{\mathbf{l}}M_q)^2 + C_{vq}(p(\mathbf{X}),\ \mathbf{v}_K,\ D_{\mathbf{k}}M_q,\ D_{\mathbf{l}}M_q)(D_{\mathbf{v}}M_q)^2\Big]. \tag{4.18}$$

The idea of dependence of C_{lq} and C_{vq} on $D_{\mathbf{k}}M_q$ and $D_{\mathbf{l}}M_q$ follows from (4.17). If $D_{\mathbf{k}}M_q$ is large enough then C_{lq} and C_{vq} vanishes and development in the $\mathbf{k}$ direction is preferred. Next degree of this hierarchy consists in the fact that the surface is straight in direction $\mathbf{k}$. As a result, we have $D_{\mathbf{k}}M_q = 0$ and then $\mathbf{l}$ is the second direction of development. Third degree of this hierarchy is evidently the $\mathbf{v}_K$ direction.

Let us note that formula (4.18) takes into considerations the symmetry of crystal structure of both the austenite and martensite. It consists in taking into account the distribution of directors $\mathbf{p}_{K\mu}$ which define the habit planes and vectors $\mathbf{v}_K$. Position of habit planes uniquely defines the kind of martensite variant which is fitted together with austenite on this plane. This is just connected with crystal symmetries of these two structures.

Summing up the above considerations, let us notice that we have constructed four summands of the free energy. However, they depend on multi-indices I, J, K. Therefore, the domain of the free energy is not determined clearly enough.

Let us observe that independent variables and their higher gradients do not take all possible values but only some admissible ones. Indeed, we do not expect that, for instance, $\mathbf{w}_\lambda$ takes a very large value. Rather, we define only some admissible domains in the set of all possible values of variables. These domains are defined here by means of multi-indices I, J, K.

Let $\partial S_{AI} = \{\mathbf{e} :\ \mathbf{d}_{I1}\mathbf{e}\mathbf{d}_{I2} = e^*_{I12},\ \mathbf{d}_{I'1}\mathbf{e}\mathbf{d}_{I'2} < e^*_{I'12},\ I \neq I'\}$. With the help of this we obtain $\partial S_A = \bigcup \partial S_{AI}$. The set ∂S_{AI} determines the validity of index I for a further stage of deformation. If the deformation attains this set then it means that the first e^*_{I12} is attained still before $e^*_{I'12}$. As a result, two paths for bifurcation for $\mathbf{w}_\lambda$ are determined and two other for the internal rotation given

in $\mathbf{F}^s$. The equilibrium paths for the relative displacement vector $\mathbf{w}_\lambda$ are given by $\mathbf{w}_{\lambda\alpha} = w_\lambda \mathbf{d}'_{I\alpha}$. We assume that these vectors develop only in some neighbourhood $U(\mathbf{w}_{\lambda\alpha})$ of this paths. It means that the domain of admissible $\mathbf{w}_\lambda$ is

$$W_J = W_{I\alpha} = \{\mathbf{w}_\lambda : \mathbf{w}_\lambda \in U(\mathbf{w}_{\lambda\alpha}),\ \lambda \in \Lambda\} = \Pi_\lambda U(\mathbf{w}_{\lambda\alpha}) . \tag{4.19}$$

Similarly, we assume that $\mathbf{F}_s$ develops near its path $K_{J\beta} = K_K$ in some neighbourhood $U(K_{J\beta})$. Thus, we have

$$V_K = V_{J\beta} = \{\mathbf{F}^s : \mathbf{F}^s \in U(K_{J\beta})\}. \tag{4.20}$$

Dependence of the free energy on higher gradients is connected with the habit plane HP_K. Thus, the set of admissible higher gradients of deformation takes the form

$$H_K = \left\{ \left\{ \frac{\partial}{\partial X_i} M_q \right\} : \quad i = 1, 2, 3 \right\} . \tag{4.21}$$

Finally, we define subdomains of the free energy with the help of multi-indices $K = (I,\ \alpha,\ \beta) = (J,\ \beta)$ as $D_K = E \times W_J \times V_K \times H_K$. Thus, the total domain is assumed as

$$D = \bigcup_K (E \times W_J \times V_K \times H_K). \tag{4.22}$$

The total form of the free energy is then described by means of the expression

$$F_K(g) = F_E + F_{W(J)} + F_{R(K)} + F_{G(K)}, \qquad g \in D_K . \tag{4.23}$$

The free energy can be also expressed with the aid of graph manifold in the following form,

$$\{g,\ F(g)\} = \bigcup_K \bigcup_{g \in D_K} \{g,\ F_K(g)\}. \tag{4.24}$$

It is assumed that in regions where $D_K \cap D_{K'} \neq \emptyset$, the free energy is determined equivalently.

Let us note that such a form of the free energy is relatively simple in comparison with those given in the Landau theory [29]. The expression given by (4.23) reflects many properties which are introduced by the geometrical skeleton of this construction. This skeleton is based on ∂S_A, $\mathbf{d}_I$, symmetries near $\mathbf{e} = \mathbf{0}$, $\mathbf{e} = \mathbf{e}_{MI}$ and directors $\mathbf{p}_{K\mu}$. Accordingly, we are able to introduce terms of the free energy which are responsible for separate phenomena.

Let us observe that second or third-order terms of the free energy in three-dimensional case in the Landau theory [29] are very long polynomials. They are difficult for physical interpretations. In order to express the free energy which is discussed in the paper, the degrees of polynomials have to be much more higher.

The expression (4.23) has a good physical interpretation. It takes place owing to the mentioned geometrical skeleton which is connected just with interpretation of the physical processes.

Summing up this comment we may say that the form of the free energy is relatively simple in comparison with those known from the Landau theory. On the other hand, this form is relatively complicated in comparison with those from the more averaged level of description.

5. Thermodynamical description of the martensitic transformation

The model with small volume of averaging describes the detailed behaviour of microstructure. Therefore, the free energy introduced in the previous section is relatively complicated. This function is a basis for the model discussed in the paper. As a next step, balance equations and a more general form of constitutive equations will be discussed.

Let us note that during kinematical considerations, a few displacement functions have been introduced. It follows from the micrononhomogeneous deformation which appears during the martensitic transformation. Such a deformation is connected with complex crystal lattice. It suggests a multicomponent description. However, in general, we would like to avoid such a description since it is too complicated. On the other hand, relative displacement of atoms are not a large deviation from homogeneity. Consequently, the one-component description is most appropriate. In such a case the presence of relative displacement vectors can be viewed as a result of a multicomponent approach.

In the first stage of our considerations, energy balance equations for multicomponent body are introduced. Next, we approximate them by a balance equation connected with one-component description, with some effects which are a result of the initial approach.

Let us introduce a set of displacement functions discussed in Sec. 3

$$\mathbf{z}_\mu(\mathbf{X},\ t) = \{\mathbf{x}(\mathbf{X},\ t),\ \mathbf{y}_\lambda(\mathbf{X},\ t) = \mathbf{x} + \mathbf{R}\mathbf{w}_\lambda\}, \tag{5.1}$$

where $\lambda \in \Lambda$, $\mu \in \{0\} \cup \Lambda$. The approximation assumed for function $\mathbf{y}_\lambda$ was discussed in the previous section.

Let us introduce the expressions for energy related to various components of the body

$$\Psi_0 = \int\limits_{\chi(\mathcal{B})} \left(\varrho_0 e + \frac{1}{2}\varrho_0 \dot{x}_i \dot{x}_i\right) dv\,, \qquad \Psi_\lambda = \int\limits_{\chi_\lambda(\mathcal{B})} \left(\varrho_\lambda e + \frac{1}{2}\varrho_\lambda \dot{y}_{\lambda i} \dot{y}_{\lambda i}\right) dv, \tag{5.2}$$

where e is the internal energy density, ϱ_0, ϱ_λ are densities related to individual components and $(\varrho_0 + \sum_\lambda \varrho_\lambda) = \varrho$. In this notation we have also $\Psi_\mu = \{\Psi_0,\ \Psi_\lambda\}$.

The following general form of the balance equation is assumed for considerations [26] as an initial stage

$$\sum_\mu \frac{d}{dt}\Psi_\mu = \sum_\mu \left(-\Phi_\mu(\Psi_\mu) + P_\mu(\Psi_\mu) + S_\mu(\Psi_\mu)\right), \tag{5.3}$$

where Φ_μ is outflow of the conserved quantity Ψ_μ through the boundary of the body, P_μ is the production and S_μ is the source of this quantity.

Taking into account higher gradients of deformation discussed in the model of the free energy, we assume the following form of the outflow Φ_μ:

$$\Phi_\mu(\Psi_\mu) = \int\limits_{\partial\chi_\mu(\mathcal{B})} \left(q_\mu - \sum_{\phi=0}^{G-1} t_{\mu M_1 \ldots M_\phi i} \dot{x}_{i,M_1 \ldots M_\phi} - \sum_{\phi=0}^{H-1} f_{\mu N N_1 \ldots N_\phi} \dot{w}_{\mu N, N_1 \ldots N_\phi} \right) da_\mu , \tag{5.4}$$

where the last term exists only for $\mu = \lambda > 0$.

The remaining parts of equation (5.3) are postulated as

$$P_\mu(\Psi_\mu) = \int\limits_{\chi_\mu(\mathcal{B})} p_{e\mu} dv_\mu \tag{5.5}$$

and

$$S_\mu(\Psi_\mu) = \int\limits_{\chi_\mu(\mathcal{B})} \varrho_\mu (r_\mu + b_{\mu i} \dot{z}_{\mu i}) dv_\mu . \tag{5.6}$$

Let us substitute (5.2), (5.4)–(5.6) into (5.3). Next we perform the limit approximation. Assuming that $\mathbf{w}_\lambda \to 0$ we obtain a one-component body. Then, we assume that

$$\chi_\mu(\mathcal{B}) \to \chi(\mathcal{B}), \qquad \sum_\mu q_\mu \to q, \qquad \sum_\mu t_{\mu M_1 \ldots M_\phi i} \dot{x}_{i,M_1 \ldots M_\phi} \to t_{M_1 \ldots M_\phi i} \dot{x}_{i,M_1 \ldots M_\phi} ,$$

$$\sum_\mu p_{e\mu} \to p_e , \qquad \sum_\mu \varrho_\mu r_{e\mu} \to r_e , \qquad \sum_\mu \varrho_\mu b_{\mu i} \dot{z}_{\mu i} \to b_i \dot{x}_i .$$

However, we do not carry out this transformation consistently. The last term of the sum (5.4) and the kinetic energy in (5.2) related to relative displacement vectors remain. After applying the well-known steps in deriving the balance equations and assuming that $q = \mathbf{qn}$, we obtain the following form of the energy balance equation:

$$\int\limits_{\chi(\mathcal{B})} \left[\varrho \dot{e} + \varrho_0 \ddot{x}_i \dot{x}_i + \sum_\lambda \varrho_\lambda \ddot{y}_{\lambda j} \dot{y}_{\lambda j} + q_{j,j} - p_e - r_e - b_i \dot{x}_i \right] dv$$
$$- \int\limits_{\partial\chi(\mathcal{B})} \left(\sum_{\phi=0}^{G-1} t_{M_1 \ldots M_\phi i} \dot{x}_{i,M_1 \ldots M_\phi} + \sum_\lambda \sum_{\phi=0}^{H-1} f_{\lambda N N_1 \ldots N_\phi} \dot{w}_{\lambda N, N_1 \ldots N_\phi} \right) da = 0. \tag{5.7}$$

Let us consider the kinetic energy part more carefully. Using definition of $\mathbf{y}_\lambda$ we have

$$(5.8)\qquad \sum_\mu \varrho_\mu \ddot{z}_{\mu i}\,\dot{z}_{\mu i} = \varrho_0\,\ddot{x}_i\,\dot{x}_i + \sum_\lambda \varrho_\lambda\,\ddot{y}_{\lambda i}\,\dot{y}_{\lambda i} = \left(\varrho_0 + \sum_\lambda \varrho_\lambda\right)\ddot{x}_i\,\dot{x}_i + \sum_\lambda \varrho_\lambda\,(\ddot{y}_{\lambda i} - \ddot{x}_i)\,\dot{x}_i + \sum_\lambda \varrho_\lambda\,(\ddot{y}_{\lambda i} - \ddot{x}_i)\,\dot{\xi}_i + \sum_\lambda \varrho_\lambda\,\ddot{x}_i\,\dot{\xi}_i \approx \varrho\,\ddot{x}_i\,\dot{x}_i + \sum_\lambda \varrho_\lambda\,\ddot{w}_{\lambda N}\,\dot{w}_{\lambda N}\,.$$

In the last step, interactions between the macroscopic inertia effects represented by time derivatives of x_i and the microscopic inertia effects represented by relative displacement vectors are neglected. It means that the influence of macroscopic motion on relative displacement vectors is due to the internal forces in the material represented by the free energy.

Next problem is related to the internal rotation. The free energy depends not only on the strain tensor but also on the internal rotation in the spinodal region. This suggests the necessity to investigate more carefully the balance of angular momentum. It will be done later. The internal rotation mentioned is connected also with certain inertia effects.

The moment of inertia tensor for the part $\mathcal{P}$ of the body $\mathcal{B}$ is defined by formula $I_{mn} = \int_{\mu(\mathcal{P})} \varrho\varepsilon_{mri}\varepsilon_{ink}r_r r_k dv$, where $\mathbf{r} = \mathbf{x} - \mathbf{x}_c$ is position of the point with respect to the center of mass of $\mathcal{P}$. The moment of inertia density can be defined as

$$i_{mn} = \frac{\partial I_{mn}}{\partial \mu(\mathcal{P})} = \varrho\varepsilon_{mri}\varepsilon_{ink}r_r r_k\,.$$

However, if $\mu(\mathcal{P}) \to 0$ then $\mathbf{r} \to 0$ and finally $i_{mn} = 0$.

The martensitic structure created during the phase transformation tends to fit together with austenite. It happens with the help of material forces which are created by locally nonhomogeneous deformation. It means that atoms are shifted from the averaged positions which are determined by the deformation function. As a result, a local distribution of density with respect to the assumed averaged density is changed. Consequently, we admit for qualitative considerations, that there is a translation $\delta\mathbf{r}$ of the averaged density from the material point in nonequilibrium state with respect to the internal rotation. This shift of density is not connected with the introduced relative displacement vectors since they characterize durable shift of atoms and are constant in martensitic phase. Accordingly, we assume that

$$i_{mn} = \frac{\partial I_{mn}}{\partial \mu(\mathcal{P})} = \varrho\varepsilon_{mri}\varepsilon_{ink}(r_r + \delta r_r)(r_k + \delta r_k) = \varrho\varepsilon_{mri}\varepsilon_{ink}\delta r_r \delta r_k\,.$$

We assume here that during $\mu(\mathcal{P}) \to 0$, an averaging shift of density $\delta\mathbf{r} \neq 0$ can be considered.

In order to take into account the inertia effects related to internal rotations, the kinetic energy term

$$I_k = \frac{1}{2}\int i_{mn}\omega_m\omega_n dv,$$

where $\omega_n = \frac{1}{2}\varepsilon_{nij}(\dot{x}_i)_{,j}$. The term I_k should be added to the formula for the total energy of the body. If we investigate the expression $\frac{d}{dt}I_k$ then we obtain a formula with two main parts. The first one is connected with conservation of i_{mn} and the second one has the form $\int i_{mn}\dot{\omega}_m\omega_n dv$. In the considered case we assume for simplicity, that the term related to conservation of i_{mn} is equal to zero. The author introduces this simplification in order to avoid complicated considerations accompanied by relatively simple effects of a rotational inertia. However, total neglecting of these inertial effects leads to qualitative complications in the balance of angular momentum. Therefore, in what follows, only the last term will be introduced into the balance of energy equation.

In order to predict the final form of energy balance equation and balance of linear momentum, it is assumed that dissipation is introduced by adding and then subtracting the same term in the balance of energy equation (5.7).

$$(5.9)\qquad T^d_{iM}\dot{x}_{i,M} + \sum_\lambda f^d_{\lambda N}\dot{w}_{\lambda N} - T^d_{iM}\dot{x}_{i,M} - \sum_\lambda f^d_{\lambda N}\dot{w}_{\lambda N}$$
$$= -T^d_{iM,M}\dot{x}_i + \sum_\lambda f^d_{\lambda N}\dot{w}_{\lambda N} + (T^d_{iM}\dot{x}_i)_{,M} - T^d_{iM}\dot{x}_{i,M} - \sum_\lambda f^d_{\lambda N}\dot{w}_{\lambda N}.$$

Let $F = \varrho\psi$ and $e = \psi + sT$. We assume that ψ depends on higher gradients of deformation and, furthermore, on some internal state variables $\boldsymbol{\mu}$ which will be discussed in what follows. Then, taking into account the above discussion, the energy balance equation (5.7) is modified and assumes the form

$$(5.10)\qquad \int_{\chi(\mathcal{B})}\Bigg[(-T_{iM,M} + \varrho\,\ddot{x}_i - b_i)\dot{x}_i + \sum_\lambda (f_{\lambda N} + \varrho_\lambda\,\ddot{w}_{\lambda N})\dot{w}_{\lambda N} + \varrho\Big(\frac{\partial\psi}{\partial T} + s\Big)\dot{T}$$
$$+ \varrho\dot{s}T - T^d_{iM}\dot{x}_{i,M} - \sum_\lambda f^d_{\lambda N}\dot{w}_{\lambda N} + q_{i,i} - r_e + \varrho\frac{\partial\psi}{\partial\mu_i}\dot{\mu}_i\Bigg]dv$$
$$+ \int_{\partial\chi(\mathcal{B})}\Bigg[\sum_{\phi=0}^{G-1}(\bar{t}_{iM_1\ldots M_\phi j}n_j - t_{iM_1\ldots M_\phi})\dot{x}_{i,M_1\ldots M_\phi} + (T^d_{iM}x_{j,M})n_j\dot{x}_i$$
$$+ \sum_\lambda\sum_{\phi=0}^{H-1}(\bar{f}_{\lambda NN_1\ldots N_\phi j}n_j - f_{\lambda NN_1\ldots N_\phi})\dot{w}_{\lambda N,N_1\ldots N_\phi}\Bigg]da = 0,$$

where

$$T_{iM} = \tilde{T}_{iM} + B_{iM} + T^d_{iM}, \qquad f_{\lambda N} = \varrho\frac{\partial\psi}{\partial w_{\lambda N}} + F_{\lambda NN_1,N_1} + f^d_{\lambda N},$$

and furthermore

$$\tilde{T}_{iM_1} = \sum_{s=1}^{G}(-1)^{s+1}\left(\varrho\frac{\partial\psi}{\partial x_{i,M_1\ldots M_s}}\right)_{,M_s\ldots M_2},$$

$$B_{iM} = \frac{1}{2}i_{mn}\dot{\omega}_m\varepsilon_{nij}x_{M,j},$$

$$F_{\lambda NN_1} = \sum_{s=1}^{H}(-1)^{s}\left(\varrho_\lambda\frac{\partial\psi}{\partial w_{\lambda N,N_1\ldots N_s}}\right)_{,N_s\ldots N_2},$$

$$\bar{t}_{iM_1\ldots M_\phi j} = \sum_{s=\phi+1}^{G}(-1)^{s-\phi+1}\left(\varrho\frac{\partial\psi}{\partial x_{i,M_1\ldots M_s}}\right)_{,M_sM_{s-1}\ldots M_{\phi+2}} x_{j,M_{\phi+1}},$$

$$\overline{f}_{\lambda NN_1\ldots N_\phi j} = \sum_{s=\phi+1}^{H}(-1)^{s-\phi+1}\left(\varrho_\lambda\frac{\partial\psi}{\partial w_{\lambda N,N_1\ldots N_s}}\right)_{,N_sN_{s-1}\ldots N_{\phi+2}} x_{j,N_{\phi+1}}.$$

Assuming the processes in Eq. (5.10) to be time-independent, the balance of linear momentum is expressed by

$$-T_{iM,M} + \varrho\,\ddot{x}_i - b_i = 0 \tag{5.11}$$

in the body $\mathcal{B}$, and

$$\bar{t}_{iM_1\ldots M_\phi j}n_j = t_{iM_1\ldots M_\phi} \tag{5.12}$$

on $\partial\mathcal{B}$, where $\phi = 0, \ldots, G-1$. Furthermore, the term $\bar{t}_{iM_1}$ is modified by adding $T^d_{iM_1}$ to the above defined expression. The remaining equations are

$$f_{\lambda N} + \varrho_\lambda\,\ddot{w}_{\lambda N} = 0 \tag{5.13}$$

in $\mathcal{B}$, and

$$\overline{f}_{\lambda NN_1\ldots N_\phi j}n_j - f_{\lambda NN_1\ldots N_\phi} = 0 \tag{5.14}$$

on $\partial\mathcal{B}$, $\lambda \in \Lambda$.

If the above linear momentum equations are fulfilled then the local form of energy balance equation is given by

$$\varrho\dot{s}T - T^d_{iM}\dot{x}_{i,M} - \sum_\lambda f^d_{\lambda N}\dot{w}_{\lambda N} + q_{i,i} - r_e + \varrho\frac{\partial\psi}{\partial\mu_i}\dot{\mu}_i = 0. \tag{5.15}$$

Let us consider the balance of angular momentum which can be expressed in the well-known form

$$\int_{\chi_\mu(\mathcal{B})}\left[\varepsilon_{ijk}x_j(t_{mk,m} + b_k - \varrho\,\ddot{x}_k) + \varepsilon_{ijk}t_{jk}\right]dv = 0, \tag{5.16}$$

where $t_{jk} = J^{-1}x_{k,M}T_{jM}$. Assuming that the balance of linear momentum is fulfilled we obtain $\varepsilon_{ijk}t_{jk} \equiv \varepsilon_{ijk}J^{-1}x_{k,M}T_{jM} = 0$ what leads to

$$\varepsilon_{ijk}x_{k,M}\overline{T}_{jM} = -\varepsilon_{ijk}x_{k,M}B_{jM}\,, \tag{5.17}$$

where $\overline{T}_{jM} = \widetilde{T}_{jM} + T^d_{jM}$. Consequently, introducing the corrective moment of inertia density field gives a possibility of taking into account the inertial reaction of the material on the internal forces acting there during the martensitic transformation.

Equation (5.13) obtained as a result of balance of linear momentum is close to phonon dynamics and it is difficult to expect that in dynamical case it will give correct results. Therefore, rather an approximation procedure is suggested in this place. Equation (5.13) can be discussed in case of slow deformational processes. In such a case we can assume that $\dot{\mathbf{w}}_\lambda \approx 0$. Then, the relation $f_{\lambda N} = 0$ is obtained. Let us consider the theory with $H = 1$. It means that only the first gradients of $\mathbf{w}_\lambda$ are considered. Then, the discussed equation takes the form

$$-\left(\varrho\frac{\partial\psi}{\partial w_{\lambda N,N_1}}\right)_{,N_1} + \varrho\frac{\partial\psi}{\partial w_{\lambda N}} = 0. \tag{5.18}$$

Gradients of $\mathbf{w}_\lambda$ generate a bifurcation of $\mathbf{w}_\lambda$ in some neighbourhood occurring in the same direction.

Equation (5.18) creates a relation $\mathbf{w}^*_\lambda = \mathbf{w}^*_\lambda(g')$, where g' is the part of the deformation measure which does not contain $\mathbf{w}_\lambda$. However, this relation is not a function since bifurcation processes are considered. Therefore, it is difficult to neglect equation (5.13). This equation in the approximate form (5.18) allows to eliminate $\mathbf{w}_\lambda$ but all complications related to modelling the bifurcations remain. Finally, the variable $\mathbf{w}_\lambda$ seems to be appropriate for modelling the free energy even in the simplified version by means of the relation $\mathbf{w}^*_\lambda = \mathbf{w}^*_\lambda(g')$.

On the other hand, micrononhomogeneous deformation increases the amount of dissipation. Then, it is assumed, it would be appropriate to plot an internal state variable with evolution of $\mathbf{w}^*_\lambda$.

Summing up these considerations we state that equation (5.13) could be replaced by Eq. (5.18) and dynamical effects related to phonon mechanics level could be described by an internal state variable and their evolution equation.

The problem of dissipation is accompanied also by the stabilization of martensite. During heat treatment of the material undergoing the martensitic transformation we obtain considerable differences in temperatures of transformations for different cycles of this process. Such a phenomenon is called the stabilization of martensite. Main reason for the changes of transformation temperatures is the evolution of vacancy density ϱ which can block the interfaces [24, 25]. This is an important phenomenon from the termomechanical point of view. In general, we admit thermal processes with miscellaneous time scales. Deformational processes

are also responsible for defects and dislocation densities. Therefore, in general, internal state variables ϱ which represent densities of dislocations and defects should have influence on temperatures of transformations by the free energy.

Let us introduce notations $\mathcal{R} = \{\psi,\ \mathbf{T},\ \mathbf{f}_\lambda,\ s,\ \mathbf{q}\}$, $\mathcal{H} = \{g,\ T_{,j}\}$, where $g \in D$ was introduced in the previous section. Let $\boldsymbol{\alpha}$ be a group of internal state variables responsible for dissipation induced by micrononhomogeneous deformation and phase transformation. Let ϱ be a set of variables for description of the stabilization of martensite phenomenon. Then, a general form of constitutive equations is assumed in the form

$$\mathcal{R} = \mathcal{R}(\mathcal{H},\ \boldsymbol{\alpha},\ \varrho), \tag{5.19}$$

$$\dot{\boldsymbol{\alpha}} = A(\mathcal{H},\ \boldsymbol{\alpha},\ \varrho), \tag{5.20}$$

$$\dot{\varrho} = B(\mathcal{H},\ \boldsymbol{\alpha},\ \varrho), \tag{5.21}$$

where some equations have been previously discussed in detail.

The introduced constitutive equations have to satisfy the Clausius–Duhem inequality which in the considered case has the form

$$T^d_{iM}\dot{x}_{i,M} + \sum_\lambda f^d_{\lambda N}\dot{w}_{\lambda N} - (q_i T_{,i})/T - \varrho\frac{\partial\psi}{\partial\alpha_i}\dot{\alpha}_i - \varrho\frac{\partial\psi}{\partial\varrho_i}\dot{\varrho}_i \geq 0. \tag{5.22}$$

The last inequality is derived with the help of the well-known Clausius–Duhem inequality [28] and local form of the balance energy equation (5.15).

Internal state variables are considered in continuum theory in order to take into account phenomena or effects of a smaller scale. The model is related to small volume of averaging. Then, the question is what scale is appropriate for justification or interpretation of internal state variables and their evolution equations (5.20), (5.21). Undoubtedly, it has to be a discrete level of description. Thus, variables $\boldsymbol{\alpha}$ are related to phonon behaviour during micrononhomogeneous deformation or jump over an energetic barrier which appears during the phase transformation. Similarly, micrononhomogeneous deformation given by ϱ is close to a discrete level.

It follows that the model of the martensitic transformation discussed in the paper should be supported by discrete calculations.

6. Final remarks

The model with small volume of averaging introduced in the paper can be used for the description of evolution of microstructure which appears during the martensitic transformation. In particular, it is referred to motion of separate interfaces and their behaviour during various forms of loading. Therefore the model of the free energy is relatively complicated and consists of many constants and functions. Unfortunately, they are not entirely identified. Some of them can

be determined by experiments. In general, it is assumed that this model will be supported by discrete calculations. Consequently, the introduced description of the martensitic transformation is viewed to be a bridge between more averaged models and descriptions on atomic level.

Furthermore, the introduced scale of averaging seems to be very convenient for modelling the interactions between various phenomena occurring in materials and the martensitic transformation.

References

1. Z. NISHIYAMA, *Martensitic transformation*, Academic Press, 1978.
2. Z. NISHIYAMA and S. KAJIWARA, *Electron microscope study of the crystal structure of the martensite in a copper aluminium alloy*, Jap. J. App. Phys., **2**, 8, 1963.
3. K. OTSUKA, H. SAKAMOTO and K. SHIMIZU, *Successive stress-induced martensitic transformation and associated transformation plasticity*, Acta Metall., **27**, 585, 1979.
4. F. FALK, *One-dimensional model of shape memory alloys*, Arch. Mech., **35**, 63–84, 1983.
5. R.D. JAMES, *The propagation of phase boundaries in elastic bars*, Arch. Rational Mech. Anal., **77**, 125, 1980.
6. R.D. JAMES, *Displacive phase transformations in solids*, J. Mech. Phys. Solids, **34**, 359, 1986.
7. K. BHATTACHARYA, *Self-accommodation in martensite*, Arch. Rational Mech. Anal., **120**, 201–244, 1992.
8. K. BHATTACHARYA, *Comparison of geometrically nonlinear and linear theories of martensitic transformation*, Continuum Mech. Thermodyn., **5**, 205–242, 1993.
9. I. MÜLLER and K. WILMAŃSKI, *A model for phase transition in pseudoelastic bodies*, Il Nuovo Cim., **57**, 283–318, 1980.
10. I. MÜLLER, *Pseudoelasticity in shape memory alloys – an extreme case of thermoelasticity*, Proc. Symp. "Thermoelasticita Finita" Acc. Naz. dei Lincei, Centro Interdisciplinare, N. 76, 1986.
11. B. RANIECKI and C. LEXCELLENT, *R_L-models of pseudoelasticity and their specification for some shape memory solids*, Eur. J. Mech. A/Solids, **13**, 21–50, 1994.
12. B. RANIECKI, C. LEXCELLENT and K. TANAKA, *Thermodynamic models of pseudoelastic behaviour of shape memory alloys*, Arch. Mech., **44**, 261–284, 1992.
13. T. INOUE and Z. WANG, *Coupling between stress, temperature, and metallic structures during processes involving phase transformations*, Mater. Sci. Technol., **1**, 845, 1985.
14. K. TANAKA and S. NAGAKI, *A thermomechanical description of materials with internal variables in the process of phase transitions*, Ing. Archiv, **51**, 287–299, 1982.
15. S. FU, Y. HUO and I. MÜLLER, *Thermodynamics of pseudoelasticity – an analytical approach*, Acta Mech., **99**, 1–19, 1993.
16. F.D. FISCHER, M. BERVEILLER, K. TANAKA and E.R. OBERAIGNER, *Continuum mechanical aspects of phase transformations in solids*, Arch. Appl. Mech., **64**, 54–85, 1994.
17. J. KACZMAREK, *A thermodynamical model of solids undergoing martensitic phase transformation with shuffles*, Arch. Mech., **45**, 167–181, 1993.
18. J. KACZMAREK, *A model of the free energy for materials which undergo martensitic phase transformations with shuffles*, Int. J. Engng. Sci., **32**, 369–384, 1994.

19. J. KACZMAREK, *Stress-strain relation for materials which undergo two-path stress-induced displacive phase transition*, Int. J. Engng. Sci., **29**, 883–888, 1991.

20. J. KACZMAREK, *A formulation of continuum mechanics as a dimensional reduction of a finite dimensional dynamical system*, Arch. Mech., **49**, 49–66, 1997.

21. H. TAS, L. DELAEY and A. DERUYTTERE, *The self-accomodating character of the β_1' copper-alluminium martensite*, Met. Trans., **4**, 2833, 1973.

22. G.R. BARSCH and J.A. KRUMHANSL, *Twin boundaries in ferroelastic media whitout interface dislocations*, Phys. Rev. Lett., **53**, 1069–1072, 1984.

23. G.R. BARSCH and J.A. KRUMHANSL, *Nonlinear and nonlocal continuum model of transformation precursors in martensites*, Met. Trans., **19A**, 761–775, 1988.

24. J. JANSSEN, J. VAN HUMBECK, M. CHANDRASEKARAN, N. MWAMBWA and L. DELAEY, *Stabilization of martensite in copper-zinc-aluminium alloys*, J. de Phys., Supplement C4, **43**, 715–720, 1982.

25. J. VAN HUMBECK, D. SEGERS and L. DELAEY, *The stabilization of step-quenched copper-zinc-aluminium martensite III*, Scripta Met., **19**, 477–480, 1985.

26. A.C. ERINGEN and J.D. INGRAM, *A continuum theory of chemically reacting media*, Int. J. Engng. Sci., **3**, 197–212, 1965.

27. J.W. CHRISTIAN, *Deformation by moving interfaces*, Met. Trans., **13A**, 509–538, 1982.

28. C. TROUSDELL and R.A. TOUPIN, *Classical field theories*, Encyclopedia of Physics, FLÜGGE [Ed.], III/1, Springer Verlag, 1960.

29. J.K. LIAKOS and G.A. SAUNDERS, *Application of the Landau theory to elastic phase transitions*, Phil. Mag., A **46**, 217–242, 1982.

30. C. VON WESTENHOLTZ, *Differential forms in mathematical physics*, North Holland Publishing Company, 1981.

POLISH ACADEMY OF SCIENCES
INSTITUTE OF FLUID-FLOW MACHINERY
ul. J.Fiszera 14, 80-952 Gdańsk, Poland.

Received February 10, 1997; new version August 18, 1997.

Arch. Mech., 50, 1, pp. 83–89, Warszawa 1998
FIFTY YEARS OF THE ARCHIVES OF MECHANICS

Control of the mechanical systems by means of sliding modes and the solution to the problem of constraint reactions

S. KOTOWSKI (WARSZAWA)

A NEW METHOD of determination of the constraint reactions in mechanics is introduced in this paper; the methods of investigation of the sliding modes in systems of variable structure are used.

1. Introduction

IN THIS ARTICLE, the methodology of control will be presented aimed at achieving accurate tracking of a class of nonlinear systems in the presence of disturbances and parameter uncertainty, and also applications of this method to the determination of the constraint reactions in analytical mechanics. In an ideal form, the method uses piecewice continuous control laws, resulting in the fact that the trajectory is sliding along the discontinuity or sliding surfaces. Proper selection of the methods leads to a perfect tracking of the required law of motion , but in reality the disturbances cause that the trajectory chatters near the sliding surface, what results in undesirable high-frequency vibration in the state trajectory.

Let us consider a piecewice continuous differential model, with discontinuos right-hand side, on the hypersurface. If the trajectories approach the discontinuity surface and, after reaching this position, stay on this surface, the surface is named the sliding surface. The sliding surface imposes certain type of constraints on the system dynamics. By suitable choice of the nonlinear systems, application of the discontinuous control law and the sliding surface, it is possible to obtain a situation in which the sliding surface accurately describes the dynamics of the systems and their trajectory, using the simplest type of control, the on-off control. In a multidimensional problem, the trajectory lies on the intersection of all the discontinuity surfaces.

2. Systems of variable structure

Systems of variable structure, which are subjected to the sliding motion, are most often described by differential equations with a linear control input. They

have the following form:

$$\dot{x} = F(x) + Bu, \qquad s = Kx,$$

$$u = \begin{cases} u^+ & \text{for } s > 0, \\ u^- & \text{for } s < 0, \end{cases} \tag{1}$$

where $F(x)$ – n vector function, B – $n \times m$ matrix, x – n vector, u – m vector, K – $m \times n$ matrix.

The system which is described in such a way has a variable structure which is determined by the control function u, varying on the surface (in our case s is a hyperplane). We shall consider the properties of a motion which takes place on a switching surface, which is called a sliding motion. When the sliding conditions [1] are satisfied, then the sliding motion which is described by the differential equation (1) occurs on the discontinuity surface [1, 3]:

$$\dot{x} = F(x) - B(KB)^{-1}KF(x). \tag{2}$$

A situation, in which the sliding trajectory lies on the intersection of all of the discontinuity surfaces and the dynamics of the motion on this surfaces is independent of the dynamics outside the surfaces, is analogous to the mechanical systems with constraints.

3. Mechanical systems with constraints

Let us consider the mechanical system described by the first mode Lagrange equations [5]

$$m_i \ddot{\xi}_i = F_i + \sum_{k=1}^{a} \lambda_k \frac{\partial f_k}{\partial \xi_i} + \sum_{c=1}^{b} \mu_c h_{ci} \qquad (i = 1, \ldots, 3n), \tag{3}$$

$$f_k(t, \xi_1, \ldots, \xi_{3n}) = 0, \qquad k = 1, \ldots, a,$$

$$\sum_{i=1}^{3n} h_{ci}\dot{\xi}_i + D_i = 0, \qquad c = 1, \ldots, b.$$

This equation can be transformed into the form of the first order matrix equation by the substitution:

$$\xi_i = x_i, \qquad \dot{\xi}_i = x_{3n+i}.$$

Then, the equation takes the form

$$M\dot{x} = F + W\lambda + H\mu, \tag{4}$$

$$f_k(t, x_1, \ldots, x_{3n}) = 0, \qquad k = 1, \ldots, a,$$

$$\sum_{i=1}^{3n} h_{ci} x_{3n+i} + D_i = 0, \qquad c = 1, \ldots, b.$$

where the matrices and vectors have the following form:

$$M = \begin{bmatrix} 1 & 0 & \cdots & \cdots & \cdots & 0 \\ 0 & \ddots & & & & \vdots \\ \vdots & & 1_{3n} & & & \vdots \\ \vdots & & & m_1 & & \vdots \\ \vdots & & & & \ddots & 0 \\ 0 & \cdots & \cdots & \cdots & 0 & m_{3n} \end{bmatrix},$$

$$\dot{x}^T = [\dot{x}_1, \ldots, \dot{x}_{6n}],$$

$$F^T = [x_1, \ldots, x_{3n}, F_1, \ldots, F_{3n}],$$

$$W = \begin{bmatrix} 0 & \cdots & \cdots & \cdots & 0 \\ \vdots & & & & \vdots \\ 0 & & 0 & \cdots & 0 \\ \vdots & & \vdots & \dfrac{\partial f_k}{\partial x_i} & \\ 0 & \cdots & 0 & & \end{bmatrix} - 6 \times (3n + a) \text{ matrix},$$

$$\lambda^T = [0, \ldots, 0, \lambda_1, \ldots, \lambda_a] \quad - \quad (3n + a) \text{ vector},$$

$$H = \begin{bmatrix} 0 & \cdots & \cdots & \cdots & 0 \\ \vdots & & & & \vdots \\ 0 & & 0 & \cdots & 0 \\ \vdots & & \vdots & h_{ci} & \\ 0 & \cdots & 0 & & \end{bmatrix} - 6 \times (3n + b) \text{ matrix},$$

$$\mu^T = [0, \ldots, 0, \mu_1, \ldots, \mu_b] \quad - \quad (3n + b) \text{ vector}.$$

Then, we should construct the abstract variable structure system, which would be similar to our mechanical systems in the meaning that the product which represents the reactions of constraints in a mechanical system is replaced by the matrix with discontinuos control in the system of a variable structure. It realizes the sliding motion on all the constraint surfaces, which replace the discontinuity surfaces in this model. If, in this model, the conditions of existence of the sliding solutions are fulfilled, then the sliding motion is unique on the discontinuity (constraints) surfaces. Hence it corresponds to the motion of mechanical systems with constraints, so that the respective elements of these models

should be equal. This fact implies that a part of the equation which represents the equivalent control in the sliding model is equal to the part which represents the reactions of constraints in the mechanical model, which is described by the first mode Lagrange equations. Then by calculating the equivalent control in the sliding mode we could obtain the constraint reactions of the mechanical systems.

The determination of the constraint reactions is one of the most difficult problems of analytical mechanics. The possibility of solving this problem, by its replacement with a less complicated equivalent problem, is crucial to this theory and opens new opportunities for the analysis of mechanical systems.

A variable structure model similar to Eq. (4), has the form

$$M\dot{x} = F + Bu, \tag{5}$$

where B is the $6n \times (a+b)$ matrix, M, F, x are the same as in the mechanical system (4), and u is a vector of discontinuous control in the form:

$$u^T = [u_1, \ldots, u_{a+b}],$$

$$u_i = \begin{cases} u_i^+ & \text{for } s_i > 0, \\ u_i^- & \text{for } s_i < 0, \end{cases}$$

$$f_k(t, x_1, \ldots, x_{3n}) = 0, \qquad k = 1, \ldots, a,$$

$$\sum_{i=1}^{3n} h_{ci} x_{3n+i} + D_i = 0, \qquad c = 1, \ldots, b.$$

Then we can determine the matrix K, the rows of which consist of the gradient constraint surfaces s_i:

$$K = \left[\frac{\partial f_k}{\partial x_i}, h_{ci}\right] \quad (a+b) \times 6n \text{ matrix}. \tag{6}$$

Once these parameters are known, we can determine the sliding mode equation for this mechanical systems (5):

$$M\dot{x} = F - B(KB)^{-1}KF. \tag{7}$$

Since this equation is unique, it describes the same motion as the Eq. (4) in [4]. It means that the components which represent the equivalent control should be the same as the elements $W\lambda + H\mu$ in the mechanical system equation (4).

Then we get the equation for the unknown reactions of constraints

$$W\lambda + H\mu = -B(KB)^{-1}KF. \tag{8}$$

This equation connects the constraint reactions with the equivalent control in the discontinuous (variable structure) systems and enable the determination

of constraint reactions without solving the equations of motion, what simplifies the problem of solution of the equations of motion.

EXAMPLE 1. Let us verify our theory on a simple example taken from the paper [3].

$$\ddot{x} = u, \qquad s = cx + \dot{x}, \qquad u = \operatorname{sgn}[s].$$

This equation can be transformed into the form

$$\begin{bmatrix} \dot{x}_1 \\ \dot{x}_2 \end{bmatrix} = \begin{bmatrix} 0 & 1 \\ 0 & 0 \end{bmatrix} \begin{bmatrix} x_1 \\ x_2 \end{bmatrix} + \begin{bmatrix} 0 \\ 1 \end{bmatrix} u, \tag{9}$$

$$s = cx_1 + x_2 .$$

Gradient of the discontinuity surface takes the form

$$\left[\frac{\partial s}{\partial x_1}, \frac{\partial s}{\partial x_2}\right] = [c, 1].$$

Then we can obtain the equivalent control by scalar multiplication

$$[c, 1] \begin{bmatrix} 0 & 1 \\ 0 & 0 \end{bmatrix} \begin{bmatrix} x_1 \\ x_2 \end{bmatrix} + [c, 1] \begin{bmatrix} 0 \\ 1 \end{bmatrix} u_{eq} = 0,$$

$$u_{eq} = -cx_2 ,$$

$$\begin{bmatrix} \dot{x}_1 \\ \dot{x}_2 \end{bmatrix} = \begin{bmatrix} 0 & 1 \\ 0 & 0 \end{bmatrix} \begin{bmatrix} x_1 \\ x_2 \end{bmatrix} - \begin{bmatrix} 0 \\ 1 \end{bmatrix} cx_2 ,$$

$$\dot{x}_1 = x_2 ,$$
$$\dot{x}_2 = -cx_2 .$$

Then $R = cx_2$, and from the equation (9) we obtain

$$\dot{x}_1 = x_2 , \qquad \dot{x}_2 = \lambda_1 .$$

By differentiating the constraint equation we obtain

$$\dot{x}_2 = -cx_2 .$$

Thus the conclusion is: by means of two different methods we obtain the same values of the constraint reactions.

EXAMPLE 2. This example is taken from the book [2], where the nonholonomic case known as Chaplygin's sleighs, is considered.

By introducing the change of variables: $x = x_1$, $y = x_2$, $\varphi = x_3$, we obtain the system:

$$\dot{x}_1 = x_4\,, \qquad \dot{x}_2 = x_5\,, \qquad \dot{x}_3 = x_6\,,$$
$$\dot{x}_4 = \lambda \sin x_3\,, \qquad \dot{x}_5 = -\lambda \cos x_3\,, \qquad \dot{x}_6 = 0,$$

with the constraint surface:

$$x_4 \sin x_3 - x_5 \cos x_3 = 0.$$

An equivalent discontinuous system can be written in the following form:

$$\begin{bmatrix} \dot{x}_1 \\ \dot{x}_2 \\ \dot{x}_3 \\ \dot{x}_4 \\ \dot{x}_5 \\ \dot{x}_6 \end{bmatrix} = \begin{bmatrix} 0 & 0 & 0 & 1 & 0 & 0 \\ 0 & 0 & 0 & 0 & 1 & 0 \\ 0 & 0 & 0 & 0 & 0 & 1 \\ 0 & 0 & 0 & 0 & 0 & 0 \\ 0 & 0 & 0 & 0 & 0 & 0 \\ 0 & 0 & 0 & 0 & 0 & 0 \end{bmatrix} \begin{bmatrix} x_1 \\ x_2 \\ x_3 \\ x_4 \\ x_5 \\ x_6 \end{bmatrix} + \begin{bmatrix} 0 \\ 0 \\ 0 \\ \sin x_3 \\ -\cos x_3 \\ 0 \end{bmatrix} u,$$

$$s = x_4 \sin x_3 - x_5 \cos x_3\,.$$

This system has the gradient vector:

$$K = [0, 0, x_4 \cos x_3 + x_5 \sin x_3, \sin x_3, -\cos x_3, 0].$$

Once this system is known, we can determine the equivalent control by scalar multiplication:

$$[0, 0, x_4 \cos x_3 + x_5 \sin x_3,\ \sin x_3,\ -\cos x_3, 0] \begin{bmatrix} 0 & 0 & 0 & 1 & 0 & 0 \\ 0 & 0 & 0 & 0 & 1 & 0 \\ 0 & 0 & 0 & 0 & 0 & 1 \\ 0 & 0 & 0 & 0 & 0 & 0 \\ 0 & 0 & 0 & 0 & 0 & 0 \\ 0 & 0 & 0 & 0 & 0 & 0 \end{bmatrix} \begin{bmatrix} x_1 \\ x_2 \\ x_3 \\ x_4 \\ x_5 \\ x_6 \end{bmatrix}$$

$$[0, 0, x_4 \cos x_3 + x_5 \sin x_3,\ \sin x_3,\ -\cos x_3, 0] \begin{bmatrix} 0 \\ 0 \\ 0 \\ \sin x_3 \\ -\cos x_3 \\ 0 \end{bmatrix} u = 0.$$

From this we obtain:

$$x_6[x_4 \cos x_3 + x_5 \sin x_3] + [\sin^2 x_3 + \cos^2 x_3]u = 0,$$

and then

$$u_{eq} = -x_6[x_4 \cos x_3 + x_5 \sin x_3].$$

By introducing this equivalent control into the discontinuous equation we obtain:

$$\begin{bmatrix} \dot{x}_1 \\ \dot{x}_2 \\ \dot{x}_3 \\ \dot{x}_4 \\ \dot{x}_5 \\ \dot{x}_6 \end{bmatrix} = \begin{bmatrix} 0 & 0 & 0 & 1 & 0 & 0 \\ 0 & 0 & 0 & 0 & 1 & 0 \\ 0 & 0 & 0 & 0 & 0 & 1 \\ 0 & 0 & 0 & 0 & 0 & 0 \\ 0 & 0 & 0 & 0 & 0 & 0 \\ 0 & 0 & 0 & 0 & 0 & 0 \end{bmatrix} \begin{bmatrix} x_1 \\ x_2 \\ x_3 \\ x_4 \\ x_5 \\ x_6 \end{bmatrix} + \begin{bmatrix} 0 \\ 0 \\ 0 \\ \sin x_3 \\ -\cos x_3 \\ 0 \end{bmatrix} (-x_6[x_4 \cos x_3 + x_5 \sin x_3]).$$

Then we get the constraint reaction in the same form as that given in the book [2].

The determination of constraint reactions is usually very complicated and, in many cases, it is an important condition necessary to find the solution to the equations of motion in various mechanical systems. Due to those difficulties, sometimes the second mode Lagrange's equations are used where the reactions do not appear. Then we propose to solve this problem in a different manner, using the sliding modes equations. This method can be used both in the analysis and synthesis of mechanical systems where the effects of constraints are crucial for determining the motion.

References

1. V.I. UTKIN, *Sliding mode and its applications to variable structure systems*, MIR, Moscow 1978.
2. J.I. NEJMARK and N.A. FUFAJEV, *Dynamics of nonholonomics systems* [in Polish], PWN, Warszawa 1971.
3. R.A. DE CARLO, S.H. ŻAK and G.P. MATTHEWS, *Variable structure control in nonlinear multivariable systems. A tutorial*, Proc. of the IEEE, **76**, 3, 1988.
4. S. KOTOWSKI, *Invariance of sliding modes with respect to control matrix*, Arch. Mech, **48**, 1, 1996.
5. R. GUTOWSKI, *Analytical mechanics* [in Polish], PWN, Warszawa 1971.

POLISH ACADEMY OF SCIENCES
INSTITUTE OF FUNDAMENTAL TECHNOLOGICAL RESEARCH
e-mail: skot@ippt.gov.pl

Received March 7, 1997; new version October 14, 1997.

Arch. Mech., 50, 1, pp. 91–112, Warszawa 1998
FIFTY YEARS OF THE ARCHIVES OF MECHANICS

Plastic propagation of band-waves in solids

K.C. VALANIS (VANCOUVER)

HEREWITH WE PRESENT a thermodynamic theory of "plastic propagation" of strain bands. The theory results in a *Wave equation* where the time of propagation is *not* the Newtonian time t but *the intrinsic time* z (in the sense of Valanis), the increment of which is proportional to the norm of the increment of the plastic strain tensor. To our knowledge the concept of plastic propagation is new in theoretical mechanics. The equation is solved exactly for the case of a flat semi-infinite strip under axial tension. The solution depicts the propagation of bands, upon plastic extension of the strip, in the axial direction, very much in accordance with observation.

1. Introduction

NUMEROUS INVESTIGATORS, see for instance LUBAHN and FELGAR [1], have reported the formation of "adiabatic" bands, commonly near the loaded boundary of an axial specimen in tension, and their propagation in the interior of the material domain. The bands become prominent, in the sense of being observable with the naked eye, when the stress reaches the vicinity of yield, and propagate in the interior as plastic deformation increases. The propagation is not time-dependent, in that it stops when the plastic deformation ceases. Therefore what we are witnessing is the propagation of plastic waves whose position in space depends parametrically on some measure of plastic deformation.

We infer on the basis of this observation, that the propagation of the bands obeys a wave equation with a "plastic inertia" term which is proportional to the second derivative of the wave function with respect to an *intrinsic* time z, *and not the clock time* t, where z is a non-decreasing measure of plastic deformation in the sense of VALANIS [2]. This inference has led to the present paper whose object is to arrive at the defining equation that describes the phenomenon of "plastic" propagation of adiabatic bands.

2. Thermodynamics

The thermodynamic theory of formation of bands – single bands or deformation patterns – in the presence of *uniform surface tractions*, was given previously in the context of a Helmholtz as well as a Gibbs formulation of *gradient thermodynamics of internal variables*, under conditions of uniform temperature and infinitesimal deformation, VALANIS [3, 4]. A cogent and detailed derivation of the equations, pertinent to the gradient theory, is also given in the Appendix.

The thermodynamic treatment in Ref. [4] addressed the general case where the Gibbs free energy density ϕ, in a material domain D, is a function of stress and three different classes of internal variables, $\mathbf{p}$, $\mathbf{q}$ and $\boldsymbol{\xi}$, each with a different physical behavior and thus, a fundamentally different form of evolution equation. The pertaining form of ϕ is given in Eq. (2.1):

$$\phi = \phi(\sigma_{ij};\ p_{ij};\ q_{i,j};\ q_i;\ \xi_{i,j};\ \xi_i), \tag{2.1}$$

where $\boldsymbol{\sigma}$ is the stress tensor, $\mathbf{p}$ stands for the class $\mathbf{p}^r$ $(r = 1, 2, ..., n_p)$, $\mathbf{q}$ for the class $\mathbf{q}^r$ $(r = 1, 2, ..., n_q)$ and $\boldsymbol{\xi}$ for the class $\mathbf{p}$ $(r = 1, 2, ..., n_\xi)$. Note that $\mathbf{p}$ are local while $\mathbf{q}$ and $\boldsymbol{\xi}$ are not-local in that their gradients are also constitutive variables of ϕ.

Following VALANIS [4], the strain in D is given by Eq. (2.2):

$$\varepsilon_{ij} = -\partial\phi/\partial\sigma_{ij}\,. \tag{2.2}$$

The stress tensor is symmetric and obeys Newton's law of motion, i.e., Eq. (2.2′) just as in the case of local theories:

$$\sigma_{ij,j} + f_i = \partial^2 u_i/\partial t^2, \tag{2.2′}$$

where f_i and u_i stand for the body force and displacement field, respectively. However, the evolution or field equation that pertains to a specific internal variable depends on whether it is local or non-local. Of the three classes, the first, p_{ij}, the local class, are tensors of the second order and obey a local evolution equation, i.e.,

$$\partial\phi/\partial p_{ij} + b_{ijkl}\,\partial p_{kl}/\partial z = 0. \tag{2.3}$$

This equation is predicated on the position that the internal force $P_{ij}(=-\partial\phi/\partial p_{ij})$ is linearly related to $\partial p_{ij}/\partial z$ through the positive definite resistance tensor b_{ijkl} which is symmetric in the indices i and j, the indices k and l and the pairs of indices (i, j) and (k, l). These variables are dissipative since the inner product $\mathbf{P}\cdot\partial\mathbf{q}/dz$ is not zero, and in fact positive – unless $\|\partial\mathbf{q}/dz\| = 0$ and/or $\|\mathbf{Q}\| = 0$, double bars denoting the Euclidean norm.

We remark that z is the intrinsic time scale in endochronic plasticity, proposed previously by VALANIS [2]. Specifically for rate-indifferent materials,

$$dz = d\zeta/f, \tag{2.3′}$$

where f is the isotropic hardening function and $d\zeta$ is the length of the increment of the plastic strain tensor, with respect to a material metric tensor $\mathbf{P}$ such that

$$d\zeta^2 = P_{ijkl}\,d\varepsilon^p_{ij}\,d\varepsilon^p_{kl}\,. \tag{2.3″}$$

In the event that the material is plastically incompressible, then:

$$d\zeta = k\|de^p_{ij}\|, \tag{2.3'''}$$

where e^p_{ij} is the strain deviator and k is an arbitrary constant, unity if convenient.

The second class q_i are *non-local* (vectorial) internal variables in that ϕ depends on the variables q_i as well as their gradients $q_{i,j}$. These variables obey the field equation (2.4):

$$(\partial\phi/\partial q_{i,j})_{,j} - \partial\phi/\partial q_i = Q_i\,, \tag{2.4}$$

where Q_i is the internal resistance force. The derivation of this equation as well as the complete set of equations pertaining to the gradient theory of internal variables, is given in the Appendix.

In this paper as well as in our previous work, we stipulate that Q_i is linearly related to $\partial q_i/\partial z$ through the resistance tensor b_{ij} symmetric in i and j and such that $\|\mathbf{b}\| \neq 0$. Hence the variables q_i obey the partial differential equation (2.5):

$$(\partial\phi/\partial q_{i,j})_{,j} - \partial\phi/\partial q_i = b_{ij}\,\partial q_j/\partial z. \tag{2.5}$$

We note that q_i are also dissipative, since again $Q_i\partial q_i/\partial z \neq 0$. Of fundamental importance is the stipulation that the evolution of the q-class of internal variables is expressed with respect to the intrinsic time z, i.e., the length of the plastic strain path, generated strictly only by virtue of the change in the local internal variables p_{ij}.

The third class ξ_i is again vectorial and non-local but inviscid, in that the internal resistance force $\Xi = 0$. These variables are either associated with dislocation glides and other changes in material conformations that take place with negligible (ideally zero) internal resistance, or are descriptors of terminal equilibrium states. Their spatial variation in the material domain D is given by Eq. (2.6):

$$(\partial\phi/\partial\xi_{i,j})_{,j} - \partial\phi/\partial\xi_i = 0. \tag{2.6}$$

REMARK. Of note is the fact that all generic internal variables of the gradient type, say ζ_i, obey one and the same fundamental equation, i.e., Eq. (2.7), where Z_i is the internal resistive force (see VALANIS [3, 4] for details):

$$(\partial\phi/\partial\zeta_{i,j})_{,j} - \partial\phi/\partial\zeta_i = Z_i\,. \tag{2.7}$$

The constitutive equation pertaining to the different sub-types of such variables depends on the nature of the resistive force Z_i. In the case of the q-class, $Z_i = Q_i = b_{ij}\partial q_j/\partial z$, while in the case of the ξ-class, $Z_i = \Xi_i = 0$.

2.1. Boundary conditions on ζ_i

Previously, VALANIS [5, 6], we demonstrated that the physical mechanism of particle migration and hence the non-affine deformation of the associated material sub-domain, is a cause for dissipative behavior. On the other hand it was also demonstrated, VALANIS [3], that internal variables ζ_i also arise as a result of heterogeneity of the internal material structure. While the field equations that describe the spatial distribution of ζ_i as well as their temporal variation are the same irrespective of their physical origin, the boundary conditions on the material surface S depend on the underlying physics. We, therefore, distinguish two different cases: (i) structural and (ii) migratory internal variables.

2.2. Structural internal variables

The surface is composed of two parts: S_T on which tractions are prescribed, and its complement S_u where displacements are prescribed. In this case the boundary conditions are as follows (VALANIS [3]):

$$\text{on } S_T: \qquad \partial\phi/\partial\zeta_{i,j} n_j = 0; \tag{2.8}$$

$$\text{on } S_u: \qquad \zeta_i = 0, \tag{2.9}$$

provided that the tractions and displacements on the boundary are "locally homogeneous" in the sense of VALANIS [3].

2.3. Migratory internal variables

Here the surface S is again composed of two parts: the permeable surface S_p on which the migratory displacements are unknown, and impermeable surface S_i on which the migratory displacements are zero. The boundary conditions are therefore as follows:

$$\text{on } S_p: \qquad \partial\phi/\partial\zeta_{i,j} n_j = 0; \tag{2.10}$$

$$\text{on } S_i: \qquad \zeta_i = 0. \tag{2.11}$$

The derivation of these equations is given in the Appendix.

REMARK. There may exist physical circumstances, though these are difficult to ascertain experimentally, where a surface is impermeable in the normal but permeable in a tangential direction; in other words, surface diffusion is possible. To deal with this situation, we construct a system of surface coordinates x_i' such that x_1' is normal to the surface and x_2' and x_3' are tangential. We also let ζ_i' be the components of $\boldsymbol{\zeta}$ in the primed system and let S_{ij} be the coordinate transformation such that:

$$\zeta_i = S_{ij}\,\zeta_j' \qquad \zeta_j' = S_{ij}\,\zeta_i\,. \tag{2.12}$$

Following VALANIS [6], the appropriate variational boundary condition is:

$$\int_S \partial\phi/\partial\zeta_{i,j} n_j \delta\zeta_i \, dS = 0 \tag{2.13}$$

for all arbitrary variations $\delta\zeta_i$ such that $Z_i \delta\zeta_i \geq 0$. Or, in view of Eq. (2.12):

$$\int_S \partial\phi/\partial\zeta_{i,j} n_j S_{im} \delta\zeta'_m \, dS = 0. \tag{2.14}$$

Since $\zeta'_1 = 0$, it follows that $\delta\zeta'_1 = 0$ and Eq. (2.14) holds for $m = 1$. However $\delta\zeta'_2$ and $\delta\zeta'_3$ are arbitrary since ζ'_2 and ζ'_3 are not prescribed. Thus, if Eq. (2.14) is to hold for $m = 2$ and $m = 3$, then:

$$\partial\phi/\partial\zeta_{i,j} n_j S_{i2} = 0, \qquad \partial\phi/\partial\zeta_{i,j} n_j S_{i3} = 0. \tag{2.15}$$

It was demonstrated, VALANIS [3, 4], that the band formation is attributable to the presence of a non-local internal field. If such multiple fields are present, the material domain is then an ensemble of sub-domains, the behavior of each of which is governed by its own internal field. The geometric extent of each sub-domain is the same as the entire domain D.

3. Wave variables

In this paper we add a *fourth* class of vectorial variables, which we call *wave variables*. These come in pairs, i.e., for each "primary" variable ω_i with a resistance force Ω_i, there is a "dual" variable ω'_i with associated resistance force Ω'_i. Of importance is the fact that though $\|\Omega_i\|$ and $\|\Omega'_i\|$ are different from zero in the course of plastic deformation ($\|\mathbf{p}\| \neq 0$), the scalar product $\Omega_i \delta\omega_i + \Omega'_i \delta\omega'_i$ is zero, for all arbitrary variations $\delta\omega_i$ and $\delta\omega'_i$, and thus *the dissipation of the dual pair is zero*. However, ω_i is non-local while ω'_i is local. Thus ϕ depends on ω_i as well as on $\omega_{i,j}$ and on ω'_i (and not its gradient).

As we shall demonstrate, the primary variable ω_i has an evolution equation which is a pertial differential equation of the wave (hyperbolic) type – the desired form for the propagation of plastic bands.

The Gibbs free energy density ϕ now has the augmented form:

$$\phi = \phi(\sigma_{ij};\ p_{ij}\ q_{i,j};\ q_i;\ \xi_{i,j}\ \xi_i;\ \omega_{i,j};\ \omega_i;\ \omega'_i) \tag{3.1}$$

with the resulting additional equations (3.2) and (3.3) that govern the wave-variables ω_i and ω'_i:

$$\Omega_i = (\partial\phi/\partial\omega_{i,j})_{,j} - \partial\phi/\partial\omega_i \tag{3.2}$$

$$\Omega'_i = -\partial\phi/\partial\omega'_i\,. \tag{3.3}$$

A coupling between ω_i and ω_i' is now introduced through a relation between Ω_i and Ω_i' on one hand, and $\partial\omega_i/\partial z$ and $\partial\omega_i'/\partial z$ on the other, by means of the resistance matrix $\boldsymbol{\eta}$ in the manner of Eqs. (3.4):

$$\begin{aligned} \Omega_i &= \eta_{11}\partial\omega_i/\partial z + \eta_{12}\partial\omega_i'/\partial z, \\ \Omega_i' &= \eta_{21}\partial\omega_i/\partial z + \eta_{22}\partial\omega_i'/\partial z. \end{aligned} \tag{3.4}$$

We remark that the Onsager form of η_{rs} is symmetric. Here, however, it is not.

We now recall that the *pair* of variables ω_i and ω_i' is *inviscid* giving rise to zero dissipation. This being the case, the matrix η_{ij} must be such that:

$$\Omega_i\partial\omega_i/\partial z + \Omega_i'\partial\omega_i'/\partial z = 0. \tag{3.5}$$

This is accomplished by letting $\boldsymbol{\eta}$ be an *antisymmetric* matrix, in which event $\eta_{11} = \eta_{22} = 0$; $\eta_{12} = -\eta_{21} \equiv \beta$. Equations (3.4) now reduce to the form:

$$\Omega_i = \beta\partial\omega_i'/\partial z, \tag{3.6}$$

$$\Omega_i' = -\beta\partial\omega_i/\partial z. \tag{3.7}$$

Note that the pair (ω_i, ω_i') is in fact inviscid since Eqs. (3.6) and (3.7) satisfy the inviscid condition (3.5) identically.

In the light of Eqs. (3.2) and (3.3), the field equations for the wave variables ω_i and ω_i' are now the following:

$$(\partial\phi/\partial\omega_{i,j})_{,j} - \partial\phi/\partial\omega_i = \beta\partial\omega_i'/\partial z, \tag{3.8}$$

$$\partial\phi/\partial\omega_i' = \beta\partial\omega_i/\partial z. \tag{3.9}$$

REMARK. We remark that, in irreversible thermodynamics, the resistance matrix, such as η_{rs} for instance, that relates the internal resistance forces to their dual internal velocities, need not be symmetric, provided that the work done by these forces is non-negative to satisfy the constraint of positive rate of dissipation. In our specific case above, where the material is inviscid, their inner product is zero.

It is of interest that the "resistance" matrix is now antisymmetric. The off-diagonal terms play the role of thermal inertia giving rise, as we shall see shortly, to a wave equation, instead of a diffusion equation, which is the case when the resistance matrix is symmetric – and positive definite.

4. The wave equation

To avoid complexities associated with the generality of dependence of ϕ on the variables of the various mechanisms, we make the reasonable stipulation

that the energies of the mechanisms are additive, in which event Eq. (3.1) has the partitioned form:

$$\phi = \phi_p + \phi_q + \phi_\xi + \phi_\omega \,, \tag{4.1}$$

where

$$\phi_p = \phi(\boldsymbol{\sigma}, \mathbf{p}), \qquad \phi_q = \phi_q(\boldsymbol{\sigma}, \nabla\mathbf{q}, \mathbf{q}), \qquad \phi_\xi = \phi_\xi(\boldsymbol{\sigma}, \nabla\boldsymbol{\xi}, \boldsymbol{\xi}), \tag{4.2}$$

$$\phi_\omega = \phi_\omega(\boldsymbol{\sigma}, \nabla\boldsymbol{\omega}, \boldsymbol{\omega}, \boldsymbol{\omega}'). \tag{4.3}$$

The strain in the domain D consists of the contributions of the various mechanisms that are active during loading. In fact, and in view of Eqs. (2.2′) and (4.1), the strain $\boldsymbol{\varepsilon}$ is the *sum* of the strains produced by the individual mechanisms. Thus:

$$\boldsymbol{\varepsilon} = \boldsymbol{\varepsilon}_p + \boldsymbol{\varepsilon}_q + \boldsymbol{\varepsilon}_\xi + \boldsymbol{\varepsilon}_\omega \,. \tag{4.4}$$

We remark that the suffix p denotes the strain contribution of the local mechanism and that $\boldsymbol{\varepsilon}_p$ will consist of the elastic strain $\boldsymbol{\varepsilon}^{(e)}$ plus the plastic strain $\boldsymbol{\varepsilon}^{(p)}$.

Equations (3.8) and (3.9) now become:

$$\begin{aligned} (\partial\phi_\omega/\partial\omega_{i,j})_{,j} - \partial\phi_\omega/\partial\omega_i &= \beta\partial\omega_i'/\partial z, \\ \partial\phi_\omega/\partial\omega_i' &= \beta\partial\omega_i'/\partial z. \end{aligned} \tag{4.5}$$

4.1. The wave equation in one dimension

Because, to begin with, we are interested in the essential physics of the problem, we do the analysis in a one-dimensional domain D signified by the variable x, $-\infty < x < \infty$ and in the context of a linear theory and, therefore, a quadratic form of ϕ_ω.

Historically, quadratic forms of the free energy densities, Helmholtz or Gibbs, have been powerful in giving insight to the constitutive behavior of solids. For instance, in local viscoelasticity a quadratic form of the Helmholtz free energy density ψ results in the stress being a linear hereditary functional of the strain, while a quadratic Gibbs free energy density ϕ results in the strain being a linear hereditary functional of the stress. The same situation arises in plasticity except that the functionals are taken with respect to the intrinsic time ζ – in the manner of endochronic plasticity, VALANIS [7].

We begin, therefore, with ψ because under isothermal conditions it has the physical significance of stored energy, with the attending stability condition that it must be a positive function of its arguments. Thus, in one dimension, we let ψ_ω have the form shown in Eq. (4.6):

$$\psi_\omega = (1/2)A_\omega(u_x^\omega)^2 - B_\omega u_x^\omega \omega_x + (1/2)C_\omega\omega_x^2 + (1/2)F_\omega(\omega^2 + \omega'^2), \tag{4.6}$$

where a suffix x denotes differentiation with respect to x, u^{ω} is the displacement field, u_x^{ω} is the (uniaxial) strain field ε_{ω} and A_{ω}, B_{ω} and C_{ω} are material constants. Quite clearly and without loss of generality we may put B_{ω} equal to unity, since we may define a new variable $\omega^* = B_{\omega}\omega$, substitute in Eq. (4.6) and drop asterisks. Thus:

$$\psi_{\omega} = (1/2)A_{\omega}(u_x^{\omega})^2 - u_x^{\omega}\omega_x + (1/2)C_{\omega}\omega_x^2 + (1/2)F_{\omega}(\omega^2 + \omega'^2). \tag{4.7}$$

Note that ω' is of the *local* type so that its gradient does not appear in the expression for ψ. Also because ψ is a positive function,

$$A_{\omega} > 0, \qquad C_{\omega} > 0, \qquad F_{\omega} > 0 \qquad \text{and} \qquad A_{\omega}C_{\omega} > 1. \tag{4.8}$$

Our purpose is to use Eq. (4.7) to obtain the ancillary form of ϕ_{ω} by means of the Legendre transformation:

$$\phi_{\omega} = \psi - \sigma_{\omega}\varepsilon_{\omega} \tag{4.9}$$

in the light of the fact that

$$\sigma_{\omega} = \partial\psi_{\omega}/\partial\varepsilon_{\omega}\,. \tag{4.10}$$

Following a simple computation and since $\sigma_{\omega} = \sigma$, common to all mechanisms in the light of Eq. (4.2), we find that:

$$\phi_{\omega} = -\sigma^2/2A_{\omega} - (\sigma/A_{\omega})\omega_x + (C_{\omega}^*/2)\omega_x^2 + (F_{\omega}/2)(\omega^2 + \omega'^2), \tag{4.11}$$

where we have set $C_{\omega}^* = C_{\omega} - A_{\omega}^{-1}$. In view of the inequality $(4.8)_4$: $C_{\omega}^* > 0$.

Equations (4.4) and (4.5) in one dimension become:

$$(\partial\phi_{\omega}/\partial u_{\omega}^x)_x - \partial\phi_{\omega}/\partial\omega = \beta\partial\omega'/\partial z, \tag{4.12}$$

$$\partial\phi_{\omega}/\partial\omega' = \beta\partial\omega/\partial z \tag{4.13}$$

while, in view of Eq. (2.2') and for quasi-static processes without a body force field:

$$\sigma_x = 0. \tag{4.14}$$

At this juncture and as a result of Eqs. (4.10), (4.11), (4.12) and (4.13), the following equations for ω and ω' are obtained:

$$C_{\omega}^*\omega_{xx} - F\omega = \beta\partial\omega'/\partial z, \tag{4.15}$$

$$F\omega' = \beta\partial\omega/\partial z. \tag{4.16}$$

Elimination of ω' from Eqs. (4.15) and (4.16) gives the following *wave equation* for ω:

$$C_{\omega}^*\omega_{xx} - F\omega = \varrho_{\omega}\partial^2\omega/\partial z^2, \tag{4.17}$$

where $\varrho_\omega = \beta^2/F$. Thus ϱ_ω plays the role of the plastic inertia which is not related to the mass density but to the off-diagonal coefficient of the resistance matrix that relates the internal forces to the rates of the dual variables ω and ω'.

The strain contribution ε_ω of the internal field ω to the total strain in D, in the light of Eqs. (2.2) and (3.1) is given by Eq. (4.18):

$$u_x^\omega = -\partial\phi/\partial\sigma. \tag{4.18}$$

In view of Eq. (4.11):

$$u_x^\omega = \sigma/A_\omega + \omega_x/A_\omega\,. \tag{4.19}$$

Note that u_x^ω consists of the elastic "local" contribution σ/A_ω and the "gradient" contribution ω_x/A_ω. Also note that the dual variable ω' does not contribute to the strain in D.

It is also pointed out that ϕ_ω in Eq. (4.11) consists of the "local term" $-\sigma^2/2A_w$ and the non-local remainder. Furthermore and in view of Eq. (4.1), the local terms in that equation are additive to one grand total local term, which in conjunction with ϕ_p constitutes the local part of ϕ, which as it happens, is of the same form as ϕ_p. Thus in conclusion we may say that ϕ may be partitioned in the form of Eq. (4.1), but with the proviso that the terms ϕ_q, ϕ_ξ and ϕ_ω contain σ as a variable, but only in algebraic terms that are coupled with the gradients of the internal field variables.

4.2. The wave equation in three dimensions

With the above discussion we have laid the foundation for the three-dimensional generalization of the expression for ϕ_ω as it appears in Eq. (4.11). We thus set:

$$\phi_w = -A_w^{-1}\sigma_{ij}\omega_{i,j} + (C_\omega/2)\omega_{i,j}\omega_{i,j} + (F_\omega/2)(\omega_i\omega_i + \omega_i'\omega_i'). \tag{4.20}$$

This is not the most general form of ϕ_ω but it will serve us well in the present study of the physics of propagation of band-waves in solids.

At this point in the light of Eq. (2.2′) and in the absence of body and acceleration forces, Eqs. (4.5) become:

$$C_\omega\omega_{i,jj} - F_\omega\omega_i = \beta\partial\omega_i'/\partial z, \tag{4.21}$$

$$F_\omega\omega_i' = \beta\partial\omega_i/\partial z. \tag{4.22}$$

The variable ω_i' is now eliminated from Eqs. (4.21) and (4.2) and the following wave equation for ω_i is thereby obtained:

$$C_\omega\omega_{i,kk} - F_\omega\omega_i = \varrho_\omega\partial^2\omega_i/\partial z^2, \tag{4.23}$$

where as before $\varrho_\omega = \beta^2/F$.

4.3. Boundary conditions

The boundary conditions depend on whether ω_i is a structural or a migratory variable. The following cases arise.

(i) Structural variables. We recall Eqs. (2.8) and (2.9) according to which and in conjunction with Eq. (4.11):

$$\text{on } S_T: \qquad \omega_{i,j} n_j = (1/A_\omega C_\omega) T_i\,, \tag{4.24}$$

$$\text{on } S_u: \qquad \omega_i = 0. \tag{4.25}$$

(ii) Migratory variables. Substitute p for subscript T in Eq. (4.24) and i for u in Eq. (4.25). For more complex conditions follow the discussion subsequent to Eq. (2.14).

REMARK. The propagation of the "plastic" wave generated by the wave Eq. (4.23) is in terms of the intrinsic time z – where z is the length of the plastic strain path, within a proportionality constant – and not in terms of the clock time t. When the deformation is brought about by application of tractions (or tractions and displacements) on the surface of the material domain D, the plastic wave will propagate from the surface toward the interior of the domain and will stop either when the surface tractions (or displacements) cease to increase, or when these change in a manner that constitutes "elastic unloading". We illustrate the above plenomenon by solving the problem of plastic strain bands propagating in a longitudinal direction in a flat strip under axial loading.

5. Band propagation in a flat thin strip under uniform axial traction

We consider the domain D to be a semi-infinitive flat strip, $|x_1| \leq a$, $0 \leq x_2 < \infty$, $|x_3| \leq b$. At $x_2 = 0$ a uniform tensile traction $T(z)$ – independent of x_1 and x_3 – is applied while the edges $|x_1| = a$ and $|x_3| = b$ are stress-free. The initial conditions in D are such that ω_i and $\partial\omega_i/\partial z$ are equal zero at $z = 0$. One can verify that $\omega_1 \equiv 0$ and $\omega_3 \equiv 0$ on the basis of the fact that Eq. (4.23), the initial conditions and the boundary condition (4.24) are satisfied identically. Furthermore, the boundary condition at $x_2 = 0$, i.e.,

$$A_\omega C_\omega \omega_{2,2} = T(z) \tag{5.1}$$

and the boundary condition at $|x_1| = a$ and $|x_3| = b$, i.e.,

$$\omega_{2,1} = 0, \tag{5.2}$$

$$\omega_{2,3} = 0, \tag{5.3}$$

require that ω_2 be a function of x_2 and z only.

Briefly, Eq. (5.1) demands that ω_2 be of the form:

$$\omega_2 = X_1(x_1, x_3, z) + X_2(x_2, z), \tag{5.4}$$

where X_1 and X_2 are arbitrary functions, while Eq. (5.2) and (5.3) demand that X_1 be, at most, a constant field. Thus:

$$\omega_2 = \omega_2(x_2, z). \tag{5.4'}$$

At this point we change the notation to simplify the presentation of the analysis and set: $\omega_2 \equiv \omega$ and $x_2 \equiv y$, $A_\omega \equiv A$, $C_\omega \equiv C$ and $F_\omega \equiv F$. Equations (4.23) and (4.24) then reduce to the following equations. In D:

$$C\partial^2\omega/\partial y^2 - F\omega = \varrho_\omega \partial^2\omega/\partial z^2. \tag{5.5}$$

On S at $y = 0$:

$$AC\,\partial\omega/\partial y = T(z) \tag{5.6}$$

while at $y = \infty$, ω is bounded.

5.1. Solution by Laplace transform

Let $\overline{\omega}(y, p)$ be the Laplace transform of $\omega(y, z)$. Then in view of the initial conditions, Eq. (5.5) becomes:

$$C\,\partial\overline{\omega}^2/\partial y^2 - F\overline{\omega} = \varrho_\omega p^2 \overline{\omega}. \tag{5.7}$$

Let

$$c^2 = C/\varrho_\omega\,, \qquad a^2 = F/\varrho_\omega\,, \qquad x = y/c, \tag{5.8}$$

where c is the wave velocity. Then Eq. (5.5) becomes:

$$\partial\overline{\omega}^2/\partial x^2 - (a^2 + p^2)\overline{\omega} = 0 \tag{5.9}$$

while Eq. (5.6) leads to the boundary conditions:

$$\Gamma\partial\overline{\omega}/\partial x = \overline{T}(p), \tag{5.9'}$$

where $\Gamma = AC/c$. In view of the required boundedness of the solution at $y = \infty$, it follows from Eq. (5.9) that

$$\overline{\omega} = K \exp\left\{-(a^2 + p^2)^{1/2} x\right\}, \tag{5.10}$$

where K is to be determined from the boundary condition at $y = 0$.

It thus follows from Eqs. (5.9') and (5.10) that:

$$\overline{\omega} = -\frac{\overline{T}(p)}{\Gamma\sqrt{(a^2 + p^2)}} e^{-x\sqrt{(a^2+p^2)}}, \tag{5.11}$$

where $\overline{T}(p)$ is th Laplace transform of $T(z)$.

Discussion. Before we consider, in its generality, the inverse transform of $\overline{\omega}$, we discuss some special cases of interest. Specifically we pose the case where the local constitutive behavior of the material is that of an elastic perfectly plastic solid, in which event the function $T(z)$ is a Heaviside step function, i.e.,

$$T(z) = T^0 H(z), \tag{5.12}$$

where T^0 is the value of yield stress. In this event $\overline{T} = T^0/p$. Noting that the Laplace transform of $\partial\omega/\partial z$ is $p\overline{\omega}$ ($\omega(0) = 0$), then:

$$p\overline{\omega} = -\frac{T^0}{\Gamma\sqrt{(a^2+p^2)}} e^{-x\sqrt{(a^2+p^2)}}. \tag{5.13}$$

The inverse transform of Eq. (5.13) is now standard and in fact,

$$\partial\omega/\partial z = (T^0/\Gamma) J_0\left\{a(z^2-x^2)^{1/2}\right\} \qquad (z \geq x), \tag{5.14}$$

where J_0 is the Bessel function of order zero. One must note, however, that because the intrinsic time z is the length of the plastic strain path, $\partial\omega/\partial z$ is not a "velocity" in the normal sense, but the rate of change of the internal displacement ω with respect to the "magnitude" of the plastic *local* strain. Specifically at $x = 0$:

$$\partial\omega/\partial z = (T^0/\Gamma) J_0(az). \tag{5.14'}$$

Equation (5.14) is that of a wave propagating into the interior of the strip at a speed c, since $x = y/c$.

In reference to Eq. (5.14) and because of the properties of J_0, we observe that at fixed z, $\partial\omega/\partial z$ is an alternating function of x with decreasing amplitude, i.e., its absolute value is largest at the wavefront but diminishes as x approaches the boundary $x = 0$. A plot of $\partial\omega/\partial z$ vs. z, for $a = 10$, is given in Fig. 1.

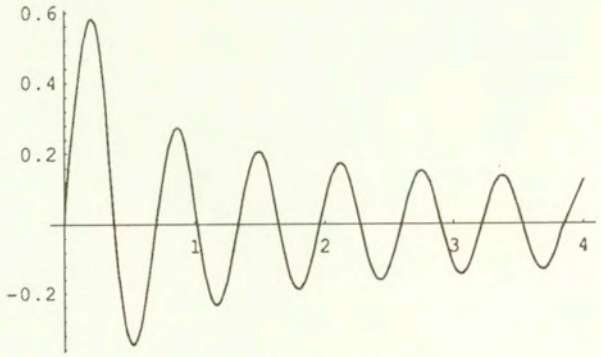

FIG. 1. Displacement (arbitrary units) vs. z. Displacement history at $x = 0$ ($a = 10$).

The displacement field is found by integrating the right-hand side of Eq. (5.14) with respect to z. Thus:

$$\omega(x,z) = (T_0/\Gamma)\int_x^z \left\{a\sqrt{(z_1^2 - x^2)}\right\} dz_1 . \tag{5.15}$$

The lower limit of integration reflects the nature of the solution whereby $\partial\omega/\partial z$ is null for $z_1 \leq x$. Of particular interest is the displacement history at $y = 0$, i.e. at $x = 0$. Then by simple integration:

$$\omega(x,z) = (T^0/a\Gamma)J_1(az), \tag{5.15'}$$

where J_1 is the Bessel function of order one.

The remarkable feature of the solution is that the displacement is highly oscillatory – particularly for large values of a – even though the traction at $x = 0$ is a constant of z. Figure 2 shows a plot of ω vs. z for $a = 10$.

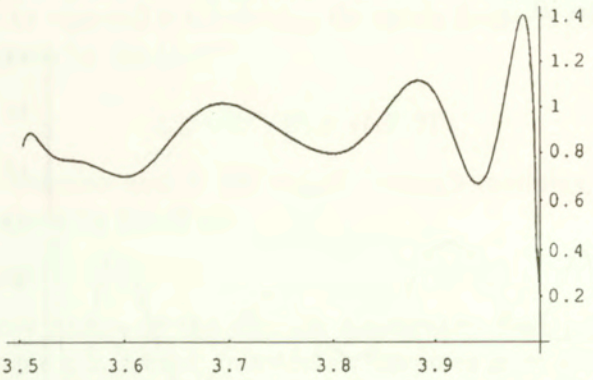

FIG. 2. Displacement vs. x. Displacement distribution close to the propagating wave-front.

5.2. The strain field

The strain is found upon using Eqs. (2.2) and (4.20). Thus:

$$\varepsilon_{ij}^{\omega} = -\partial\phi/\partial\sigma_{ij} = (1/A_{\omega}\omega_{(i,j)}, \tag{5.16}$$

where $\omega_{(i,j)}$ is the symmetric part of $\omega_{i,j}$. In the case at hand only the axial strain $\varepsilon_{22}^{\omega} \equiv \varepsilon_x^{\omega}$ is non-null. A simple calculation shows that

$$\varepsilon_x^{\omega} = (1/CA)\partial\omega/\partial x. \tag{5.17}$$

Thus, and in view of Eq. (5.11):

$$\varepsilon_x^{\omega} = \frac{\overline{T}(p)}{C} e^{-x\sqrt{(a^2+p^2)}}. \tag{5.18}$$

At this point we note that the inverse transform of the function $f(p)$, where

$$\overline{f}(p) = e^{-x\sqrt{(a^2+p^2)}}, \tag{5.19}$$

is given by Eq. (5.20)

$$f(z) = \delta(z-y) - \frac{ax}{\sqrt{(z^2-x^2)}} J_1\left\{a(z^2-x^2)^{1/2}\right\}, \tag{5.20}$$

where $\delta(\cdot)$ is the Dirac delta function. Thus in the event that $\overline{T} = T^0/p$, as above,

$$\varepsilon_x^\omega = (T_0/C)\left\{H(z-x) - ax\int_x^z \frac{J_1\left\{a(z'^2-x^2)^{1/2}\right\}}{(z'^2-x^2)^{1/2}}dz'\right\}. \tag{5.21}$$

The spatial strain distribution ε_x^ω behind the wave front is given in Fig. 3 for a value of a equal to 10.

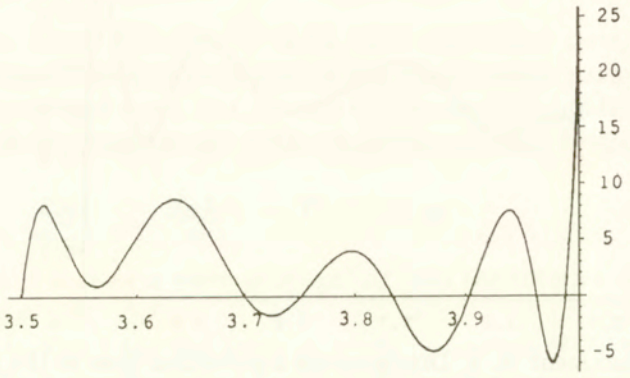

FIG. 3. Strain (arbitrary units) vs. x. Strain band-waves close to the propagating front.

We note that $T(z)$, in the general case, pertains to and is the function of the "local" stress-plastic strain curve of a plastic hardening solid. In this general case, ε_x^ω is given by the convolution integral depicted in Eq. (5.22):

$$C\varepsilon_x^\omega = T(z-x) - ax\int_x^z T(z-z')\frac{J_1\left\{a(z'^2-x^2)^{1/2}\right\}}{(z'^2-x^2)^{1/2}}dz'. \tag{5.22}$$

Discussion. As pointed out earlier, the strain field in D consists of the separate contributions of the several activated mechanisms. To bring out the effects of the wave mechanism, we assume that only the local and wave-mechanisms are active, so that

$$\varepsilon = \varepsilon_p + \varepsilon_\omega\,. \tag{5.23}$$

Prior and up to yielding, the strain field is local, elastic and $z = 0$. When the plate is stretched at and beyond yield, if the material hardens, z increases and the local strain field is given by Eq. (5.24):

$$\varepsilon_p = \varepsilon^{(p)} + \varepsilon^{(e)}, \tag{5.24}$$

where $\varepsilon^{(p)}$ is the local plastic strain while $\varepsilon^{(e)}$ is its elastic counterpart. Note that z is the Euclidean norm of the plastic strain tensor, i.e.,

$$z = \|\varepsilon^{(p)}\| \tag{5.25}$$

so that in simple tension:

$$z = \sqrt{(2/3)}\,\varepsilon_2^{(p)} = \sqrt{(2/3)}\,\varepsilon_x^{(p)} \tag{5.26}$$

assuming plastic incompressibility.

Thus during extension at yield, if the material is elastic-perfectly plastic, or beyond yield if the material is hardening, the strain field will consist of a uniform local field ε_{px}, given by Eq. (5.27):

$$\varepsilon_{px} = (T/E) + \sqrt{(3/2)}\,z, \tag{5.27}$$

where T is the traction and E the elastic Young's modulus, and the internal (wave) field ε_x^{ω} given by Eq. (5.22).

5.3. One final note

The oscillatory nature of the solution has already been pointed out. As the material parameter a increases, the solution becomes more and more oscillatory and its spatial visual representation will be that of numerous bands of increasing thinness. Likewise, the history of the solution will become highly oscillatory. This is illustrated in Fig. 4, where the displacement history is shown at $x = 0$ for $a = 20$.

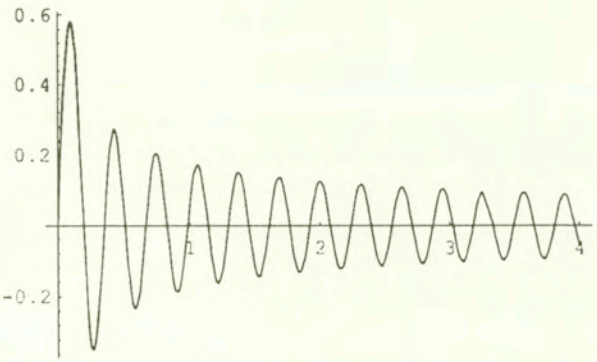

FIG. 4. Displacement (arbitrary units) vs. z. Displacement history at $x = 0$ ($a = 20$).

Appendix

The field equations and boundary conditions, pertaining to the gradient theory of internal variables, have been derived elsewhere [3, 4, 6]. However, because at times the analysis has been too concise and because the physics of the problem needs to be well understood, we give here a detailed and cogent derivation for the sake of completeness. Specifically, the boundary conditions are discussed at some length.

We begin a mathematical derivation, without concern for the physical nature of the internal variables, but discuss the resulting equations and boundary conditions, in the context of the pertaining physics, later in the Appendix. We limit the analysis to small deformation and isothermal conditions. The large deformation case has been discussed elsewhere [6]. Both the Helmholtz and Gibbs formalism are presented.

A.1. Helmholtz formulation

Let the material domain of a body of volume V and surface S be a *closed* thermodynamic system in the sense that it cannot exchange matter with its surroundings, is devoid of sources and sinks (either of the heat or material type), and is free of chemical reactions and electromagnetic fields. Then the following fundamental thermodynamic inequality applies under isothermal conditions:

$$\dot{\Psi} \leq \int_S T_i v_i \, dS + \int_V f_i v_i \, dV, \tag{A.1}$$

where Ψ is the Helmholtz free energy of the domain, T_i the surface tractions, f_i the body forces (including inertia forces) and v_i the velocity field, real or virtual, i.e., due to the set $(T_i; f_i)$ or an external agency.

Let D denote the internal dissipation in the sense that

$$D = \int_V Q_i \dot{q}_i \, dV \,, \tag{A.2}$$

where Q_i are internal dissipation forces, q_i are dual internal displacements, different and independent of the continuum average displacements u_i, and a superposed dot denotes a time derivative. Both u_i and q_i are continuous and twice differentiable in V.

Note that D is the rate of work done by Q_i and is always non-negative for $|\dot{q}_i| \neq 0$, bars denoting the Euclidean norm. Thus:

$$D = \int_V Q_i \dot{q}_i \, dV \geq 0 \tag{A.3}$$

and therefore, applying Eq. (A.2) to infinitesimal volumes,

$$Q_i \dot{q}_i \geq 0 \tag{A.4}$$

the equality in Eq. (A.4) pertaining to the case only when $|\dot{q}_i| = 0$. Inequality (A.1) may now be stated in terms of the dissipation D, i.e.,

$$\dot{\Psi} = \int_S T_i v_i \, dS + \int f_i v_i \, dV - D \tag{A.5}$$

or,

$$\dot{\Psi} = \int_S T_i v_i \, dS + \int f_i v_i \, dV - \int Q_i \dot{q}_i \, dV. \tag{A.6}$$

Quite clearly, if $|\dot{q}_i| = 0$, then the body behaves as non-dissipative and the rate of change of the free energy is equal to the rate of work of the surface tractions and the body forces, as in the case of an elastic body. Equation (A.6) is true for all actual and virtual v_i and $\dot{q}_i$ in V, subject to Ineq. (A.4).

At this point we introduce the free energy density ψ where

$$\Psi = \int_V \psi \, dV \tag{A.7}$$

such that,

$$\psi = \psi(u_{i,j};\ q_{i,j};\ q_i). \tag{A.8}$$

In view of Eqs. (A.7) and (A.8) and upon use of the Green – Gauss theorem, we now have the following identity:

$$\dot{\Psi} = \int_S (\partial\psi/\partial u_{i,j}) n_j v_i \, dS - \int_V (\partial\psi/\partial u_{i,j})_{,j} v_i \, dV + \int_S (\partial\psi/\partial q_{i,j}) n_j \dot{q}_i \, dS - \int_V (\partial\psi/\partial\psi_{i,j})_{,j} \dot{q}_i \, dV + \int_V (\partial\psi/\partial q_i) \dot{q}_i \, . \tag{A.9}$$

REMARK. Quite clearly $\dot{q}_i$ on S are not subject to Ineq. (A.3). They constitute a set of measure zero in so far as the integral $\int_V Q_i \dot{q}_i \, dV$ is concerned, in the sense that their value on S contributes nothing to the integral. However, other physical considerations apply. We have given two different physical interpretations for q_i in the literature: 1) where q_i are material *migratory* vectors, VALANIS [6], and 2) where they are *structural* vectors, i.e., deviations from the average continuum displacements u_i – the averaging volume depending on the heterogeneity of the material *structure*, VALANIS [3].

CASE 1. Here q_i are migratory vectors and their behavior at the surface is determined by the physical nature of the latter. We shall deal with two cases: a) when the surface $S_p \subseteq S$ is totally permeable and b) when $S_i \subseteq S$ is totally impermeable, where $S_p \cap S_i = 0$. On S_p, q_i are generally different from zero but are unknown since they are not measurable. However on S_i $q_i = \dot{q}_i = 0$. This is an inviolated kinematic constraint.

Thus, the virtual integral velocities $\dot{q}_i$ are arbitrary on S_p but zero on S_i.

The more general case where a surface is impermeable in the normal direction but permeable in the transverse directions, is treated in the text.

CASE 2. Here q_i are structural variables. We shall treat the case where u_i are "almost" uniform on the part of the surface $S_u \subseteq S$ where they are prescribed, in the sense of VALANIS [3]. Then on S_u, $q_i = \dot{q}_i = 0$. On the part of the surface $S_T \subseteq S$ where "almost" uniform tractions T_i are prescribed, q_i are not known and generally different from zero.

Thus virtual $\dot{q}_i$ are arbitrary on S_T and zero on S_u.

A.2. Derivation of field equations

Equation (A.6) and Eq. (A.9) combine to give rise to Eq. (A.10):

$$\text{(A.10)} \qquad \int_S \left[\left(\frac{\partial \psi}{\partial u_{i,j}}\right) n_j - T_i\right] v_i \, dS + \int_S \frac{\partial \psi}{\partial q_{i,j}} n_j \dot{q}_i \, dS - \int_V \left[\left(\frac{\partial \psi}{\partial u_{i,j}}\right)_{,j} + f_i\right] v_i \, dV + \int_V \left[\left(\frac{\partial \psi}{\partial q_{i,j}}\right)_{,j} - \frac{\partial \psi}{\partial q_i} - Q_i\right] \dot{q}_i \, dV = 0.$$

Let v_i and $\dot{q}_i$ be virtual and set $\dot{q}_i = 0$ in V and on S. Also set $v_i = 0$ on S. Then since v_i are otherwise arbitrary in V, it follows that

$$\text{(A.11)} \qquad \left(\frac{\partial \psi}{\partial u_{i,j}}\right)_{,j} + f_i = 0.$$

This is the equation of (dynamic) equilibrium. For instance if f_i are inertia forces then according to Newton's law, $f_i = -\varrho_0 \partial^2 u_i / \partial t^2$.

Since $\dot{q}_i$ is zero on S and in V and for all arbitrary v_i on S, it follows from Eq. (A.10) that

$$\text{(A.12)} \qquad \left(\frac{\partial \psi}{\partial u_{i,j}}\right) n_j = T_i$$

which is the boundary condition for the tractions T_i.

In the light of Eq. (A.10), the following identity now holds for all virtual $\dot{q}_i$ subject to Ineq. (A.6):

$$\int_V \left[\left(\frac{\partial \psi}{\partial q_{i,j}} \right)_{,j} - \frac{\partial \psi}{\partial q_i} - Q_i \right] \dot{q}_i \, dV = 0. \tag{A.13}$$

Since Eq. (A.13) must be true for infinitesimal dV, then:

$$\left[\left(\frac{\partial \psi}{\partial q_{i,j}} \right)_{,j} - \frac{\partial \psi}{\partial q_i} - Q_i \right] \dot{q}_i = 0 \tag{A.14}$$

for all virtual $\dot{q}_i$ such that $Q_i \dot{q}_i \geq 0$. Let $\dot{q}_i^{(r)}$ be three linearly independent vectors that satisfy the foregoing inequality. The existence of such a triad is geometrically obvious since thay lie in the open half-plane of vectors that make an acute angle with Q_i. Further let

$$\left[\left(\frac{\partial \psi}{\partial q_{i,j}} \right)_{,j} - \frac{\partial \psi}{\partial q_i} - Q_i \right] \dot{q}_i = R_i \, . \tag{A.15}$$

It then follows that

$$\dot{q}_i^{(r)} R_i = 0. \tag{A.16}$$

This is a set of three linear and homogeneous algebraic equations in R_i. The determinant of the coefficients is different from zero since $\dot{q}_i^{(r)}$ are linearly independent. Thus:

$$R_i = 0 \tag{A.17}$$

and hence:

$$\left(\frac{\partial \psi}{\partial q_{i,j}} \right)_{,j} - \frac{\partial \psi}{\partial q_i} = Q_i \, . \tag{A.18}$$

Equation (A.18) constitutes an internal equilibrium equation for the internal forces Q_i.

A.3. Boundary conditions

In view of Eqs. (A.11), (A.12) and (A.18) and in the light of Eq. (A.10), it follows that

$$\int_S (\partial \psi / \partial q_{i,j}) n_j \dot{q}_i \, dS = 0. \tag{A.19}$$

CASE 1. In view of Eq. (A.19):

$$\int_{S_p} (\partial\psi/\partial q_{i,j}) n_j \dot{q}_i \, dS + \int_{S_i} (\partial\psi/\partial q_{i,j}) n_j \dot{q}_i \, dS = 0. \tag{A.20}$$

But, $\dot{q}_i = 0$ on S_i. Thus,

$$\int_{S_p} (\partial\psi/\partial q_{i,j}) n_j \dot{q}_i \, dS = 0. \tag{A.21}$$

However, $\dot{q}_i$ are arbitrary on S_p. Letting $\dot{q}_i$ be non-zero on an infinitesimal part of S_p and zero elsewhere, it follows that:

$$(\partial\psi/\partial q_{i,j}) n_j \dot{q}_i = 0 \tag{A.22}$$

for all $\dot{q}_i$. Now letting $\dot{q}_i$ be equal to (1,0,0), (0,1,0) and (0,0,1), we find in turn that

$$(\partial\psi/\partial q_{i,j}) n_j = 0 \qquad \text{on} \quad S_p \,. \tag{A.22'}$$

On the other hand, on S_i, per force:

$$\dot{q}_i = q_i = 0. \tag{A.23}$$

CASE 2. In a similar manner:

$$(\partial\psi/\partial q_{i,j}) n_j = 0 \qquad \text{on} \quad S_T \,, \tag{A.24}$$

while:

$$\dot{q}_i = q_i = 0 \qquad \text{on} \quad S_u \,. \tag{A.25}$$

A.4. Conservation of linear and angular momentum

In the presence of migratory motion and similar types of non-affine deformation one cannot assume *a priori* that the local equations of conservation of linear and angular momentum will be preserved. To arrive at these laws we invoke the following axiom.

AXIOM. $\dot{\Psi} = 0$ and $\dot{q}_i = 0$, whenever $v_i = v_i^*$ are virtual rigid body velocities.

The physics of the Axiom is self-evident and was discussed at length elsewhere, see VALANIS [6]. It follows from Eq. (A.6) that:

$$\int_S T_i v_i^* \, dS + \int_V f_i v_i^* \, dV = 0. \tag{A.26}$$

Let v_i^* be a translational velocity, constant in V and on S. Then since it is also arbitrary:

$$\int_S T_i \, dS + \int_V f_i \, dV = 0. \tag{A.27}$$

Then by the usual arguments of continuum mechanics,

$$T_i = \sigma_{ji} n_j \quad \text{on} \quad S, \tag{A.28}$$

$$\sigma_{ij,i} + f_j = 0, \tag{A.29}$$

where σ_{ij} is the stress tensor. On the other hand if v_i^* are the result of rigid body rotation, i.e.,

$$v_i^* = e_{ijk} \Omega_j x_k \,, \tag{A.30}$$

where e_{ijk} is the permutation tensor, x_k are the reference coordinates and Ω_j is the angular velocity vector, then in view of Eqs. (A.26), (A.28) and (A.29):

$$\sigma_{ij} = \sigma_{ji} \,. \tag{A.31}$$

It then follows by straightforward analysis, using Eqs. (A.6), (A.7), (A.8), (A.18), (A.28) and (A.29) that

$$\sigma_{ij} = \partial \psi / \partial u_{i,j} \tag{A.32}$$

and thus,

$$\partial \psi / \partial u_{i,j} = \partial \psi / \partial u_{j,i} \tag{A.33}$$

whereby

$$\psi = \psi(\varepsilon_{ij}, \ldots), \tag{A.34}$$

where $\varepsilon_{ij} = (1/2)(u_{i,j} + u_{j,i})$.

A.5. Gibbs formulation

Let ϕ be the Gibbs free energy density of the domain, where

$$\phi(\sigma_{ij};\ q_{i,j};\ q_i) = \psi - \sigma_{ij} \varepsilon_{ij} \,. \tag{A.35}$$

Upon use of Eqs. (A.6), (A.7) and (A.35) one finds the following expression for $\dot{\phi}$:

$$\int_V \dot{\phi} \, dV = - \int_S u_i \dot{T}_i \, dS - \int_V u_i \dot{f}_i \, dV - \int_V Q_i \dot{q}_i \, dV. \tag{A.36}$$

Equation (A.36) is the variational principle, in terms of ϕ, true for virtual traction rates $\dot{T}_i$, body force rates $\dot{f}_i$ and migration velocities $\dot{q}_i$. Use of the Green – Gauss theorem on the surface integral in Eq. (A.36) gives the following result:

$$\text{(A.37)} \qquad \int_V [\partial\phi/\partial\sigma_{ij} + \varepsilon_{ij}]\,\dot{\sigma}_{ij}\,dV + \int_S (\partial\phi/\partial q_{i,j}) n_j \dot{q}_i\,dS - \int_S [(\partial\phi/\partial q_{i,j})_{,j} - \partial\phi/\partial q_i - Q_i]\,dV = 0.$$

Repeating the standard variational arguments presented earlier, we find the following equations in V:

$$\text{(A.38)} \qquad \varepsilon_{ij} = -\partial\phi/\partial\sigma_{ij}\,,$$

$$\text{(A.39)} \qquad (\partial\phi/\partial q_{i,j})_{,j} - \partial\phi/\partial q_i = Q_i\,.$$

On S:

$$\text{(A.40)} \qquad \partial\phi/\partial q_{i,j} n_j = 0 \quad \text{on } S_p\,, \qquad q_i = \dot{q}_i = 0 \quad \text{on } S_i$$

for migratory q_i. However, for structural q_i:

$$\text{(A.41)} \qquad \partial\phi/\partial q_{i,j} n_j = 0 \quad \text{on } S_T\,, \qquad q_i = \dot{q}_i = 0 \quad \text{on } S_u\,.$$

The analysis is now complete.

References

1. D.J. LUBAHN and R.P. FELGAR, *Plasticity and creep in metals*, John Wiley and Sons, New York 1951.
2. K.C. VALANIS, *Fundamental consequences of a new intrinsic time measure. Plasticity as a limit of the endochronic theory*, Arch. Mech., **32**, 171–191, 1980.
3. K.C. VALANIS, *A gradient theory of internal variables*, Acta Mech., **116**, 1–14, 1996.
4. K.C. VALANIS, *A thermodynamic theory of patterned deformation*, Acta Mech. [in press].
5. K.C. VALANIS, *The concept of physical metric in thermodynamics*, Acta Mech., **113**, 169–184, 1995.
6. K.C. VALANIS, *A gradient theory of finite viscoplasticity*, Arch. Mech., **49**, 589–606, 1997.

ENDOCHRONICS
8605 NW Lakecrest Court, Vancouver WA 98665, USA.

Received May 27, 1997; new version October 24, 1997.

Arch. Mech., 50, 1, pp. 113–126, Warszawa 1998
FIFTY YEARS OF THE ARCHIVES OF MECHANICS

Optimization of local heating for a spherical shell made of titanium alloy BT-23

S.F. BUDZ, W.I. ASTASHKIN, I.S. BUDZ
and I.I. CHUPYK (LVIV)

THE PROBLEM of optimization of local heating for a spherical shell made of titanium alloy BT-23 in order to reduce maximal transient or residual stresses is posed and solved. The effect of the volume changes occurring during phase transition is taken into account. The minimum of the transient or residual stresses is adopted as an optimization criterion for determination of optimal temperature fields.

1. Introduction

THIN-WALLED SHELL constructions during manufacturing and exploitation often undergo local heating, which is used for various technological reasons. This process produces the stressed state of construction which causes appearing of the cracks, plastic deformation etc. Therefore the task of local heating optimization is very important. Minimization of the stresses is performed by choosing such heating regime which leads to the stress distribution similar to a homogenous one. As it is shown in [1], non-optimal local heating may significantly reduce effectiveness of the heating.

Solution of the problem of local optimal heating is connected with using constitutive equations of the thermoelastic theory [2, 3], and the calculation methods of constructions exposed to various thermal and thermo-mechanical influences [4, 5]. Mathematical theory of optimal local heating is considered in [6] and [7–10]. However, those approaches are valid for the materials and heating regimes if there are no structural transformations.

In this paper we consider the problem of optimization of local heating for thin-walled shell constructions. In contrast to the papers [6–10], the following problems have been analyzed:

1. Phase transition during heating, and casting during cooling are taken into account.

2. The problem of choice of optimal heating is reduced to calculation of temperature fields which minimize the transient and residual stresses. Minimization of residual stresses was provided by preliminary optimization of heterogeneous phase distribution and calculation of the appropriate temperature field.

In direct solving and optimization of the problem of local heating, the residual stresses are calculated which are produced by heterogeneous phase distribution due to casting, but not by thermoplastic deformation. The authors have not

found the above formulation of the problem of local optimal heating in the literature. The inhomogeneous distribution of phases was established, what is a novelty in local heating problems.

2. The subject of the paper and constitutive equations

The purpose of this paper is to define the stress state of a spherical shell made of titanium alloy BT-23 during local equatorial heating, and to optimize it. We assume that the shell is free from any external mechanical influences and no stresses have been introduced by previous technological operations during its production and processing. Local heating of the shell is a technological process of heating of its equator from the initial temperature of 20° C to the temperature previously defined (in our case that temperature was 720° C). We consider the heating to depend upon the radial coordinate.

Alloy BT-23 during heating in the temperature range of 520 – 920° C undergoes phase transition. During rapid cooling it is cast and the phase state is fixed, which is different from the one appearing during very slow cooling. During ordinary cooling of locally heated shell in the air, the casting conditions for the heated zone are provided because the cooling is not only due to the heat exchange with environment but also to the intensive heat flow to cooler parts of the shell.

We consider two reasons of appearing the stresses in the shell:

1. The stresses are produced by thermal dilatation of phase transitions. In this case the stresses are simple functions of temperature and can be defined by thermoelastic methods [2, 3].

2. After cooling, the material is cast and the spatially inhomogeneous phase state is fixed. The residual stresses are the result of the difference of the specific volumes of the phases. The phase state of the material after complete cooling depends on the temperature from which the cooling was started, and on the speed of the cooling. We consider the speed of cooling when the phase state depends only on the temperature from which the cooling was initiated.

In the normal state, when temperature is 20° C, the alloy BT-23 contains 80% of α-phase (hexahedral dense-packed lattice) and 20% of β-phase (body-centered cubic lattice). This alloy has the following chemical composition: Al – 5.4%, Mo – 1.9%, V – 4.7%, Cr –1.2%, Fe – 0.5%, Ti – 86.3%. By heating the alloy in the temperature range of 520° C – 920° C, the quantity of β-phase increases to 100%. As it was shown in [2], the difference in the specific volumes between α and β phases is about 2 – 5% which influences significantly the value and distribution of the transient and residual stresses.

Figure 1 presents the diagram of linear approximation of the β-phase mass fraction (Ξ) as a function of temperature t of the uniformly heated material (curve *1*), and of the experimentally determined dependence of the residual fraction of β-phase in the material on the initial temperature of cooling (curve *2*).

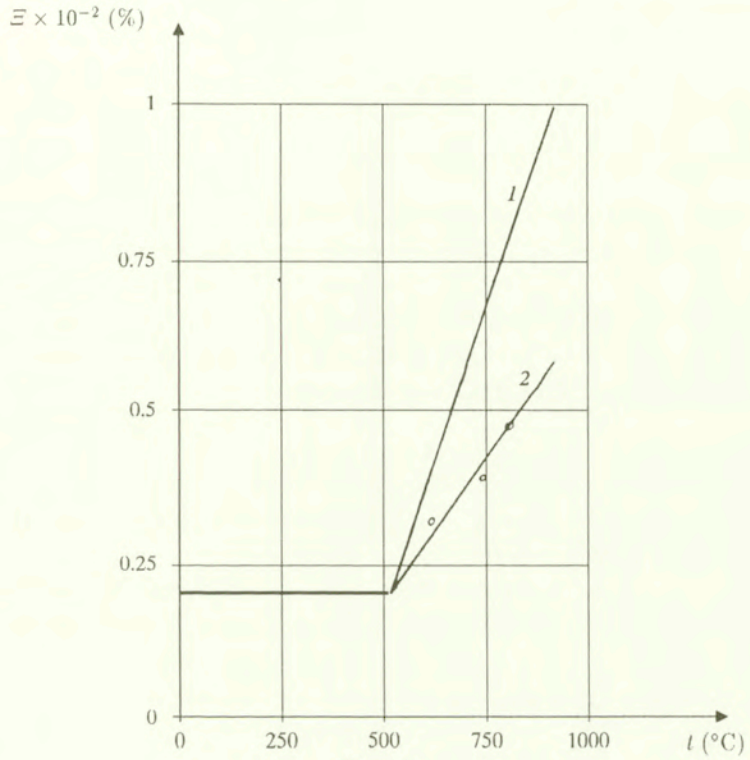

FIG. 1.

During heating the total change of shell volume de_T consists of two parts – thermal volume increment de_t and structural volume increment de_ξ:

$$de_T = de_t + de_\xi\,, \tag{2.1}$$

where $de_t = 3\alpha_* dt$, $de_\xi = 3\beta_* d\Xi$, α_* is the linear coefficient of thermal expansion, β_* is the linear coefficient of structural dilatation (dilatation which depends on phase transition). In general, α_* and β_* are functions of temperature. It should be noticed that in the temperature range of phase transition of alloy $520^\circ\,\mathrm{C} < t < 920^\circ\,\mathrm{C}$, the thermal component of the volume e_t is increasing, and the structural one e_ξ is decreasing [2].

During very slow or stationary heating, at each point of the material certain phase distribution, which depends on temperature of the point, is established. Therefore, under these conditions, the phase transition fraction Ξ is a simple function of temperature t ($\Xi = \Xi(t)$), and the total change of the volume can be determined from the equation:

$$de_T = 3\alpha^*(t)\, dt, \tag{2.2}$$

where $\alpha^*(t) = \alpha_* + \beta_*(t)\, d\Xi/dt$ is the generalized linear coefficient of thermal expansion which depends on all volume changes which occured in the material

during heating. In the paper we assume:

$$\alpha^*(t) = \begin{cases} \alpha_1, & t < 520^\circ\,\mathrm{C}, \\ (\alpha_1 + \alpha_2)/2 + \beta_*(t)d\Xi/dt, & 520^\circ\,\mathrm{C} < t < 920^\circ\,\mathrm{C}, \\ \alpha_2, & t > 920^\circ\,\mathrm{C}, \end{cases} \tag{2.3}$$

where α_1 is the linear coefficient of thermal expansion in the temperature range of $20^\circ\,\mathrm{C} < t < 520^\circ\,\mathrm{C}$, α_2 is the linear coefficient of thermal expansion in the temperature range of $t > 920^\circ\,\mathrm{C}$, $\beta_*(t)$ is an experimentally found function [11]. Figure 2 presents the graph of this coefficient $\alpha^*(t)$ (the graph has been taken from [11, 12]). It should be noticed that function β_* may be considered to be constant and it may be found from the equation:

$$\beta_* = (V_1 - V_2)/V_1\,, \tag{2.4}$$

where V_1 is the specific volume of the alloy when $t = 520^\circ\,\mathrm{C}$, V_2 is the specific volume of the alloy when $t = 920^\circ\,\mathrm{C}$.

After cooling, certain residual stress state is produced by inhomogeneous β-phase distribution. In this case, the volume change is defined by changing

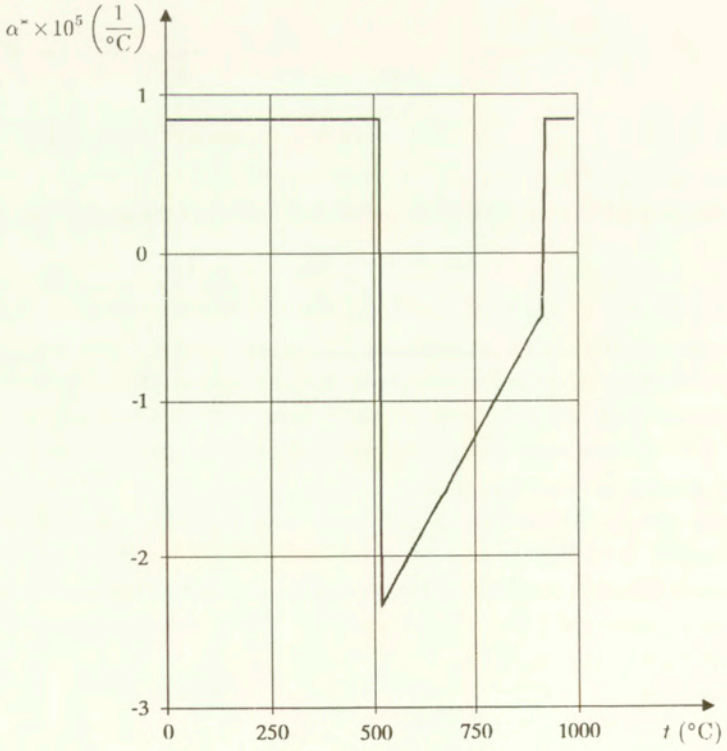

FIG. 2.

the function $d\Xi$:

$$de_\Xi = 3\beta_0\, d\Xi, \tag{2.5}$$

where β_0 is the linear coefficient of structure dilatation. It was determined in [11]:

$$\beta_0 = \begin{cases} -0.013 & \text{for the points, which have experienced phase transitions,} \\ 0 & \text{for the points, which did not experience phase transitions.} \end{cases}$$

The generalized Hooke's law for the discussed case in a differential form can be written as

$$d\sigma_{ij} = \frac{E}{1+\nu}\left\{de_{ij} + \frac{1}{1-2\nu}\left[\nu\, de - (1+\nu)de_a\right]\delta_{ij}\right\}, \tag{2.6}$$

where $d\sigma_{ij}$ are components of the stress tensor, de_{ij} are components of the strain tensor, E is the elastic modulus, ν is Poisson's ratio, $e = e_{11} + e_{22} + e_{33}$, δ_{ij} is Kronecker's delta, $a = T, \Xi$, $i, j = (1, 2, 3)$.

It should be noticed that transient stresses during heating and residual stresses after heating are determined from Eq. (2.6). In this case the reason for residual stresses to appear is not the thermoplastic deformation but the inhomogeneous phase state which is fixed by rapid cooling.

From Eqs. (2.2), (2.5) and (2.6) we derive the equation for volume changes during the heating:

$$e_T = 3\int_{t_0}^{t} \alpha_*(t)\, dt, \tag{2.7}$$

where t_0 is the initial temperature; and during the casting:

$$e_\Xi = \begin{cases} 3\displaystyle\int_{\Xi_0}^{\Xi_S} \beta\, d\Xi & \text{for the points, which have experienced phase transitions,} \\ 0 & \text{for the points, which did not experience phase transitions.} \end{cases} \tag{2.8}$$

The generalized Hooke's law for the discussed case can be written in the form

$$\sigma_{ij} = \frac{E}{1+\nu}\left\{e_{ij} + \frac{1}{1-2\nu}\left[\nu\, e - (1+\nu)e_a\right]\delta_{ij}\right\}. \tag{2.9}$$

3. The phase distribution and state of stress of spherical shell during and after the heating

At first we will define the state of stress of the spherical shell during heating. It is assumed that the shell is free from any external mechanical influences. Stationary, axisymmetric heating uniform across the width is provided along the equator of the sphere.

The meridional (σ_1) and circumferential (σ_2) stresses in the spherical shell are found from the relations [11]:

$$\sigma_1 = 1/(2h)(N_1 + 3\gamma/h^2 M_1), \qquad \sigma_2 = 1/(2h)(N_2 + 3\gamma/h^2 M_2), \tag{3.1}$$

where γ is the distance from the middle surface of the shell ($-h < \gamma < h$),

$$N_1 = -D_1 V \operatorname{ctg}\varphi/R, \quad M_1 = -D_1/R(d\theta/d\varphi + \nu\theta \operatorname{ctg}\varphi),$$
$$N_2 = -D_1/R dV/d\varphi, \quad M_2 = -D_1/R(\theta \operatorname{ctg}\varphi + \nu d\theta/d\varphi), \quad V = 1/R(L(\theta) - \nu\theta).$$

N_1, N_2 are meridional and circumferential strains; M_1, M_2 are meridional and circumferential moments; θ is the angle of inclination of the normal to the middle surface of the shell, and it is determined from the equation [6]:

$$LL(\theta) + (D_* R^2 - \nu^2) = D_* R^2 \frac{d}{d\varphi} e_a, \tag{3.2}$$

where

$$L = \frac{d^2}{d\varphi^2} + \operatorname{ctg}\varphi \frac{d}{d\varphi} - \operatorname{ctg}\varphi,$$

φ is the arc length of the meridian, R is the radius of the middle surface of the shell, $D_* = D_0/D_1$, $D_0 = 2Eh$ is the tensile rigidity; $D_1 = 2Eh^3/(3(1-\nu^2))$ is the bending rigidity, $2h$ is the thickness of the shell, $a = T, \Xi$.

During such a heating regime, the function θ will be defined when the equator does not rotate ($\theta(\pi/2) = 0$), the meridional strains are equal zero there ($N_1(\pi/2) = 0$), and meridional σ_1 and circumferential σ_2 stresses are symmetric with respect to the equatorial section.

Equation (3.1) was solved by means of the finite element method for the shell with the following physical and geometrical parameters: the radius of the middle surface of the shell $R = 0.1815$ m, the thickness $2h = 0.009$ m, $E = 106$ MPa, $\nu = 0.3$. While solving the direct problem, we used the practically local equatorial heating shown in Fig. 3, curve *1*. Here $s = R\varphi$ is the distance measured along the meridian from the equator ($\varphi = 0, \pi/2$). This heating regime does not account for the phase transformation in the material. This temperature field corresponds to the transient heterogeneous phase distribution (Fig. 4, curve *1*), which was defined by Fig. 1, curve *1*, and the distribution of transient internal (Fig. 5, curves *1*) and external (Fig. 6, curves *1*) stresses; $\sigma_1^{\pm}$ and $\sigma_2^{\pm}$ are

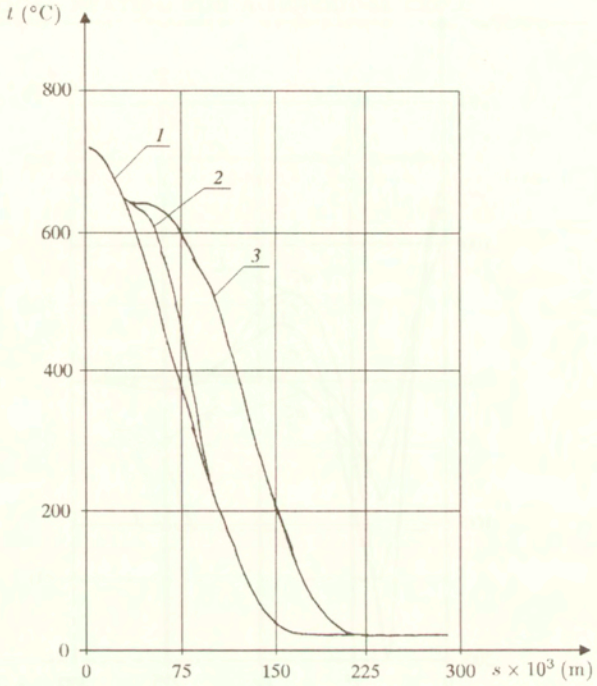

FIG. 3.

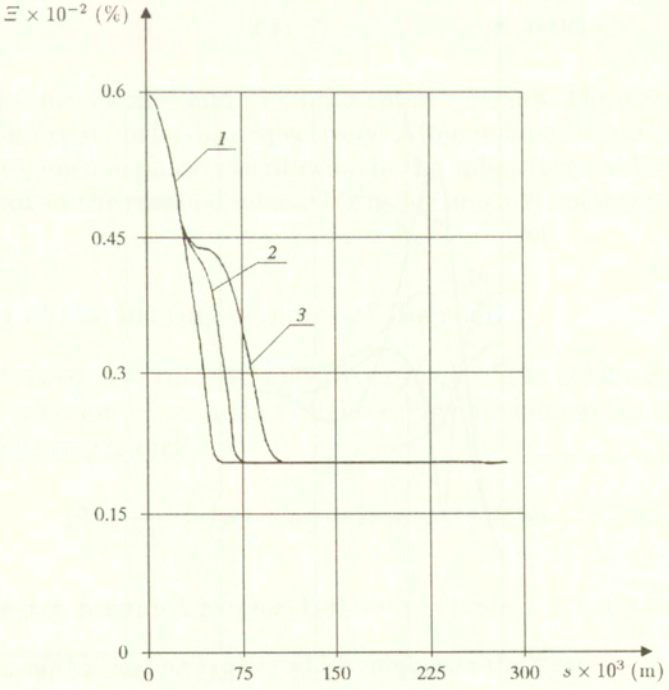

FIG. 4.

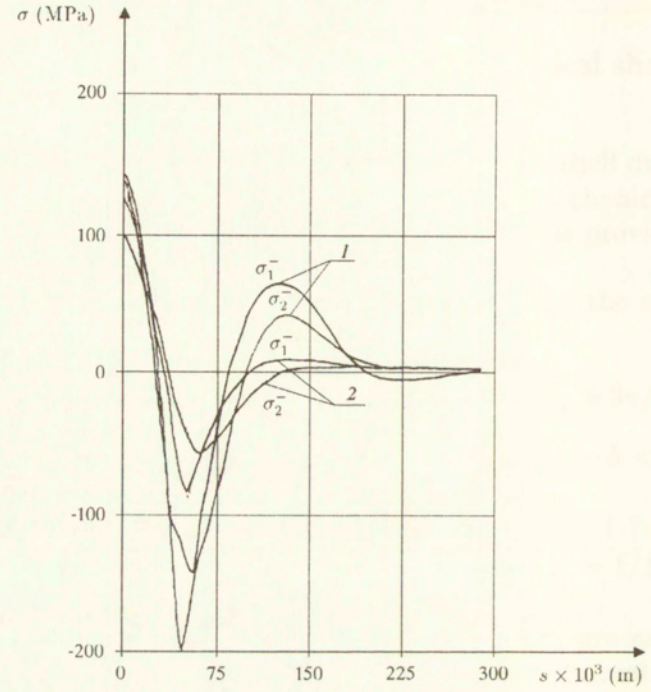

FIG. 5.

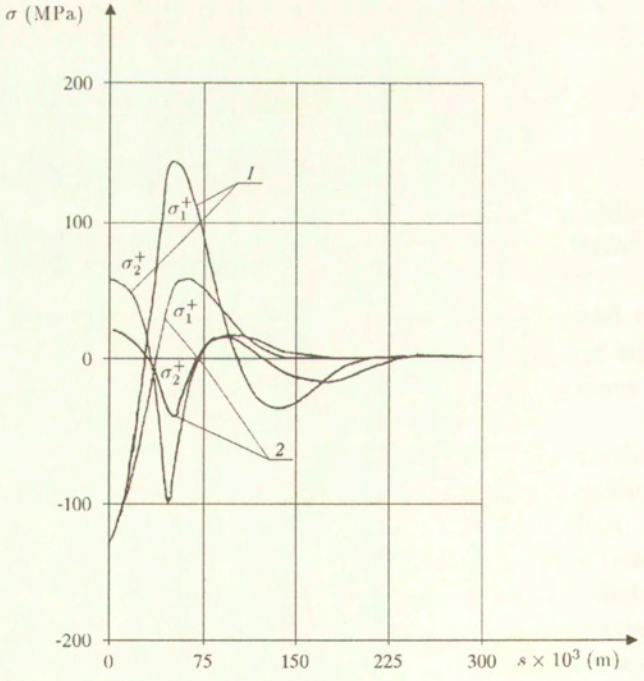

FIG. 6.

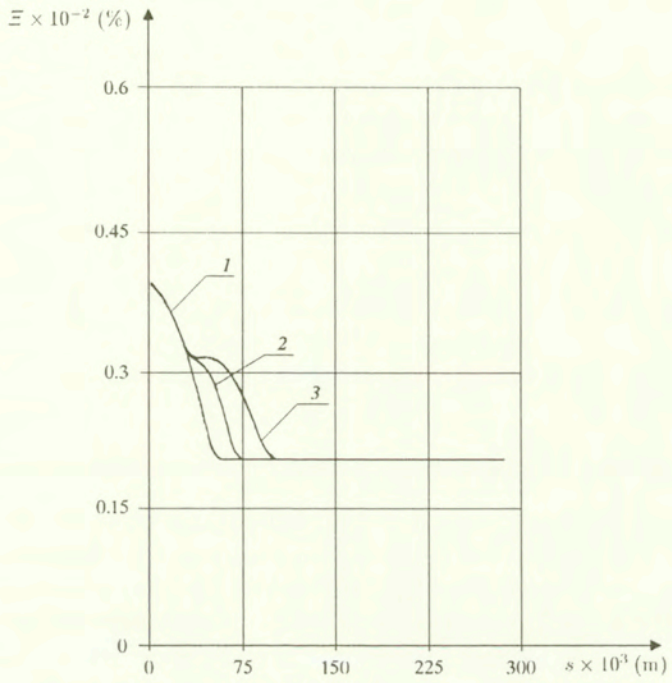

FIG. 7.

components of the meridional and circumferential stresses. The signs ± apply to external and internal surfaces, respectively. After instantaneous stopping of heating, the heterogeneous phase distribution in the sphere is established (Fig. 7, curves *1*) which causes the residual internal (Fig. 5, curves *2*) and external (Fig. 6, curve *2*) stresses.

4. Optimization of the heating regimes of the shell

The optimization of axi-symmetric heat treatment of the sphere is performed according to the criterion of minimum of the energy functional for transient or residual elastic deformation [8]:

$$F = \frac{1}{2E} \int_{\Omega} \left(\sigma_1^2 + \sigma_2^2 - 2\nu(\sigma_1 \sigma_2) \right) d\Omega, \tag{4.1}$$

where Ω is the region occupied by the shell.

4.1. Determination of the heating regime which minimizes the stresses during the heating

The problem of determination of axi-symmetric stress during optimal heat treatment in the spherical shell with limitation imposed on temperature and

stress is considered. It is assumed that heating is homogeneous across the width. In the initial state there are no stresses in the shell. During and after the heating the shell is free from any mechanical influences. The local heating will be defined under limitation imposed on temperature ($t = t_*$) along the equator. The problem is solved under the following conditions:

$$t(^{\pm}S_1) = t_0, \qquad t(0) = t_*, \qquad \left.\frac{\partial t}{\partial S}\right|_{S=\pm S} = 0, \tag{4.2}$$

where $S_1 = 0.2\,\mathrm{m}$ is the range of heating, t_0 is the initial temperature. The optimal temperature field is the solution of the following problem: define the extremum of the elastic energy functional (4.1) which satisfies Eq. (3.2) and the condition of freedom from mechanical loading (4.2).

4.2. Determination of the heating regime which minimizes residual stresses

Residual stresses which appear in the shell after cooling are defined by inhomogeneous phase distribution. Therefore we optimize the phase state of the shell and then define the temperature field which leads to that phase state. Therefore the problem of determination of optimal phase distribution in the material subject to local heating uniformly distributed across the width is posed. There are no initial stresses in the shell. After the heating it is free from any mechanical influences. Local phase distribution will be defined with limitation of the β-phase mass fraction (Ξ_*) in the equator. The problem is solved with the following boundary conditions:

$$\Xi(^{\pm}S_1) = \Xi_0\,, \qquad \Xi(0) = \Xi_*\,, \qquad \left.\frac{\partial \Xi}{\partial S}\right|_{S=\pm S} = 0, \tag{4.3}$$

where Ξ_0 is initial phase distribution in the material. The optimal phase distribution is the solution of the problem of defining the extremum of the elastic energy functional (4.1) which satisfies Eq. (3.2) and condition (4.3). The temperature field which corresponds to the optimal phase distribution is shown in Fig. 1, curve *2*.

The optimization was accomplished by the Hooke – Jeeves method [13]. The temperature shown in Fig. 3, curve *1*, was taken as an initial assumption in determining the optimal one, which minimizes the transient stresses in the sphere. The functional (4.1) was found from this initial approximation and its optimization was provided by variation of that temperature. Optimization of the functional was accomplished when its n-th step did not differ by more than 1% from the preceding one. The optimal temperature obtained by that method is presented in Fig. 3, curve *2*. The transient phase fistribution (Fig. 4, curve *2*) and transient internal nad external stresses (curves *1* in Fig. 8 and Fig. 9) are produced by that optimal temperature. After the cooling, the residual heterogeneous phase distribution (Fig. 7, curve *2*) and the corresponding residual internal and external

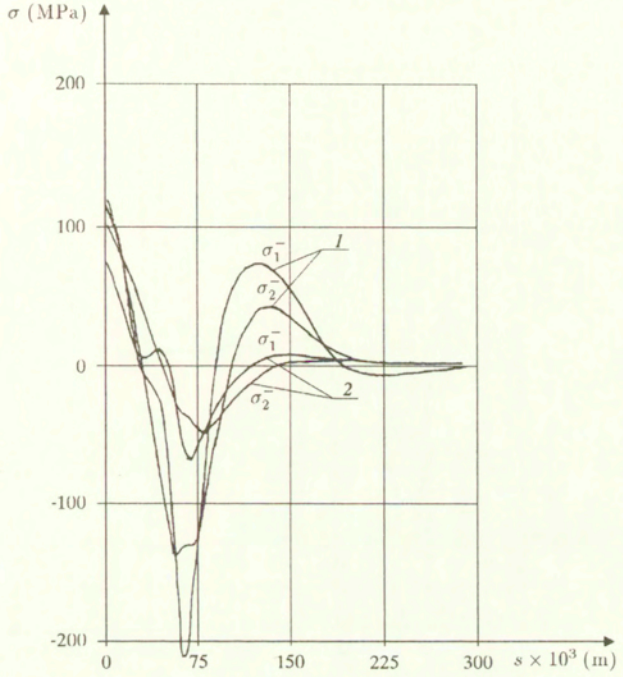

FIG. 8.

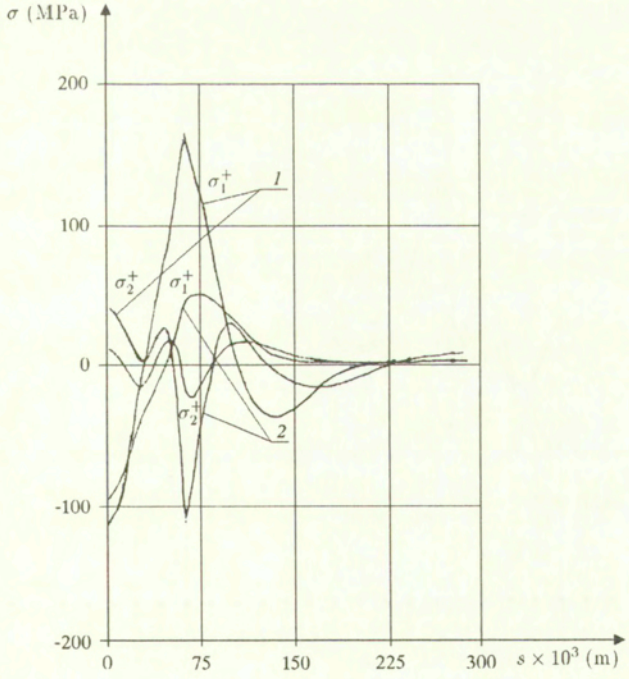

FIG. 9.

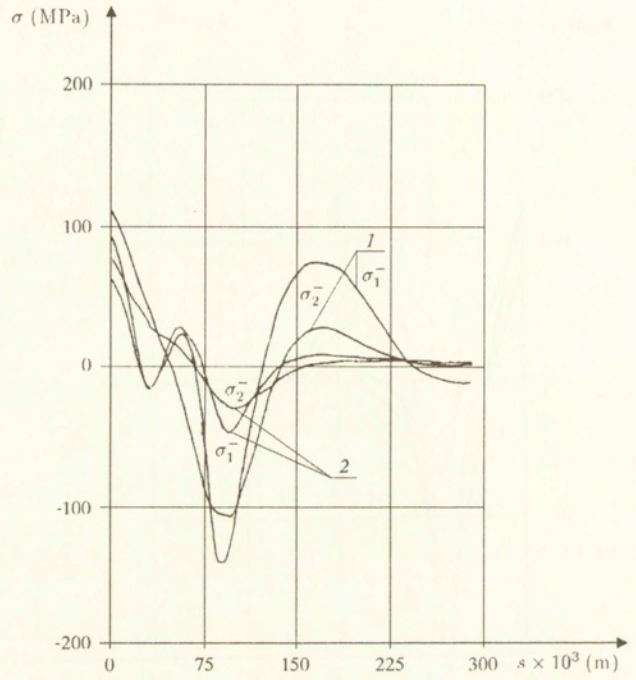

FIG. 10.

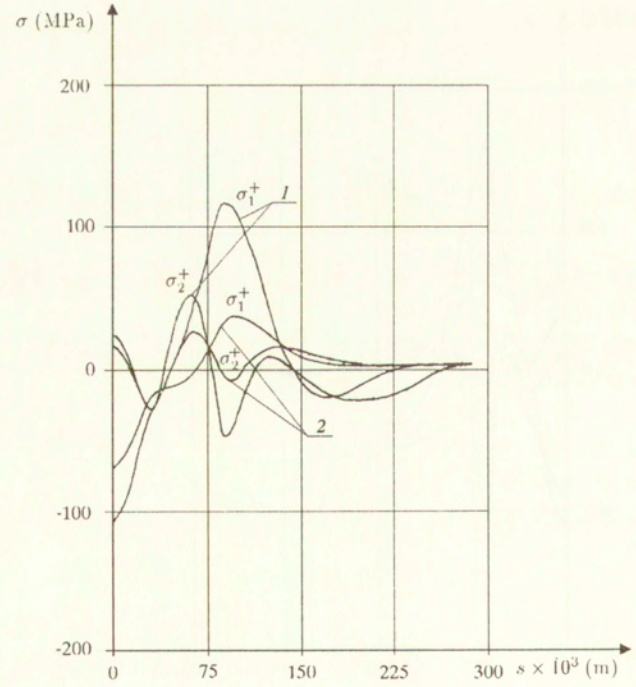

FIG. 11.

stresses (curve *2* in Fig. 8 and Fig. 9) are established. The temperature (Fig. 3, curve *2*) minimizes the transient stresses in the sphere, that are the stresses which appear *during this heating regime.*

During minimization of the residual stresses, the initial functional (4.1) was defined by residual phase distribution (Fig. 7, curve *1*) which was established after the same initial heating (Fig. 3, curve *1*). The optimal residual phase distribution (Fig. 7, curve *3*) was found by the Hooke – Jeeves method. The residual internal and external stresses (curves *2* in Fig. 10 and Fig. 11) correspond to that optimal residual phase distribution. The heating regime (Fig. 3, curve *3*) which creates this phase distribution was defined by function $\Xi = \Xi(t)$ shown in Fig. 1, curve *2*. The temperature (Fig. 3, curve *3*) minimizes the residual stresses in the sphere which appear *after this heating regime.*

5. Conclusions

The optimal heating of the spherical shell made of titanium alloy BT-23 which undergoes phase transition exhibits some peculiarities following that phenomenon. Rapid cooling after heating and casting were taken into account by determining the residual stresses.

The determination of optimal temperature fields is performed under the assumption that temperature was not controlled once the heating had been stopped. From the obtained data we can see that optimal temperature field which minimizes the transient stresses (Fig. 3, curve *2*) has a negligible effect on the stresses (compare curves *1* in Figs. 5, 6 with curves *1* in Figs. 8, 9 for transient stresses and curves *2* in Figs. 5, 6 with curves *2* in Figs. 8, 9 for residual stresses). The most significant effect was obtained by optimization of the residual phase distribution (Fig. 7, curve *3*) which was established in the material after cooling. In this case we can reduce the residual stresses by approximately 35% (compare curves *2* in Figs. 5, 6 with curves *2* in Figs. 10, 11). The heat regime (Fig. 7, curve *3*) which reflects that optimal residual phase distribution, was found by using the phase transition function $\Xi(t)$ presented in Fig. 1, curve *1*. It turned out that, during that heat regime, the transient stresses have been reduced by approximately 20% in comparison with the initial heat treatment (Fig. 3, curve *1*), compare curves *1* in Figs. 5, 6 with curves *1* in Figs. 10, 11.

References

1. YA.S. PODSTRIGACH, E.I. GORIACHEVA, YA.I. BURAK, L.P. BESEDINA, L.A. KOZAKOVA and V.A. KANYGIN, *On the influence of temperature field on residual relaxation stresses during local haeting of circumferential joints* [in Russian], Physico-Chemical Mechanics of Material, No. 1, 1970.
2. A.D. KOVALENKO, *Foundations of thermoelasticity* [in Russian], Naukova Dumka, Kiev 1970.

3. W. NOWACKI, *Theory of elasticity* [in Russian translation], Mir, 1975.
4. Y.I. NYASHIN and P.V. TRUSOV, *Residual stresses. Simulation and control*, Advances in Mech., **12**, 4, 77–109, 1989.
5. Y.I. NYASHIN and P.V. TRUSOV, *Residual stress optimization in material treatment. Residual stresses – III. Science and technology*, Vol. 1, FUJIWARA, T. ABE and K. TANAKA [Eds.], Elsevier Applied Science, London and New York, 1260–1266, 1992.
6. E.I. GRIGOLYUK, YA.S. PODSTRIGACH and YA.I. BURAK, *Optimizarion of heating of shells and plates* [in Russian], Naukova Dumka, Kiev 1979.
7. YA.S. PODSTRIGACH, *Foundations of the theory of optimal heating regimes for casting joints* [in Russian], Bull. of AS USSR, No. 5, 1969.
8. YA.I. BURAK, E.I. GRIGOLYUK and YA.S. PODSTRIGACH, *On various methods of determination of optimal heating of thin-walled shells* [in Russian], Bull. of the VII-th All-Union Conference on the Theory of Shells and Plates, Dniepropetrovsk 1969, Nauka, 1970.
9. E.I. GRIGOLYUK, YA.I. BURAK and YA.S. PODSTRIGACH, *On a certain external thermoelastic problem of an infinite cylindrical shell* [in Russian], Bull. of AS USSR, **174**, 3, 1967.
10. E.I. GRIGOLYUK, YA.I. BURAK and YA.S. PODSTRIGACH, *Solution of a variational thermoelastic problem of thin-walled shells and determination of optimal heating regimes* [in Russian], J. of Appl. Mech. and Tech. Physics, 4, 1968.
11. A.A. ILIN, M.YU. KOLLEROV, V.V. ZASYPKIN and V.I. MAISTROV, *Voluminal change occurring in $(\alpha + \beta)$-titanium alloys at polymorphic transformations* [in Russian], Metallovedenie i Termicheskaya Obrabotka, 1, 1986.
12. *Handbook of physical magnitudes* [in Russian], I.K. KIKOIN [Ed.], Atomizdat, 1976.
13. D. HIMMELBLAU, *Applied nonlinear programming* [in Russian], Mir, 1975.

PIDSTRYGACH INSTITUTE OF APPLIED PROBLEMS
OF MECHANICS AND MATHEMATICS, NASU
Lviv, Ukraine.

Received August 19, 1996; new version October 27, 1997.

Arch. Mech., 50, 1, pp. 127–138, Warszawa 1998
FIFTY YEARS OF THE ARCHIVES OF MECHANICS

Effect of miss-distance on the airfoil-vortex interaction Numerical study

J. PIECHNA and A.P. SZUMOWSKI (WARSZAWA)

THE EFFECT of a strong vortex interacting with an airfoil flow is investigated numerically. The finite volume method for Euler equations is applied. Instantanous flow patterns, including pressure distributions along the airfoil and lift coefficients, were calculated for various miss-distances of the vortex passing parallel to the airfoil plane. It was found that the effects of interaction are much stronger when the vortex approaching the airfoil accelerates the flow at the pressure surface than in the case when the vortex decelerates the flow at the suction surface.

1. Introduction

IN CERTAIN CASES of helicopter flight, e.g. descent with deep turns or low-powered approach to landing, the rotor blade tip vortices strongly disturb the flow at the following blades. As a result, the blade loading considerably varies. This leads to vibrations of the blade and of the remaining elements of the helicopter structure. The variations of blade loading are accompanied by impulsive noise of high intensity.

The strongest effects of the airfoil-vortex interaction (AVI) occur when the vortex passes parallel and close to the airfoil plane. This was the main reason why the majority of the investigators who studied the AVI phenomenon considered two-dimensional model of interaction.

The vortex filament can pass at various miss-distances along both the upper and bottom surfaces of the airfoil. When it is equal to zero, a head-on impact occurs. This problem was investigated by LEE and BERSHADER [1, 2]. They solved the Navier–Stokes equations using a fifth order upwind scheme based on Osher-type of flux differencing. The isolines of density calculated by the above authors qualitatively coincide with those observed in the corresponding interferometric photographs. The sound wave which appears due to an expansion of high pressure air in the stagnation region was also predicted in the papers mentioned above. Pressure in the stagnation region increases when the vortex approaches the leading edge.

Variations of the surface pressure during the AVI for the vortex passing under the airfoil plane (increasing the flow velocity along the bottom surface of the airfoil) were calculated by DAMODARAN and CAUGHEY [3], EHRENFRIED [4] and GALLMAN [5]. The unsteady Euler equations [3, 4] or full-potential equation for transonic flow [5] were solved. DAMODARAN and CAUGHEY [3] and EHRENFRIED [4] noted a strong influence of the vortex on the lift and pitching moment

coefficients. Unfortunately, only one value of the miss-distance, equal to a quarter of the chord lengh, was considered by the above authors.

In the present work, an effect of miss-distance for the vortex passing over or under the NACA 0012 airfoil at 0 deg. angle of attack is considered. The miss-distance was changed in the range from -0.5 to $+0.2$ chords. A constant flow Mach number at infinity $M_\infty = 0.69$ and a constant circulation of a clockwise rotating vortex were assumed.

2. Equations

A coherent vortex of relative core radius $r/c = 0.045$ (r_0 – core radius, c – chord length of the airfoil) which is the subject of the present calculations causes rapid changes of actual flow properties during its passage along the airfoil. It can be supposed that these changes are controlled, first of all, by inertia effects but not by viscous ones.

By this assumption the Euler equations seem to be adequate for these calculations.

The two-dimensional Euler equations in integral form are as follows:

$$\frac{\partial}{\partial t}\int_S U\,ds + \int_L F\,dy + \int_L G\,dx = 0, \tag{1}$$

where

$$U = \begin{pmatrix} \varrho \\ \varrho u \\ \varrho v \\ e \end{pmatrix}, \qquad \begin{pmatrix} \varrho u \\ \varrho u^2 + p \\ \varrho uv \\ (e+p)u \end{pmatrix}, \qquad G = \begin{pmatrix} \varrho v \\ \varrho uv \\ \varrho v^2 + p \\ (e+p)v \end{pmatrix},$$

$$e = \varrho\frac{(u^2+v^2)}{2} + p/(\gamma - 1).$$

The first integral is related to the control area S and the remaining ones to the control circuit L (encircling the control area).

3. Boundary and initial conditions

The calculations performed in the present work correspond to experimental investigations of the AVI process with the use of shock tubes. To reproduce the experimental conditions, a control area shown in Fig. 1 is considered. Its upper and bottom surfaces correspond to the shock tube walls. Hence, the fluxes accross these walls are assumed to be zero. The remaining surfaces represent the cross-sections of the shock tube located upstream and downstream of the test airfoil. For these surfaces, a one-dimensional Riemann flow is considered.

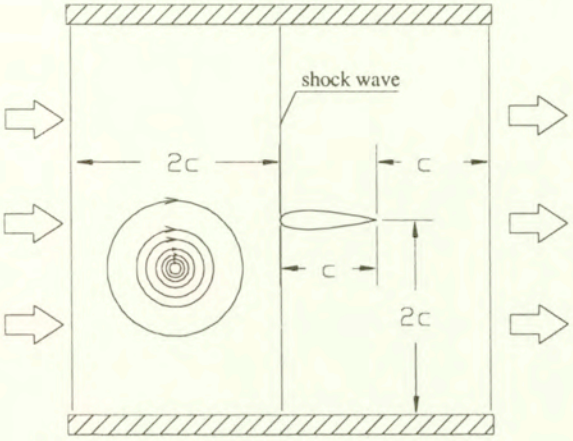

FIG. 1. Control area, $c = 120$ mm.

For the initial conditions it is assumed that the shock wave running in motionless air reaches the leading edge of the airfoil. The shock wave is followed by an axisymmetric vortex convected in a uniform flow. The vortex center in the initial phase of computation is located at half the distance between the shock front and the upstream control surface. It is assumed that the flow velocity induced by the vortex at the upper and bottom walls, as well as at the upstream cross-section and at the shock front, is small enough to be neglected. For the vortex considered (see below) it is under 5% of the flow velocity behind the shock wave. The calculations were stoped when the vortex leaves the trailing edge of the airfoil.

The flow velocity induced by the vortex for the initial phase of interaction is obtained from the following relationship:

$$V_\theta = \frac{\Gamma}{2\pi r} \frac{r^2(2+\alpha)}{r^2 \exp\left(\alpha(r-r_0)/r_0\right) + (1+\alpha)r_0^2}, \tag{2}$$

where V_θ – tangential velocity, r_0 – vortex core radius, Γ_0 – circulation at $r = r_0$, α – coefficient controlling velocity distribution.

The coefficient strongly influences the velocity distribution outside the vortex core but weakly inside it (Fig. 2).

For the experimental data which can be found in Ref. [6] $\alpha = 0.15$. For this α the velocity decay (in the radial direction) in the vortex is much stronger than for the clasical vortex model with $\alpha = 0$ (see Fig. 2). Taking into account this feature, one can consider a smaller control volume for $\alpha > 0$ than in the case of the clasical vortex. The pressure distribution corresponding to $V_\theta(r)$ can be found using the momentum

$$\frac{p}{r} = \frac{\varrho V_\theta^2}{r} \tag{3}$$

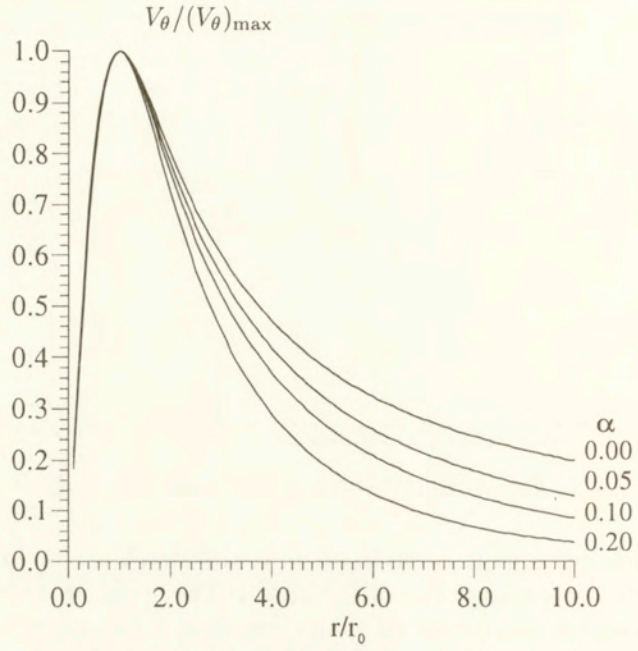

FIG. 2. Velocity distributions in the vortex.

and energy equation for adiabatic flow:

$$\frac{\gamma}{\gamma-1}\frac{p}{\varrho}+\frac{V_\theta^2}{2}=\frac{\gamma}{\gamma-1}\frac{p_\infty}{\varrho_\infty}, \tag{4}$$

where p_∞ and ϱ_∞ mean the pressure and density far from the vortex core, respectively.

The parameters Γ_0, r_0 and α in Eq. (1) can be chosen to match the real pressure distribution in the vortex. To obtain these parameters the pressure in the vortex center, the maximum of pressure derivative $(dp/dr)_{\max}$ and the radius corresponding to $(dp/dr)_{\max}$ determined from the measured function $p(r)$ can be used. The apropriate procedure is presented in Ref. [6]. In the present calculations the following values for Γ_0, r_0/c and α were assumed: 50 m^2/s, 0.045, 0.15, respectively. These values correspond to the measured pressure distribution in the vortex presented in Ref. [6].

4. Numerical procedure

The finite volume method is used. Equation (1) for a cell j of finite area ΔS yields:

$$\frac{dU_j}{dt}=\frac{1}{\Delta S}\sum(F\Delta y+G\Delta x). \tag{5}$$

In case of a quadrilateral cell (Fig. 3) the right-hand side of the above equation is

$$\frac{1}{\Delta S}\begin{Bmatrix} -(F_{i+1/2,j})(y_P - y_Q) + (G_{i+1/2,j})(x_P - x_Q) \\ -(F_{i-1/2,j})(y_R - y_S) + (G_{i-1/2,j})(x_R - x_S) \\ -(F_{i,j+1/2})(y_S - y_P) + (G_{i,j+1/2})(x_S - x_P) \\ -(F_{i,j-1/2})(y_Q - y_R) + (G_{i,j-1/2})(x_Q - x_R) \end{Bmatrix}.$$

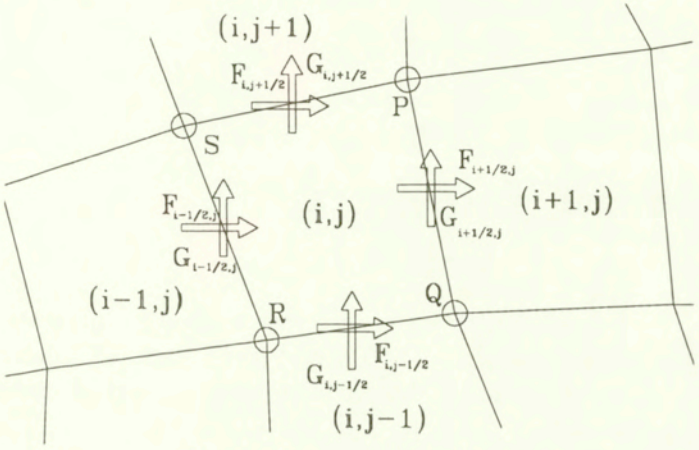

FIG. 3. Notation of the fluxes.

Each flux vector shown in Fig. 3 is composed of two terms, e.g.

$$F_{i+1/2,j} = F^{+}_{i,j} + F^{-}_{i+1,j}\,. \tag{6}$$

The first and the second term on the right-hand side are the forward and the backward contributions of the fluxes produced by the neighbouring cells i, j and $i+1, j$, respectively (Fig. 4).

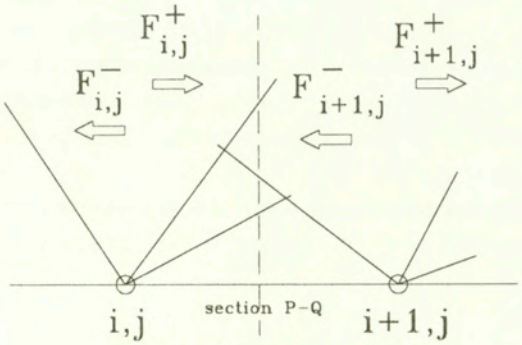

FIG. 4. Flux splitting.

The contributions are obtained by splitting the flux vector F, in the way proposed by VAN LEER [7], as follows:

for $-a < u < a$ (a means the speed of sound)

$$F^{\pm} = \begin{Bmatrix} f^{\pm} \\ f^{\pm}\left[(\gamma-1)u \pm 2a\right]/\gamma \\ f^{\pm}v \\ f^{\pm}\left\{\left[(\gamma-1)u \pm 2a\right]/\left[2(\gamma^2-1)\right] + v^2/2\right\} \end{Bmatrix},$$

where

$$f^{\pm} = \varrho(u+a)^2/(4a)$$

for $u > a$

$$F^{+} = F, \qquad F^{-} = 0,$$

and for $u < -a$

$$F^{+} = 0, \qquad F^{-} = F.$$

The second order Runge–Kutta procedure was applied to integrate Eq. (5).

Almost 360 000 cells uniformly distributed in the control volume were used. Such a large number of cells was chosen to prevent numerical dispersion of the vortex during its passage.

5. Results

Figures 5 show the pressure isolines for six phases of the AVI process. The vortex was initially positioned under (at $h/c = -0.2$) or over ($h/c = 0.2$) the airfoil symmetry plane for the figures in the first and the second column, respectively. In Figs. 5 a and 5 g one can see the clockwise rotating vortex approaching the airfoil.

The vortex disturbs the bow shock wave which appears when the incident shock wave reflects at the leading section of the airfoil. Due to the vortex, the stagnation point leaves its initial position at the leading edge and shifts on to the upper surface independently of the vortex initial location ($h/c = -0.2$ and 0.2). However, beginning from the following phase when the vortex reaches the region very close to the leading edge, the flow patterns become strongly dependent on the vortex trajectory, i.e. on wheather the vortex passes over or under the airfoil. In the former case (Fig. 5 h) the stagnation point moves in the bottom surface of the airfoil. It comes back again to the leading edge after some delay (Fig. 5 j) as the vortex is being convected. The remaining flow region does not show remarkable changes.

In contrast to this, the latter case exhibits much stronger variations of the flow pattern. The vortex, when it passes the leading edge (Fig. 5 c), induces a supersonic flow region at the bottom surface of the airfoil. In this region there

is a shock wave. Simultaneously, a strong disturbance (compressive wave) is created at the leading section of the airfoil. It appears due to the expansion of the air in the stagnation region as the vortex passes the leading edge (the air in the stagnation region was initially compressed to high pressure owing to high velocity induced by the vortex). The compressibility wave which expands in the space under the airfoil is visible in Figs. 5 d – f. The shock wave in the supersonic flow region (Fig. 5 c) initially precedes the vortex and moves with it. However, the spacing between the shock wave and the vortex decreases. In the phase shown in Fig. 5 d the shock is in the plane normal to the airfoil and crossing the vortex core. In the following phases (Fig. 5 e, f) when the vortex passes the compression region at the trailing section of the airfoil, the shock wave disappears. The bow shocks visible in Fig. 5 e at both the upper and the bottom surfaces, form due to steepening of the compressibility waves. They appear at the trailing edge when it is left by the incident shock wave. Additional shocks emerge at the trailing edge when the vortex approaches it (Fig. 5 f).

The pressure distributions along the upper and bottom surfaces of the airfoil, corresponding to instantaneous flow patterns described above, are shown in Figs. 6 a – f. They are compared with those for the flow without vortex. For the phase of interaction shown in Fig. 6 a, at which the vortex only weakly influences the airfoil flow, the pressure distributions along the upper and bottom surfaces are very close to those obtained for case without the vortex. The compressibility waves mentioned above, induced by the incident shock wave when it leaves the trailing edge, can be observed in the trailing section. The difference between the pressure distributions increases as the vortex approaches the leading edge (Fig. 6 b). In the phase shown in Fig. 6 c, the supersonic flow region divided into two parts by a shock wave can be noted at the bottom surface. This suggests that the shock in this phase moves upstream and is followed by a compressive wave. The shock gains in strength during its motion down the airfoil. It achieves its maximum strength for the phase when it passes through the vortex (Fig. 5 d and 6 d). One can see that for the initial phases of the AVI, when the vortex passes the leading section, the average pressure at the bottom surface ($\overline{p}_b$) is lower than that at the upper surface ($\overline{p}_u$). The relationship between $\overline{p}_b$ and $\overline{p}_u$ changes as the vortex passes the airfoil, $\overline{p}_u$ increases whereas $\overline{p}_b$ decreases.

Eventually, for the vortex at the trailing edge, we have $\overline{p}_u < \overline{p}_b$. Variations of pressure do not disappear when the vortex leaves the airfoil. The experiments conducted in Ref. [8] prove that they exist for a relatively long time afterwards.

Analogous behaviour of the surface pressure can be also found for the vortex passing over the airfoil. In this case, however, the pressure variations are much weaker than for the vortex passing under the airfoil at the same miss-distance.

Histories of the lift coefficient (C_l) for four values of the miss-distance of the vortex passing under the airfoil are presented in Fig. 7. It can be noted that variations of C_l show cosine-like character. Its amplitude decreases with increasing miss-distance. Figure 8 shows a comparison of C_l for two vortex trajectories

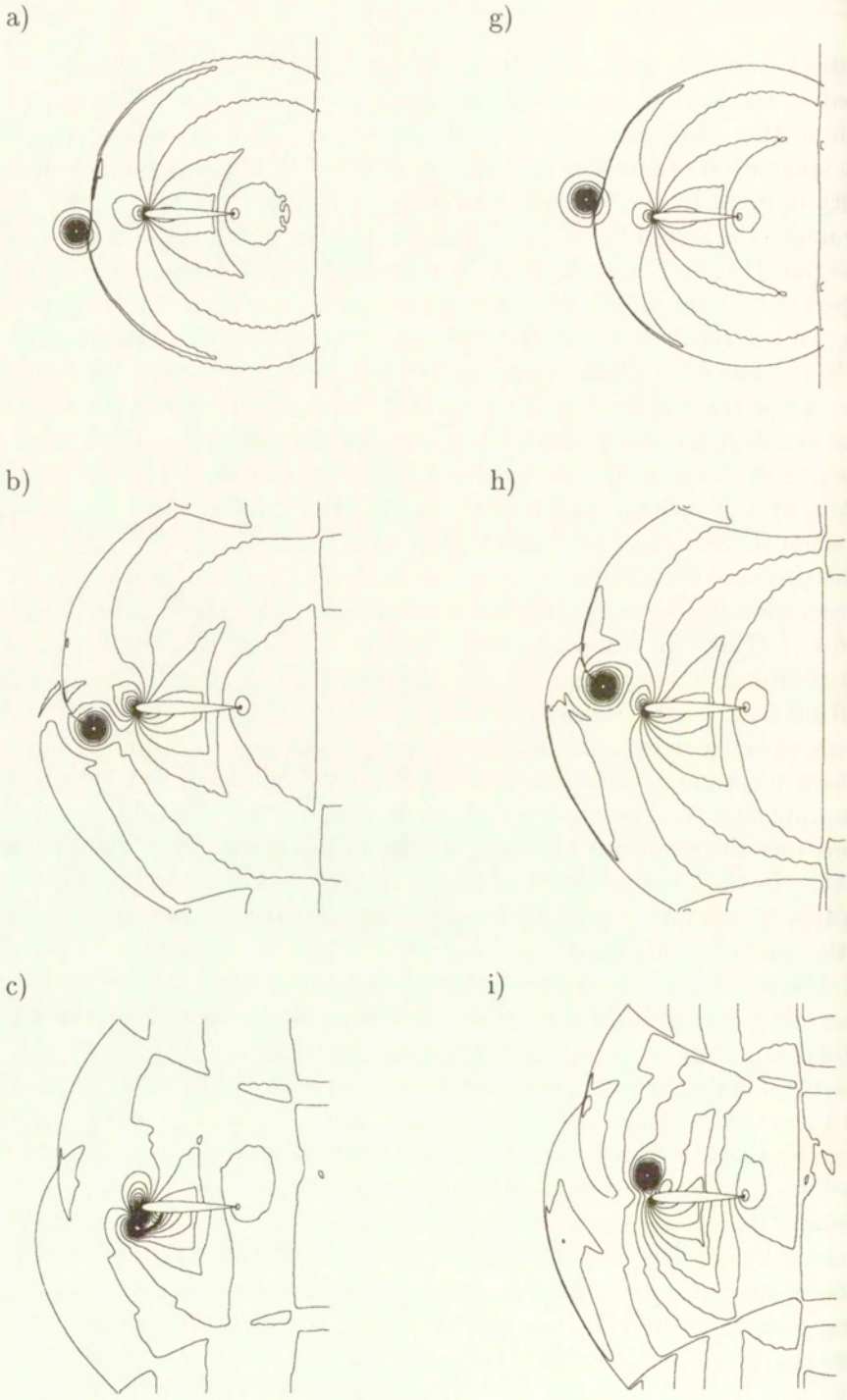

[FIG. 5]

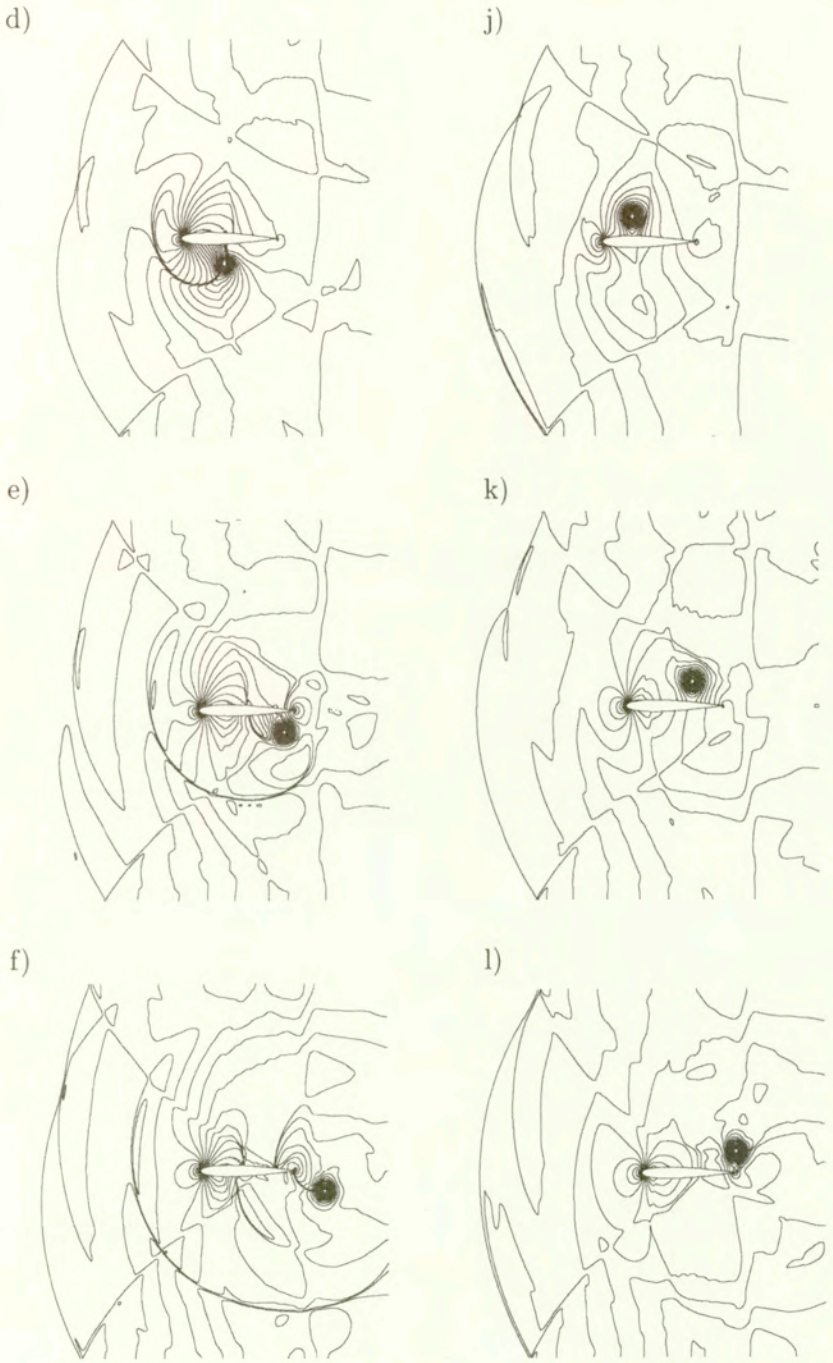

FIG. 5. Instantanous pressure isolines for the vortex passing under (first column) and over (second column) the airfoil. Delay in relation to the moment when the incident shock wave reaches the leading edge: (a,g) 0.508 ms, (b,h) 0.678 ms, (c,i) 0.848 ms, (d,j) 1.017 ms, (e,k) 1.186 ms, (f,l) 1.355 ms.

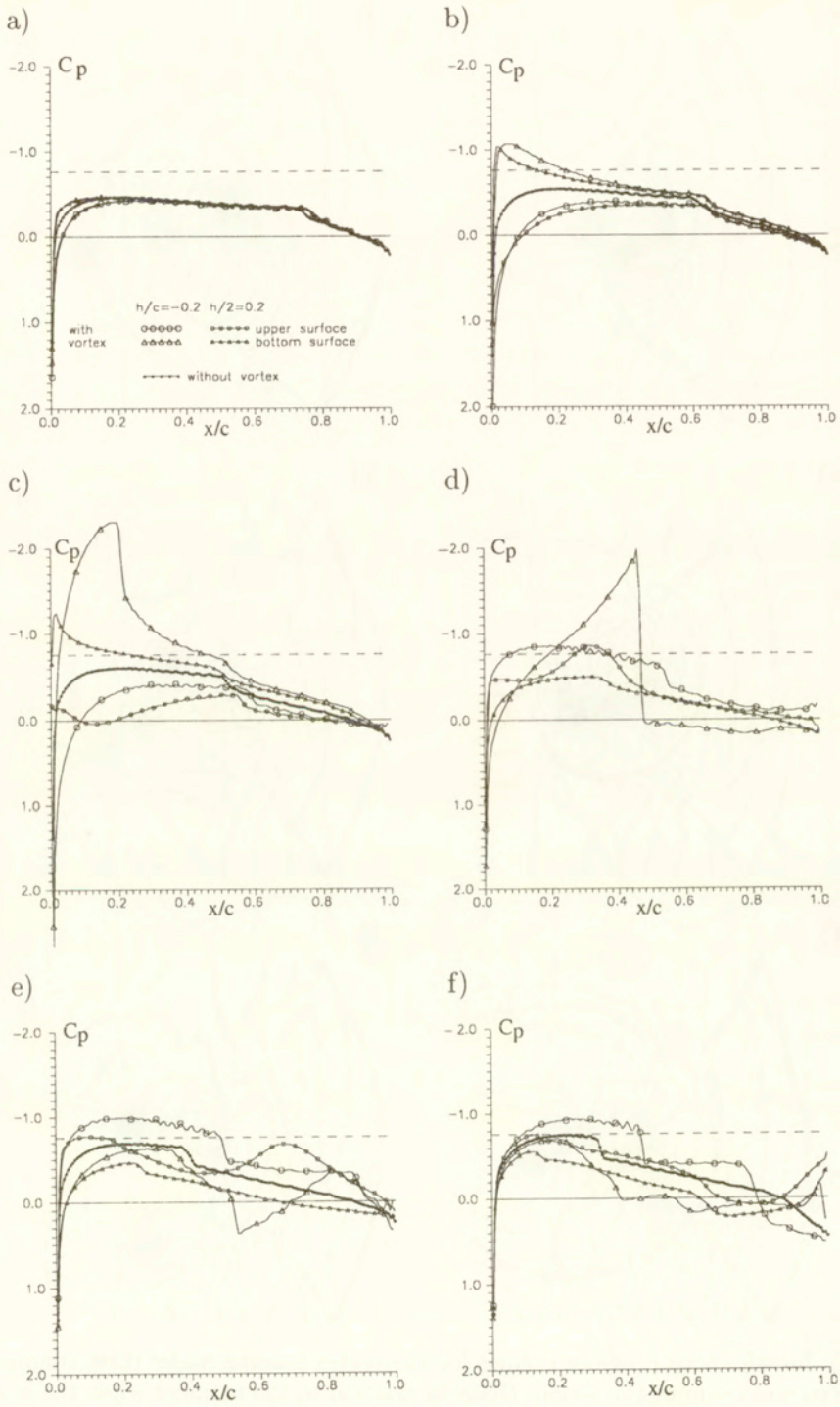

FIG. 6. Instantanous surface pressure coefficient (C_p) distributions corresponding to flow patterns shown in Fig. 5. Dashed line means sonic flow.

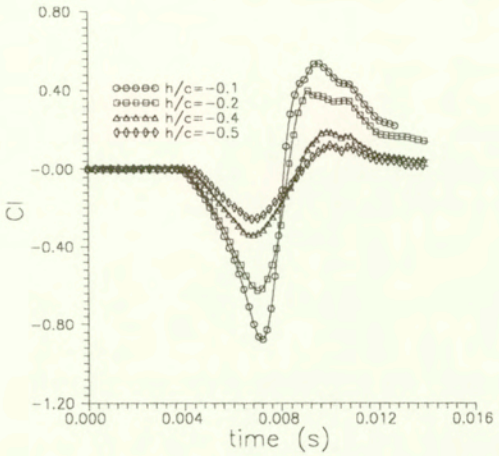

FIG. 7. Lift coefficients for various trajectories of the vortex passing under the airfoil.

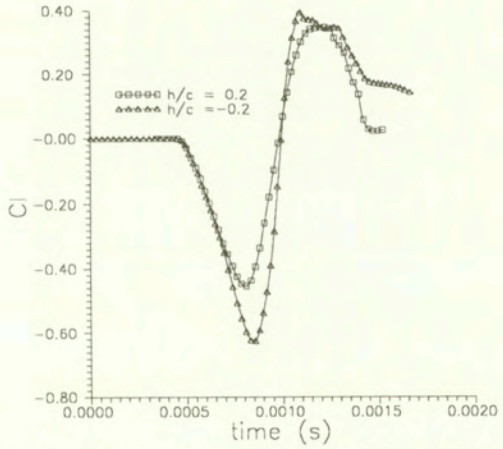

FIG. 8. Lift coefficients for the vortex passing over ($h/c = 0.2$) and under ($h/c = -0.2$) the airfoil.

$h/c = 0.2$ and $h/c = -0.2$. It is visible that the amplitude of C_l is larger for negative miss-distance.

6. Conclusions

Vortex trajectory appears to be an important parameter controlling the airfoil-vortex interaction. The effects of the AVI are much stronger when the vortex approaching to the airfoil accelerates the flow at the pressure surface of the airfoil than in the case when the vortex decelerates the flow at the suction surface. These cases correspond to the clockwise rotating vortex passing under or over the airfoil

considered in the present studies, respectively. The miss-distance strongly affects the instantaneous pressure distributions along the airfoil which leads to strong variations of the lift coefficient.

The background flow on which the vortex is superimposed has been induced in the present numerical investigation by a preceding shock wave passing along the airfoil at 0 deg. angle of attack. Nevertheless, the results obtained, at least qualitative, can be also considered for the case of fully developed steady background flow.

References

1. S. LEE and D. BERSHADER, *An experimental and computational study of 2-D parallel blade. Vortex interaction*, AIAA Paper, 91-3277.
2. S. LEE and D. BERSHADER, *Head-on parallel blade-vortex interaction*, AIAA J., **1**, 1, pp. 16–22, 1994.
3. S. DAMODARAN and D. CAUGHEY, *Finite-volume computation of inviscid transonic airfoil. Vortex interaction*, AIAA J., **26**, 11, pp. 1346–1352, 1988.
4. K. EHRENFRIED, *Numerische Untersuchung von Wirbel-Tragflügel-Wechselwirkungen im transsonischen Geschwindigkeitsbereich*, Max-Planck-Institut für Stroemungsforschung Report, 8, 1991.
5. J. GALLMAN, *Parametric computational study of isolated blade-vortex interaction noise*, AIAA J., **32**, 2, pp. 232–238, 1994.
6. A. SZUMOWSKI, J. PIECHNA, W. SELEROWICZ and G. SOBIERAJ, *Modified formula for the velocity distribution in a vortex*, J. Fluid Engng. [to be published].
7. B. VAN LEER, *Flux-vector splitting for the Euler equations*, Lecture Notes in Physics., **170**, pp. 507–512, 1982.
8. W. KAMIŃSKI and A. SZUMOWSKI, *Acoustic effects of parallel vortex-airfoil interaction*, J. Sound and Vibration, **183**, 2, 209–220, 1995.

WARSAW UNIVERSITY OF TECHNOLOGY
ul. Nowowiejska 24, 00-665 Warsaw.

Received June 20, 1997; new version October 30, 1997.

DIRECTIONS FOR THE AUTHORS

The journal *ARCHIVES OF MECHANICS (ARCHIWUM MECHANIKI STOSOWANEJ)* deals with the printing of original papers which should not appear in other periodicals.

As a rule, the volume of a paper should not exceed 40 000 typographic signs, that is about 20 type-written pages, format: 210 × 297 mm, leaded. The papers should be submitted in two copies. They must be set in accordance with the norms established by the Editorial Office. Special importance is attached to the following directions:

1. The title of the paper should be as short as possible.

2. The text should be preceded by a brief introduction; it is also desirable that a list of notations used in the paper should be given.

3. The formula number consists of two figures: the first represents the section number and the other the formula number in that section. Thus the division into subsections does not influence the numbering of formulae. Only such formulae should be numbered to which the author refers throughout the paper, and also the resulting formulae. The formula number should be written on the left-hand side of the formula; round brackets are necessary to avoid any misunderstanding. For instance, if the author refers to the third formula of the set (2.1), a subscript should be added to denote the formula, viz. $(2.1)_3$.

4. All the notations should be written very distincly. Special care must be taken to write small and capital letters as precisely as possible. Semi-bold type should be underlined in black pencil. Explanations should be given on the margin of the manuscript in case of special type face.

5. It has been established to denote vectors by semi-bold type. Trigonometric functions are denoted by sin, cos, tg and ctg, inverse functions – by arc sin, arc cos, arc tg and arc ctg; hyperbolic functions are denoted by sh, ch, th and cth, inverse functions – by Arsh, Arch, Arth and Arcth.

6. Figures in square brackets denote reference titles. Items appearing in the reference list should include the initials of the first name of the author and his surname, also the full title of the paper (in the language of the original paper); moreover;

a) In the case of books, the publisher's name, the place and year of publication should be given, e.g.,
5. S. Ziemba, *Vibration analysis*, PWN, Warszawa 1970;

b) In the case of a periodical, the full title of the periodical, consecutive volume number, current issue number, pp. from ... to ..., year of publication should be mentioned; the annual volume number must be marked in black pencil so as to distinguish it from the current issue number, e.g.,
6. M. Sokołowski, *A thermoelastic problem for a strip with discontinuous boundary conditions*, Arch. Mech., **13**, 3, 337–354, 1961.

7. The authors should enclose a summary of the paper. The volume of the summary is to be about 100 words.

8. The authors are kindly requested to enclose the figures prepared on diskettes (format PCX, BitMap or PostScript).

Upon receipt of the paper, the Editorial Office forwards it to the reviewer. His opinion is the basis for the Editorial Committee to determine whether the paper can be accepted for publication or not.

The printing of the paper completed, the author receives 10 copies of reprints free of charge. The authors wishing to get more copies should advise the Editorial Office accordingly, not later than the date of obtaining the galley proofs.

The papers submitted for publication in the journal should be written in English. No royalty is paid to the authors.

Please send us, in addition to the typescript, the same text prepared on a diskette (floppy disk) 3 1/2″ or 5 1/4″ as an ASCII file, in Dos or Unix format.

EDITORIAL COMMITTEE
ARCHIVES OF MECHANICS
(ARCHIWUM MECHANIKI STOSOWANEJ)

The next number of Archives of Mechanics will contain the following papers:

W. LARECKI, *Symmetric forms of the equations of heat transport in a rigid conductor of heat with internal state variables. Part I. Analysis of the model and thermodynamic restrictions via the "main dependency relation"*

W. LARECKI, *Symmetric forms of the equations of heat transport in a rigid conductor of heat with internal state variables. Part II. Alternative symmetric systems*

Z. SZYMAŃSKI, *The gas flow through the laser-sustained plasmas*

Z. PŁOCHOCKI and A. MIODUCHOWSKI, *An idea of thin-plate thermal mirror. Part II. Mirror created by a constant heat flux*

R. KIRK and H. PETRYK, *A self-consistent model of rate-dependent plasticity of polycrystals*

Z.A. WALENTA and J. ORZEŃSKI, *Focusing a shock wave – microscopic structure of the phenomenon*

H. XIAO, *On anisotropic functions of vectors and second order tensors – all subgroups of the transverse isotropy group* $C_{\infty h}$

J.J. TELEGA, A. GAŁKA and B. GAMBIN, *Effective properties of physically nonlinear piezoelectric composites*

Archives of Mechanics

cena zł 15,-

WARUNKI PRENUMERATY

Wpłaty na prenumeratę przyjmują na okresy półroczne:

na teren kraju

— jednostki kolportażowe RUCH S.A. i wszystkie urzędy pocztowe na terenie całego kraju, właściwe dla miejsca zamieszkania lub siedziby prenumeratora, oraz doręczyciele w miejscowościach, gdzie dostęp do urzędu jest utrudniony;

— od osób zamieszkałych lub instytucji mieszczących się w miejscowościach, w których nie ma jednostek kolportażowych RUCH, wpłaty należy wnosić do RUCHU S.A. Oddział Krajowej Dystrybucji Prasy, 00–958 Warszawa, ul. Towarowa 28. Konto: PBK S.A. XIII Oddział Warszawa nr 11101053–16551–2700–1–67. RUCH S.A. zapewnia dostawę pod wskazanym adresem pocztą zwykłą w ramach opłaconej prenumeraty;

na zagranicę

— RUCH S.A. Oddział Krajowej Dystrybucji Prasy, 00–958 Warszawa, ul. Towarowa 28. Konto: PBK S.A. XIII Oddział Warszawa nr 11101053–16551–2700–1–67. Dostawa odbywa się pocztą zwykłą w ramach opłaconej prenumeraty, z wyjątkiem zlecenia dostawy pocztą lotniczą, której koszt w pełni pokrywa zleceniodawca.

Prenumerata ze zleceniem dostawy za granicę jest o 100 % wyższa od krajowej.

Terminy wpłat na prenumeratę zagraniczną:

do 20 XI na I półrocze roku następnego do 20 V na II półrocze roku bieżącego

Terminy wpłat na prenumeratę krajową:

RUCH S.A.		Poczta Polska	
do 5 XII	na I półrocze roku następnego	do 25 XI	na I półrocze roku następnego
do 5 VI	na II półrocze roku bieżącego	do 25 V	na II półrocze roku bieżącego

Dostawa zamówionej prasy następuje:

— przez jednostki kolportażowe RUCH S.A. – w sposób uzgodniony z zamawiającym,
— prenumerata pocztowa – pod wskazanym adresem, w ramach opłaconej prenumeraty.

RUCH S.A. fulfils foreign customers' orders, starting from any issue in the calendar year:
tel.: (48) (22) 620 10 39; fax: (48) (22) 620 17 62.

Bieżące numery można nabyć w Księgarni Wydawnictwa Naukowego PWN, ul. Miodowa 10, 00–251 Warszawa, tel. (22) 695 40 26. Również można je nabyć, a także zamówić (przesyłka za zaliczeniem pocztowym) we Wzorcowni Ośrodka Rozpowszechniania Wydawnictw Naukowych PAN, 00–818 Warszawa, ul. Twarda 51/55, tel. (22) 697 88 35 oraz w Redakcji.

Redakcja przyjmuje prenumeratę na wszystkie czasopisma wydawane przez IPPT PAN.

Subscription orders for all journals edited by IFTR may be sent directly to the Editorial Office of the Institute of Fundamental Technological Research, Świętokrzyska 21, 00-049 Warszawa, Poland.

All journals edited by PWN are available through:

Foreign Trade Enterprise
ARS POLONA,
Krakowskie Przedmieście 7,
00-068 Warszawa, Poland
fax (48) (22) 826 86 73

or

Polish Scientific Publishers PWN Ltd.
10 Miodowa Str.
00–251 Warszawa, Poland
fax (48) (22) 695 42 88

Arch. Mech. T. **50**, nr 1, str. 1 – 140, Warszawa 1998.